Lateral Hypothalamic Control of Motivated Behaviors through the Midbrain Dopamine System

By

Edward H. Nieh

M.S.E. in Bioengineering
B.S.E. in Bioengineering
University of Pennsylvania, 2010

Submitted to the Department of Brain and Cognitive Sciences in partial fulfillment of the requirements for the degree of

DOCTOR OF PHILOSOPHY IN NEUROSCIENCE

at the

MASSACHUSETTS INSTITUTE OF TECHNOLOGY

June 2016

Signature of Author: Signature redacted
Department of Brain and Cognitive Sciences
May 20th, 2016

Certified by: Signature redacted
Kay M. Tye
Assistant Professor of Neuroscience
Thesis Supervisor

Accepted by: Signature redacted
Matthew A. Wilson
Sherman Fairchild Professor of Neuroscience
Director of Graduate Education for Brain and Cognitive Sciences

Lateral Hypothalamic Control of Motivated Behaviors through the Midbrain Dopamine System

By

Edward H. Nieh

Submitted to the Department of Brain and Cognitive Sciences on May 20th, 2016 in partial fulfillment of the requirements for the degree of

DOCTOR OF PHILOSOPHY IN NEUROSCIENCE

Abstract

The lateral hypothalamus and ventral tegmental area are two brain regions that have long been known to be involved in processing reward and the control of feeding behaviors. We continue work in this area by identifying the functional connectivity between these two regions, providing evidence that LH neurons projecting to the VTA encode conditioned responses, while LH neurons innervated by the VTA encode conditioned and unconditioned stimuli. Activation of the LH-VTA projection can increase compulsive sugar seeking, while inhibition of the projection can suppress this behavior without altering normal feeding due to hunger. We can separate this projection into the GABAergic and glutamatergic components, and we show that the GABAergic component plays a role in promoting feeding and social interaction by increasing motivation for consummatory behaviors, while the glutamatergic component largely plays a role in the suppression of these behaviors. Finally, we show that activation of the GABAergic component causes dopamine release downstream in the nucleus accumbens via disinhibition of VTA dopamine neurons through VTA GABA neurons. Together, these experiments have profoundly elucidated the functional roles of the individual circuit components of the greater mesolimbic dopamine system and provided potential targets for therapeutic intervention of overeating disorders and obesity.

Thesis Supervisor: Kay M. Tye
Title: Assistant Professor, Department of Brain and Cognitive Sciences

Table of Contents

Dedicated to my parents, Evan and Sun,

My brothers, Vincent, Albert, and Kevin,

And my lovely wife, Lisa

Chapter 1

Introduction: The Neural Correlates for Feeding and Reward and Implications in Health and Medicine

The study of how the brain encodes reward and feeding behaviors has become even more important and relevant as obesity and related disorders shape the global population.

Portions Adapted from Nieh et al. 2013, *Brain Research*

1.1 The Fastest Rising Health Problem in the Early 21st Century

The search for food is one of the most basic motivated drives in the natural world. From single-celled organisms to human beings, sustenance is required for life. However, for the majority of the animal kingdom, food is scarce and finding it is often subject to threats that are dangerous to life. Thus animals, including humans, have learned to evaluate the balance between obtaining food and avoiding dangers, and it is in this environment that the mammalian brain has evolved over millions of years. However, in a relatively short amount of time, humans have climbed to the top of the food chain and developed technologies for efficient farming, mass production, and refrigeration. As a result, food is no longer scarce for much of the human population, nor are there any apparent or immediate dangers associated with obtaining food. It is this combination of technological advances with the ancient wiring of the mammalian brain that has resulted in humans coming upon a relatively new problem – obesity.

In 2010, a study from the World Health Organization (Alwan, 2011) reported that at least 2.8 million people die each year as a result of complications from being overweight or obese. These deaths stem from the prevalence of overweightness and obesity, as 35% of adults above the age of 20 worldwide have been found to be overweight, with the problem most severe in the Americas, where 62% of men and women fit this category. The outlook is also grim - with obesity rates having doubled from 1980 to 2008 in adults and a steady rise in infants and young children being overweight from 1990 to present-day across all socioeconomic groups. Perhaps the most dire realization of all is that due to diet-related diseases, children in the U.S. today may be the first generation to live shorter lives than their parents (Harris et al., 2009; Olshansky et al., 2005).

The rise in obesity has largely coincided with modern trends in food production/sale and eating habits (Popkin and Nielsen, 2003). Between 1977 and 2001, an additional 280 kcal/day from beverages (Nielsen and Popkin, 2004) and 145 kcal/day from snacking has been added to the American diet (Zimmerman, 2011). Dietary behavior has shifted from at-home to away-from-home consumption, which had led to large increases in total energy consumed from salty snacks, soft drinks, and pizza and large decreases in low- and medium-fat milk and medium- and high-fat beef and pork (Nielsen et al., 2002). Simply put, the frequency of consuming restaurant food has been positively associated with body fatness (McCrory et al., 1999). In addition, portion sizes have increased steadily from the 1970s to 1999 (Young and Nestle, 2002). To further exacerbate the problem, fast food restaurants have been concentrated within shorter walking distances from schools (Austin et al., 2005), and consumers who frequent these restaurants (more than twice a week) have been found to gain an extra 4-5 kg of bodyweight and have a two-fold greater increase in insulin resistance over a 15-year period (Pereira et al., 2005).

This increase in availability, type, and amount of food has also coincided with a rise in marketing. Total advertising expenditures have been estimated to have increased 60%, from ~$506 to $815 a person, from 1980 to 2000 (Klein, 2009). In the United State alone, $1.6 billion is spent by the food industry to target children and adolescents (Federal Trade Commission, 2008), and 98% of those food advertisements are for products high in sugar, fat and/or sodium (Harris et al., 2009; Powell et al., 2007). Perhaps one of the greatest examples of the effectiveness of advertising was the product placement of Reese's Pieces in the blockbuster movie, E.T., which led to a subsequent 65% increase in sales (Snyder, 1992). Advertisers also play on the psychology of consumers, appealing to their choices in lifestyle, real or imagined, and on their loyalties to certain brands, as well as on the biology of consumers, engineering

foods to be more palatable and easier to eat – faster consumption means more consumption (Drewnowski, 1997; Kessler, 2010; Zimmerman, 2011).

The prevalence of overweightness and obesity across the world's populations indicates that the problem isn't necessarily tied with culture, religion, or social/family structures. Instead, it suggests an evolutionarily conserved mechanism that is hijacked across different populations of humans living in a variety of distinct environments. The most important question of our generation for solving this obesity crisis is to uncover why we are overeating, how it is happening, and present possibilities for solutions. This thesis will explore how the brain has been wired to leave it vulnerable to hijacking by high-fat or high-sugar foods which can lead to the overeating and obesity. Increased activity in neural pathways, from the lateral hypothalamus to the midbrain dopamine system, through the ventral tegmental area and nucleus accumbens, causes increased motivation for responding to conditioned desires, including the desire to consume palatable foods.

1.2 Conditioned to Seek Reward – A Learning Mechanism

Classical, or Pavlovian, conditioning is a learning process by which a neutral stimulus (the conditioned stimulus), such as the ringing of a bell, becomes associated with an unconditioned stimulus, such as food, after repeated pairings. When Pavlov repeatedly presented the pairing of a stimulus with food, the dog began to salivate in response to the stimulus before the presentation of food (Pavlov, 1927; Pavlov and Anrep, 2003). Here, the conditioned stimulus

had obtained the rewarding aspects of the unconditioned stimulus. The dog knew that when it saw or heard the conditioned stimulus, a reward delivery was imminent.

In humans, we also experience many CS-US pairings in everyday life. Marketing and advertising rely on logos and brands on colorful boxes and bags to indicate the rewarding nature of the food contained within, and the way food is presented on a plate can alter how appealing it is, even prior to tasting (Hutchings, 1977; Jaros et al., 2000; Zellner et al., 2010, 2011). Television commercials filled with friendly animals selling candies or scantily-clad models eating burgers or even simply playing sounds of the bubbling and sizzling of your favorite soft-drinks are taking advantage of the conditioned stimuli that we have associated with palatable foods. And as it did with Pavlov's dogs, exposure to these conditioned stimuli can lead to salivation, or a desire to drive to the nearest corner store or fast food restaurant to obtain the food.

An important extension to Pavlovian conditioning is the Rescorla-Wagner model (Rescorla and Wagner, 1972), which argues that an animal learns from the discrepancy between expectations and reality. For example, once the dog has learned that a ringing bell predicts food, if that food is not given, the dog will become confused since an expectation has not been fulfilled and will react to the omission of the expected reward. However, after repeated omissions, the bell will no longer be conditioned with the food, and the dog will no longer salivate to the ringing of the bell – the learning of the pairing has become extinguished. A second layer to this idea is that the nature of a stimulus can weigh in on how strong a conditioned pairing can be. For example, the pairing of a bell with a steak will produce more salivation than pairing with normal chow. The same is also true in advertising. The pairing of a bright, happy animal mascot in a television commercial with a garden salad will never supersede the pairing of the same bright,

happy animal mascot with a much more appetizing, chocolate candy bar. Because of the prevalence and ease of obtaining the chocolate candy bar, we essentially live in a society where we are constantly exposed to conditioned stimuli that are paired with unhealthy foods that are easy to obtain. This aspect of society has generated the prevalence of obesity, but as scientists, we can uncover how the brain becomes so easily manipulated in these situations in order to find solutions to counteract the obesity epidemic.

1.3 Conditioning in the Brain – Dopamine Neurons in the VTA

To study how the Rescorla-Wagner learning model manifests itself in the brain, we can look for correlates in neural activity that reflect predictions from the model for how the brain should behave. An apparent neural correlate was found when Schultz and colleagues published findings that dopamine (DA) neurons in the ventral tegmental area (VTA) of the brain change their activity based on patterns similar to those predicted by the Rescorla-Wagner model, which became known as reward prediction error (Cohen et al., 2012; Mirenowicz and Schultz, 1994; Montague et al., 1996; Romo and Schultz, 1990; Schultz et al., 1997). In these studies, VTA dopamine neurons would increase their firing rate in the presence of an unexpected reward, but shift their firing to coincide with the predictive stimulus once the animals had learned the presence of the CS-US pairing. In addition, as predicted in the Rescorla-Wagner model, these neurons also inhibited their firing when an expected reward was omitted.

The VTA is one of the most well-known areas for the processing of reward, and as part of the greater mesolimbic dopamine system, it sends dopaminergic innervation to the nucleus

accumbens (NAc), amygdala, hippocampus (HPC), and the prefrontal cortex (PFC) (Figure 1) (Fields et al., 2007). It also carries a heterogeneous composition of neurons, consisting of dopamine neurons (~65%), GABA neurons (~30%), and glutamate neurons (~5%) (Dobi et al., 2010; Margolis et al., 2006; Nair-Roberts et al., 2008; Yamaguchi et al., 2007). Importantly, for its role in reward prediction error, the VTA can be thought of as the critic in an actor-director critic model for decision-making (Figure 2) (Atallah et al., 2007; Nieh et al., 2013; Sugrue et al., 2005), where the VTA judges valuations of higher order processes by taking in predictions about the value of a stimulus and outputting error signals comparing these predictions with the actual reward obtained. As a result of its role in judging reward predictions, it is a region likely perturbed in pathological states such as addiction and other neuropsychiatric disorders (Everitt and Robbins, 2005; Grace et al., 2007; Hyman et al., 2006; Kalivas, 2005; Lüscher and Malenka, 2011; Nestler and Carlezon Jr, 2006; Schultz, 2007; Wise, 2002, 2005).

Animal studies have shown that phasic activation of VTA dopamine neurons is sufficient to drive behavioral conditioning, where animals would spend more time in the side of an open chamber paired with phasic VTA stimulation than the side without stimulation (Tsai et al., 2009). In addition, depletion of dopamine in the nucleus accumbens, a major target for dopamine neurons of the VTA, by local injection of 6-hydroxydopamine (6-OHDA) can attenuate amphetamine-induced conditioned place preference (Spyraki et al., 1982), while direct injection of amphetamine or dopamine receptor agonist supports conditioned place preference (Carr and White, 1983, 1986; White et al., 1991). As a result, there is a clear role for VTA dopamine neurons in processing reward and that activating this system is rewarding (Ikemoto, 2007).

Meanwhile, as mentioned previously, the VTA also contains a significant population of GABA neurons, which have been found to show persistent activity during the delay between a reward-predictive cue and the reward that reflects the value of the upcoming reward (big, small or none) (Cohen et al., 2012). Combined with the lack of modulation by the delivery or omission of the reward, these data suggest that GABA neurons possibly encode reward expectation and not the reward itself. In addition, GABA neurons were also activated by aversive stimuli, potentially suppressing dopaminergic activity in response to aversive events, as it has been shown that activating VTA GABA neurons suppresses the activity of VTA dopamine neurons (Tan et al., 2012; van Zessen et al., 2012). Importantly, opiates acutely hyperpolarize these VTA GABA neurons that synapse on and inhibit dopamine neurons, which leads to a disinhibition of VTA dopamine neurons (Johnson and North, 1992).

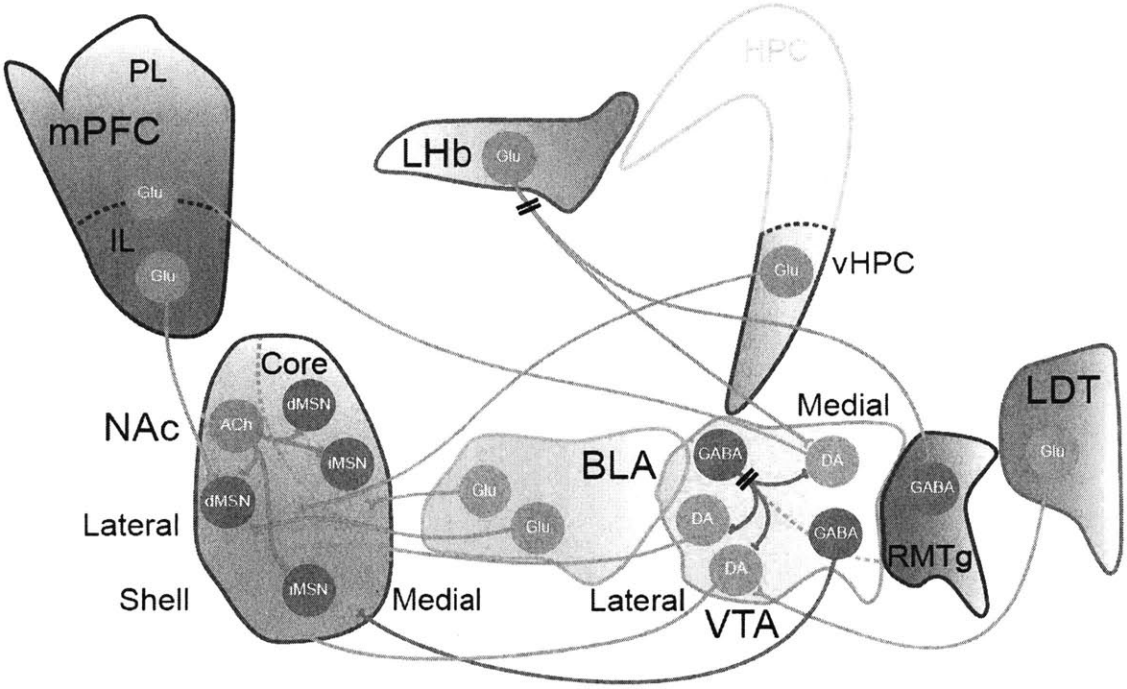
PL
mPFC
Glu
IL
Glu
HPC
LHb
Glu
Glu
vHPC
Core
NAc
dMSN
ACh
iMSN
dMSN
Lateral
Shell
iMSN
Medial
BLA
Glu
Glu
Medial
GABA
DA
DA
GABA
DA
Lateral
VTA
GABA
RMTg
LDT
Glu

Figure 1. A Model of the Mesolimbic Dopamine System

Optogenetic studies have expanded our understanding of the distal circuit dynamics, the extended inputs and outputs, and the causal relationships underlying behavior in the mesolimbic dopamine system. Individual projections through the VTA that process reward (LDT-VTA-NAc) and aversion (LHb-VTA-mPFC) have been characterized. Cell-type specific targeting of channelrhodopsin-2 (ChR2) has shown that GABAergic neurons in the VTA negatively regulate reward, while striatal dMSNs and iMSNs have opposing functions on valence processing. Dotted lines represent non-optogenetic findings. Double hash marks represent uncertainty in neuronal population from projection origin. Abbreviations: ACh, acetylcholine; BLA, basolateral amygdala; DA, dopamine; dMSN, direct pathway medium spiny neuron; Glu, glutamate; HPC, hippocampus; iMSN, indirect pathway medium spiny neuron; IL, infralimbic cortex; LDT, laterodorsal tegmentum; LHb, lateral habenula; mPFC, medial prefrontal cortex; MSN, medium spiny neuron; NAc, nucleus accumbens; PL, prelimbic cortex; RMTg, rostromedial tegmental area; vHPC,ventral hippocampus; VTA, ventral

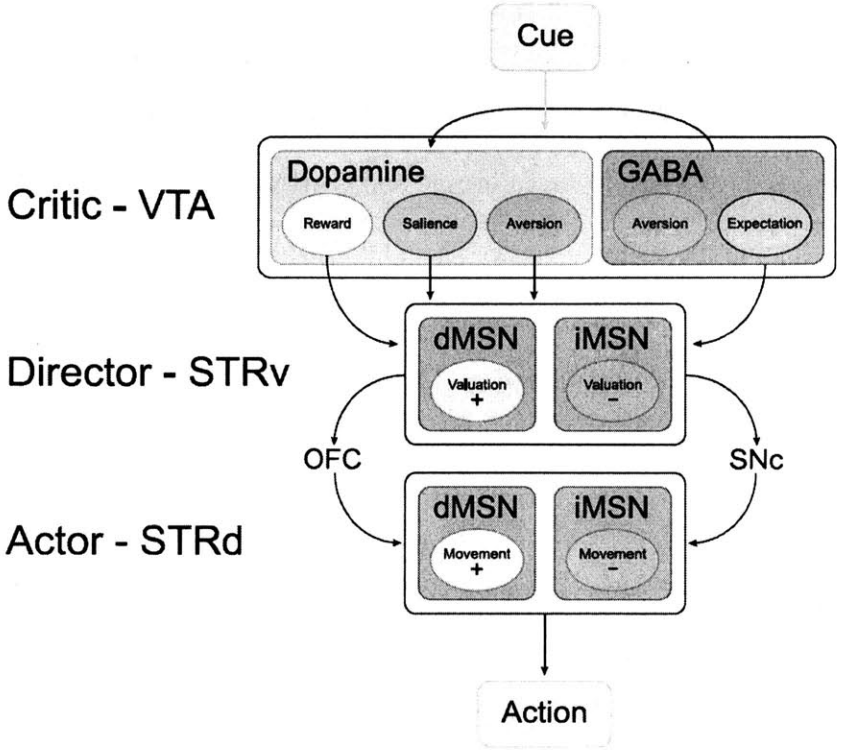
Cue
Critic - VTA
Dopamine
Reward
Salience
Aversion
GABA
Aversion
Expectation
Director - STRv
dMSN
Valuation
+
iMSN
Valuation
−
OFC
SNc
Actor - STRd
dMSN
Movement
+
iMSN
Movement
−
Action

Figure 2. Actor – Director – Critic Model for Decision-Making

In the actor-director-critic model for decision-making, the VTA plays the role of the critic, while the ventral and dorsal striatum play the roles of the director and actor, respectively. The VTA sends dopaminergic and GABAergic signals downstream to the STRv representing the value of a cue. The STRv integrates information from the VTA with inputs from other brain regions and sends a signal through the OFC or SNc to modulate STRd activity. The STRd generates an action signal that is processed downstream to generate the appropriate motor response for the cue. However, there is also evidence that STRd encodes reward and aversion as well. Abbreviations: dMSN, direct pathway medium spiny neuron; iMSN, indirect pathway medium spiny neuron; MSN, medium spiny neuron; OFC, orbitofrontal cortex; SNc, substantia nigra pars compacta; STRd, dorsal striatum; STRv, ventral striatum; VTA, ventral tegmental area.

1.4 Salience – A Measure of Importance

If we revisit Pavlovian conditioning, the Rescorla-Wagner model, and reward prediction error, we can address an issue that hasn't been brought up yet – what happens if the unconditioned stimulus is an aversive one? In this case, if the ringing bell is followed with a stimulus that causes pain, the dog will learn to fear the ringing bell, possibly by showing signs of fear, such as cowering. Importantly, in reward prediction error, we would expect dopamine neurons to show very clear inhibition to an aversive stimulus, and while many dopamine neurons do follow this trend, others are also excited by aversive stimuli (Chiodo et al., 1980; Coizet et al., 2006; Guarraci and Kapp, 1999; Mantz et al., 1989; Matsumoto and Hikosaka, 2009; Schultz and Romo, 1987). Matsumoto and Hikosaka suggested that neurons excited by both rewarding and aversive stimuli may reflect the salience of the stimulus (Matsumoto and Hikosaka, 2009). Importantly, these authors showed that dopamine neurons inhibited and excited by aversive stimuli were anatomically distinct. Lammel and colleagues showed that the projection targets of dopamine neurons could also separate their function: projections to the NAc medial shell responded to rewarding stimuli, projections to medial prefrontal cortex (mPFC) responded to aversive stimuli, and projections to NAc lateral shell responded to both rewarding and aversive stimuli, a representation of salience (Lammel et al., 2011).

In fact, there is a separate school of thought that suggests that VTA dopamine neurons encode incentive salience, instead of reward prediction error (Berridge, 2006; Berridge and Robinson, 1998; Robinson and Berridge, 1993). The incentive salience theory posits that VTA dopamine neurons mediate the incentive salience of rewards, modulating their motivational value in a manner irrespective of hedonic value and reward learning. Essentially, the idea is that

dopamine neurons signal the "wanting" of a stimulus, instead of the "liking" of a stimulus. These two separate psychological components of reward are often tied together, and using behavioral measures based on affective reactions, "wanting" can be separated from the "liking". This is important because traditional tests to measure reward, such as place preference or instrumental performance, can only estimate the amount of "liking" from the amount of "wanting" an animal has for a stimulus – we infer that because an animal is willing to work for a stimulus, that it "likes" the stimulus.

A strong piece of evidence for incentive salience is that dopamine signals are elevated prior to the consumption of a rewarding stimulus (Kiyatkin and Gratton, 1994; Phillips et al., 1993; Simansky et al., 1985), an indication that dopamine neurons have already responded before the animal has experienced the pleasurable reward. In addition, oxidopamine (6-OHDA) lesions of the striatal/accumbens dopamine system show that the affective reactions (hedonic: lateral tongue protrusions, rhythmic tongue protrusions, and paw licks; aversive: gapes, chin rubs, face washing, forelimb flairs, paw treads, and locomotion (Grill and Norgren, 1978)) were unchanged in reaction to exposure to sucrose or quinine solutions, even though animals were aphagic (Berridge and Robinson, 1998; Berridge et al., 1989). This was evidence that lesioning dopamine neurons did not change whether animals perceived the hedonic or aversive values of the solutions, and therefore dopamine neurons could not be encoding reward values. In addition, dopamine depletion did not disrupt an animal from learning a CS that changed its pairing from rewarding to aversive, and thus dopamine wasn't necessary for encoding reward learning (Berridge and Robinson, 1998). The debate between whether dopamine neurons encode reward learning or incentive salience has been ongoing for decades, but recent work has shown that

dopamine release dynamics in the nucleus accumbens core and shell could suggest parallel dopamine signals capable of supporting both theories (Saddoris et al., 2015).

Afferent projections to the VTA may also target distinct subpopulations of dopamine neurons. Matsumoto and Hikosaka showed that lateral habenula (LHb) neurons responded to reward in an opposing manner to dopamine neurons and that electrical stimulation in the LHb inhibited dopamine neurons (Matsumoto and Hikosaka, 2007). The rostromedial tegmental area (RMTg), also known as the posterior tail of the VTA (Kaufling et al., 2009; Perrotti et al., 2005), is composed of inhibitory GABA neurons that project to dopamine neurons in the midbrain (Kaufling et al., 2009). Jhou and colleagues showed robust excitatory input from the LHb to the RMTg (Jhou et al., 2009) and inhibitory input from the RMTg to the VTA (Jhou et al., 2009; Matsui and Williams, 2011), suggesting a LHb-RMTg-VTA pathway that mediates responses to aversive stimuli. Stamatakis and Stuber expressed ChR2 in LHb neurons of mice and implanted optical fibers above LHb terminals in the posterior VTA and the RMTg (Stamatakis and Stuber, 2012). Behavioral experiments showed that optical stimulation of LHb terminals caused conditioned place aversion (CPA), was capable of providing negative reinforcement, and also disrupted positive reinforcement.

The laterodorsal tegmentum (LDT) is another brain region that has been shown to innervate the VTA (Cornwall et al., 1990). In addition, electrical stimulation was shown to elicit dopamine release in the NAc, mediated by glutamatergic and cholinergic receptors in the VTA (Forster et al., 2002), suggesting a LDT-VTA-NAc pathway involved in processing reward. Lammel and colleagues used a combination of tracing techniques and retrograde/anterograde delivery of ChR2 to study both the projection targets of VTA dopamine neurons and afferent

projections to the VTA (Lammel et al., 2012). By infusing a retrograde rabies virus (RV) containing ChR2 into the VTA and differentially targeting two groups of animals with optical fibers in LDT or LHb, the authors found conditioned place preference (CPP) and conditioned place aversion (CPA) from optical stimulation of these two pathways, respectively. In addition, by combining retrobead injection in the mPFC or NAc with anterograde delivery of ChR2 into the LDT or LHb, the authors could perform whole-cell recordings of retrogradely-labeled VTA neurons that could be optically stimulated. Using this technique, LDT neurons were found to preferentially synapse onto dopamine neurons in lateral VTA projecting to the NAc lateral shell, while LHb neurons were found to preferentially synapse onto both dopamine neurons in medial VTA projecting to the mPFC and rostromedial tegmental nucleus (RMTg) GABA neurons. These data indicate a distinct separation of two circuits in the VTA – while the LDT-lateral VTA-NAc pathway encodes reward, the LHb-medial VTA-mPFC pathway encodes aversion (Lammel et al., 2012).

1.5 The Control of Feeding Behaviors in the VTA

While many studies of reward processing in the VTA have focused on drug reward, food is a potent natural reward. In fact, the intense sweetness of refined sugars such as sucrose or fructose has been shown to surpass cocaine reward, even in drug-sensitized and drug-addicted rats (Lenoir et al., 2007). This is even more concerning, given the increase in the use of sweeteners in our diets in recent years (Popkin and Nielsen, 2003). Fortunately, the dopamine system has also been well-studied in terms of its involvement in food rewards and feeding (Kelley and Berridge, 2002; Volkow et al., 2011; Wise, 2006). Dopamine-deficient mice will die

of starvation (Szczypka et al., 1999a), while dopamine antagonists will cause animals to reduce responding for food over time (Dickinson et al., 2000; Wise et al., 1978). In humans, eating has been shown to cause dopamine release in dorsal striatum with correlations to how pleasant subjects perceived the meals to be (Small et al., 2003). As mentioned above, dopamine neurons are believed to play a role in reward learning, and thus shift their firing to reward-predictive cues once a CS-US pairing is learned. Importantly, nonhedonic food stimulation, or in this case, the display of food without consumption – a compelling CS, has been shown to increase dopamine levels in dorsal striatum (Volkow et al., 2002). The increase in money spent on marketing and advertising in recent years to put such conditioned stimuli in front of consumers (Klein, 2009), combined with dopamine neural encoding of these cues, makes a strong case for study of the dopamine system for the overeating that causes obesity.

Homeostatic processes regulate food consumption (Zheng et al., 2009), and as a result, hormone signaling can modulate food reward and caloric homeostasis (Lattemann, 2008). Leptin is a hormone secreted by adipose tissue, or fat cells, and leptin concentrations fall during starvation and rise during obesity (Ahima et al., 1996; Friedman and Halaas, 1998; Maffei et al., 1995; Margetic et al., 2002; Palmiter, 2007). VTA dopamine neurons express the mRNA for leptin receptors and direct intra-VTA injection of leptin causes decrease in food intake (Hommel et al., 2006). In addition, the infusion of leptin into the lateral ventricle in rats suppresses extracellular dopamine concentrations of dopamine in the nucleus accumbens (Krügel et al., 2003), a major projection target of VTA dopamine neurons.

Another hormone that has been shown to act on VTA dopamine neurons is ghrelin, which is produced by the stomach and rises with fasting and falls after feeding (Kojima et al., 1999;

Nakazato et al., 2001; Palmiter, 2007; Tschöp et al., 2000, 2001; Wren et al., 2001). Intravenous ghrelin increased the appetite and food intake in humans (Wren et al., 2001), and it has also been shown the obese human patients have increased circulating ghrelin levels (Tschöp et al., 2001). In rodents, peripheral ghrelin administration caused weight gain by reducing the utilization of fat (Tschöp et al., 2000). With respect to the VTA, dopamine neurons have been shown to express ghrelin receptors, and direct intra-VTA administration of ghrelin was able to trigger feeding (Abizaid et al., 2006).

Importantly, opioid and cannabinoid signaling in the brain has also been shown to modulate feeding and reward through actions in the VTA, in both dopamine and local GABA interneurons (Cota et al., 2006; Johnson and North, 1992; Kirkham and Williams, 2001; Solinas and Goldberg, 2005; Tanda et al., 1997). Delta-9-tetrahydrocannabinol (THC) injection (i.p.) increased the break points for food reinforcement, suggesting that it increases the reinforcing effects of food (Solinas and Goldberg, 2005). Dynorphin (κ-opioid receptor agonist) and morphine (μ-opioid receptor agonist) intra-VTA injection caused increased feeding (Hamilton and Bozarth, 1988), as did intra-VTA injection of D-Ala^2, N-Me-Phe^4-Gly^5-Ol-enkephalin (DAMGO; μ-opioid receptor agonist) and D-Pen^2, D-Pen^5-enkephalin (DPDPE; δ-opioid receptor agonist) (Noel and Wise, 1995). This body of research shows that the VTA plays a major role in generating feeding behaviors in a system that also encodes reward processing, evidence that these two systems are largely intertwined in the midbrain dopamine system and that treating obesity will have to involve modulation of feeding and the rewards perceived from food.

1.6 The Lateral Hypothalamus – Motivational Control over the VTA

The study of the neural circuits for reward processing and feeding cannot ignore one of the largest players, the lateral hypothalamus (LH). The LH was one of the first areas of the brain to be identified where animals would repeatedly press a lever to receive electrical stimulation of the area (Olds, 1956; Olds and Milner, 1954), also known as intracranial self-stimulation (ICSS). This was the first indication that stimulation of the LH was rewarding and that the LH could play a role in positive reinforcement. Only several years prior, the LH had already been ascribed the label of "feeding center" due to evidence that bilaterally lesioning this area would cause animals to stop eating to the point of death from starvation (Anand and Brobeck, 1951a, 1951b). In addition, it was shown that electrical stimulation of this area could evoke feeding (Delgado and Anand, 1953). In fact, it was discovered that if the same animals were subjected to feeding and intracranial self-stimulation tests, all animals that fed when the LH was electrically stimulated would also show high self-stimulation rates (Margules and Olds, 1962), evidence that the feeding and reward systems were interconnected within the LH.

Evidence of the related effects of reward and feeding could be studied from the effects of satiety, and satiety was shown to affect ICSS (Hoebel and Teitelbaum, 1962). Animals that received intragastric injections of food showed slower rates of ICSS than animals that received intragastric injections of water. In addition, early recording studies showed that neurons in the LH would respond to the sight and/or taste of food, and interestingly, the responsiveness of the neurons decreased over the course of a meal as satiety increased (Burton et al., 1976; Mora et al., 1976). In addition, when drinking was shown to be evoked from LH stimulation, it was an initial indication of another motivated drive that could be tied into the LH system (Mogenson and

Stevenson, 1966), and perhaps that feeding might not be the only appetitive behavior that was encoded within the LH.

An important study by Valenstein and colleagues showed how the LH might be processing these different behaviors in the same way (Valenstein et al., 1968). Rats were placed into a chamber with access to food pellets, a water bottle with a drinking tube, and a pine wedge. Upon LH stimulation on the first day, different animals had different preferences for which stimulus they would interact with the most. On the second day of testing, experimenters removed the most preferred stimulus from the chamber for each animal, and LH stimulation was found to generate motivated behaviors towards the remaining stimuli. This phenomenon showed that LH stimulation may not be directly causing feeding or drinking, but rather it is changing the motivation for the animal towards a stimulus. In different contexts, depending on what stimuli were available, animals would perform different actions upon LH stimulation. Yet another form of substitutability was shown when animals were willing to substitute LH stimulation for water or food when given the choice (Green and Rachlin, 1991). This idea that the LH is involved in multiple motivated drives, yet unspecific to any single drive, will be addressed further in the main text as well as the final conclusion.

Sadly, stimulation studies of the LH became more difficult to interpret as more behaviors were shown to be elicited from LH stimulation, including aggression and sexual behaviors (Perachio et al., 1979; Singh et al., 1996; Woodworth, 1971). In addition, electrical stimulation inherently could not easily distinguish between fine spatial locations within the LH because electrical stimulation activates both cell bodies as well as axons of passage. As a result, the study of the LH slowed, as the field could not separate the many populations within the LH. However,

a few groups of researchers did try to alleviate the problem by focusing on one specific projection from the LH. Because there was ample evidence of both LH and VTA involvement in reward, the projection from the LH to the VTA through the medial forebrain bundle was thought to be the primary mediator of the reward and positive reinforcement behaviors evoked from LH or VTA stimulation. Many studies were done studying this LH-VTA projection using electrophysiological recordings combined with antidromic stimulation (Bielajew and Shizgal, 1986; Gratton and Wise, 1988; Murray and Shizgal, 1996a, 1996b; Shizgal, 1989). Recent work using a rabies-virus mediated tracing approach has confirmed a monosynaptic input from LH neurons onto dopamine neurons in the VTA (Watabe-Uchida et al., 2012), and this long history of work culminated in a study showing that animals will ICSS for optogenetic stimulation of LH terminals in the VTA (Kempadoo et al., 2013).

1.7 The Lateral Hypothalamus – Heterogeneity in the Population

The lateral hypothalamus is not a well-defined set of neurons that can fit under the category of a nucleus, which is likely why it has been also referred to as the "lateral hypothalamic area" (Swanson and Cowan, 1979). It receives inputs and sends outputs to many different brain areas and also plays a major role in the neuroendocrine system in the maintenance of homeostasis (Ahima et al., 2000; Barson et al., 2013; Berthoud and Münzberg, 2011; Date et al., 1999). As a result, the LH contains many different types of neurons that release a variety of neuropeptides along with the fast transmission neurotransmitters, glutamate and GABA. These include orexin/hypocretin (Gautvik et al., 1996; De Lecea et al., 1998; Sakurai et al., 1998), melanin-concentrating hormone (MCH) (Kawauchi et al., 1983; Kokkotou et al., 2005; Qu et al.,

1996; Rossi et al., 1997, 1999; Shimada et al., 1998), and neurotensin (Carraway and Leeman, 1973; Kahn et al., 1980; Kempadoo et al., 2013; Leinninger et al., 2011; Opland et al., 2013; Uhl et al., 1977).

The most well-studied of these systems is probably the orexin/hypocretin system, whose existence was first hinted at by Gautvik and colleagues when they discovered a gene in the rat brain with expression limited to only the LH (Gautvik et al., 1996). Two separate groups, Sakurai and colleagues and De Lecea and colleagues, published soon after, detailing the role of orexin for controlling feeding behavior and as a homeostatic regulator (De Lecea et al., 1998; Sakurai et al., 1998). The field is still currently undecided as to which name, orexin or hypocretin, to adopt. For this thesis, the neuropeptide will be referred to as simply orexin, respectfully noting that the name hypocretin is a viable alternative that is also commonly used. Since the foundational work by these two groups, orexins have also been characterized as a primary neurotransmitter in the LH functionally associated with reward (Aston-Jones et al., 2010; Boutrel et al., 2010; Cason et al., 2010; Georgescu et al., 2003; Harris and Aston-Jones, 2006; Harris et al., 2005; Narita et al., 2007). LH orexin neurons are activated by cues associated with food or drugs in a conditioned place preference assay (Harris et al., 2005; Narita et al., 2006), and activation of LH orexin neurons was also able to reinstate extinguished drug-seeking behavior (Harris et al., 2005). Most importantly, orexin directly affects VTA, as intra-VTA administration of orexin was shown to reinstate drug seeking for morphine (Harris et al., 2005) and cocaine (Wang et al., 2009), as well as producing dose-dependent place preference (Narita et al., 2007). In fact, genetically deleting the prepro-orexin gene was able to abolish any conditioned place preference involving morphine, and intra-VTA injection of an orexin antagonist significantly decreased place preference (Narita et al., 2006).

The second neuropeptide mentioned is melanin-concentrating hormone (MCH), which was first isolated from the salmon pituitary with antagonistic function to α-melanocyte-stimulating hormone (Kawauchi et al., 1983), and then discovered to promote feeding in the same direction as orexin (Barson et al., 2013; Edwards et al., 1999; Qu et al., 1996). However, orexin and MCH populations within the lateral hypothalamus were found to be distinct (Berthoud and Münzberg, 2011; Bittencourt et al., 1992; Peyron et al., 1998; Saito et al., 2001; Skofitsch et al., 1985; Swanson et al., 2005). Injection of MCH into the ventricles acutely stimulates feeding (Edwards et al., 1999; Qu et al., 1996; Rossi et al., 1997). In addition, mice with an overexpression of MCH become obese and develop resistance to insulin (Ludwig et al., 2001), while those with a MCH1 receptor deficiency are lean and have reduced fat mass (Marsh et al., 2002). Surprisingly, these MCH1R deficient mice are hyperphagic, and the maintenance of lean body mass is likely due to the corresponding changes resulting in hyperactivity and an altered metabolism. The stimulation of feeding is stronger with more palatable food, as intracerebroventricular (ICV) injection of MCH promotes the consumption of higher fat diets more than normal chow diets (Gomori et al., 2003; Shearman et al., 2003). It is believed that though both orexin and MCH are orexigenic, the reason they are distinct systems is because they generate feeding behavior in different ways. While orexin likely generates feeding behavior by increasing the motivation to eat, MCH appears to stimulate feeding by reinforcing ongoing intake (Barson et al., 2013). Importantly, MCH also modulates the midbrain dopamine system by playing a critical role in regulating accumbal dopamine signaling (Pissios et al., 2008). It's important to note that while it has been shown that the orexin and MCH systems both project to the VTA, a direct causal study of the orexin-VTA or MCH-VTA terminal stimulation on behavior has never been shown.

The third LH neuropeptide heavily involved in feeding and reward is neurotensin (Cador et al., 1986; Glimcher et al., 1984, 1987; Hawkins, 1986; Levine et al., 1983; Luttinger et al., 1982; Rompré, 1995; Rompré et al., 1992; Sahu, 1998; Uhl et al., 1977), which was first isolated in the bovine hypothalamus and shown to cause vasodilation (Carraway and Leeman, 1973). Early work on neurotensin showed that rats were willing to spend more time in an environment where they received bilateral injections of neurotensin on previous days – a form of conditioned reinforcement (Glimcher et al., 1984). In addition, rats were also willing to perform an operant task in order to obtain intra-VTA injections of neurotensin (Glimcher et al., 1987). In fact, the effects of intracerebroventricular injection of neurotensin have been compared to those of psychostimulants, since it potentiates brain stimulation reward in a dose-dependent manner (Rompré, 1995; Rompré et al., 1992). In contrast with orexin and MCH, ICV injection of neurotensin suppressed feeding, even in hungry animals, and it has been hypothesized that neurotensin may be a satiety factor (Cador et al., 1986; Hawkins, 1986; Levine et al., 1983). Importantly, neurotensin does not cause taste aversion (Luttinger et al., 1982). The involvement in satiety is strengthened by evidence of neurotensin in the leptin system (Leinninger et al., 2011; Sahu, 1998). Leinninger and colleagues discovered that the majority of neurons in the LH that contain leptin receptors also coexpress neurotensin, and that mice with leptin receptors knocked-out in neurotensin neurons show early-onset obesity, increased feeding, and decreased locomotion (Leinninger et al., 2011). Importantly, intra-VTA injection of neurotensin has been shown to increase locomotion and increase dopamine metabolism (Kalivas, 2005). Most recently, it was shown that mice are willing to ICSS for optogenetic stimulation of LH projections to the VTA, and that neurotensin antagonist infusion into the VTA blocks this ICSS (Kempadoo et al.,

2013), evidence that neurotensin plays a role in the brain stimulation reward previously evoked by LH electrical stimulation.

1.8 Into the Present – Dissection of the LH-VTA Circuit

The impetus for my Ph.D. work was to dig deeper into this circuit between the LH and VTA and really understand how the components of this circuit were involved in processing reward and feeding behaviors. By combining *in vivo* freely moving electrophysiology, optogenetic manipulations, fiber photometry, and fast-scan cyclic voltammetry, we could start to distinguish the individual components in this system and map the contributions to behavior of the identified components. As literature in this field has shown, feeding and reward are tied together very closely within the brain, and the interaction between the LH and the VTA is a major reason why. My goal was to understand how this interaction was taking place.

If we hope to understand obesity, we need to understand how the brain encodes eating and how it decides the rewarding value of food. The combination of the ancient wiring in our brain with this new environment of ample food, coupled with the massive amounts of advertising that invades our daily life, has placed the human brain in a situation where it is mishandling and miscalculating the rewarding value of food and other conditioned stimuli that are presented to it. If we can understand how these calculations are made, we can design ways to intervene and correct these calculations in order to stop the prevalence of overeating and obesity. It is with this sentiment that I pursue my scientific career, and the following studies are evidence that we are moving closer towards this goal.

Chapter 2

Decoding the Neural Circuits that Control Compulsive Sugar Seeking

A neural circuit loop between the lateral hypothalamus and the ventral tegmental area that selectively controls compulsive sugar consumption without preventing feeding necessary for survival provides a potential target for therapeutic interventions for compulsive overeating.

Adapted from Nieh et al. 2015, *Cell*

2.0 Contributions and Acknowledgements

Conception: Edward H. Nieh and Kay M. Tye

Surgical Injections and Implantations: Edward H. Nieh, Stephen A. Allsop, Kara N. Presbrey

In Vivo Electrophysiological Recordings: Edward H. Nieh, Stephen A. Allsop

Electrophysiology Analysis: Edward H. Nieh

Ex Vivo Patch-Clamp Experiments: Gillian A. Matthews

Patch-Clamp Analysis: Gillian A. Matthews

Behavioral Experiments – Compulsive Sucrose Seeking: Edward H. Nieh, Stephen A. Allsop, Christopher A. Leppla, Kara N. Presbrey

Behavioral Experiments – Feeding: Edward H. Nieh, Stephen A. Allsop, Kara N. Presbrey, Gillian A. Matthews

Behavioral Experiments – Tail Withdrawal: Edward H. Nieh, Stephen A. Allsop, Kara N. Presbrey, Gillian A. Matthews

Behavioral Experiments – Open-Field Task: Edward H. Nieh, Kara N. Presbrey

Behavioral Scoring: Edward H. Nieh, Stephen A. Allsop, Kara N. Presbrey

Optic Fiber Construction: Kara N. Presbrey

Optrode Construction: Edward H. Nieh

Histology: Edward H. Nieh, Gillian A. Matthews, Kara N. Presbrey, Romy Wichmann, Christopher A. Leppla

Confocal Microscopy: Edward H. Nieh, Gillian A. Matthews, Romy Wichmann

HSV-Cre Virus Creation: Rachael Neve

2.1 Summary

The lateral hypothalamic (LH) projection to the ventral tegmental area (VTA) has been linked to reward processing, but the computations within the LH-VTA loop that give rise to specific aspects of behavior have been difficult to isolate. We show that LH-VTA neurons encode the learned action of seeking a reward, independent of reward availability. In contrast, LH neurons downstream of VTA encode reward-predictive cues and unexpected reward omission. We show that inhibiting the LH-VTA pathway reduces "compulsive" sucrose-seeking, but not food consumption in hungry mice. We reveal that the LH sends excitatory and inhibitory input onto VTA dopamine (DA) and GABA neurons, and that the GABAergic projection drives feeding-related behavior. Our study overlays information about the type, function and connectivity of LH neurons and identifies a neural circuit that selectively controls compulsive sugar consumption, without preventing feeding necessary for survival, providing a potential target for therapeutic interventions to treat compulsive overeating an obesity.

2.2 Background

The lateral hypothalamus (LH) has long been linked to a wide variety of functions including reward, motivation, and feeding (Adamantidis et al., 2007; Anand and Brobeck, 1951b; Brobeck, 1946; Delgado and Anand, 1953; Gutierrez et al., 2011; Harris et al., 2005; Hoebel and Teitelbaum, 1962; Kempadoo et al., 2013; Margules and Olds, 1962; Sakurai, 2007). However, little is known about how the LH computes specific aspects of reward processing and how this information is relayed to each of its downstream targets.

Despite our incomplete understanding of the mechanisms of LH circuits, there is ample evidence indicating the complexity of LH circuits that give rise to behavior. Electrical stimulation of the LH has been shown to produce intracranial self-stimulation (ICSS) (Olds and Milner, 1954), as well as a variety of other behaviors including grooming, seizure, sexual, and gnawing behaviors (Singh et al., 1996). LH neurons have been reported to encode a variety of sensory modalities (Yamamoto et al., 1989), particularly taste (Li et al., 2013; Norgren, 1970; Schwartzbaum, 1988), in addition to reward-associated cues (Burton et al., 1976; Nakamura et al., 1987). LH neurons also fire during both feeding (Burton et al., 1976; Schwartzbaum, 1988) and drinking (Tabuchi et al., 2002) consummatory behaviors. Despite the rich literature describing LH neural responses, making sense of the remarkable functional heterogeneity observed in the LH has represented a major challenge in the field.

While the LH is interconnected with many subcortical regions, we have a poor understanding of how the functional and cellular heterogeneity of the LH is transposed upon these anatomical connections. One LH projection target of interest is the VTA, which is widely purported to be a critical component in reward processing (Phillips et al., 2003; Stuber et al.,

2008; Wise, 2004). The projection to the VTA was explored in early studies using electrophysiological recordings combined with antidromic stimulation (Bielajew and Shizgal, 1986; Gratton and Wise, 1988; Murray and Shizgal, 1996a, 1996b; Shizgal, 1989). It has since been confirmed, using a rabies-virus mediated tracing approach, that there is monosynaptic input from LH neurons onto dopamine neurons in the VTA (Watabe-Uchida et al., 2012). Additionally, the VTA also sends reciprocal projections back to the LH, both directly and indirectly via other regions such as the nucleus accumbens, amygdala, hippocampus and ventral pallidum (Barone et al., 1981; Beckstead et al., 1979; Fields et al., 2007; Rosenkranz and Grace, 2002; Simon et al., 1979; Swanson, 1982).

While both electrical (Bielajew and Shizgal, 1986; Murray and Shizgal, 1996a) and optical (Kempadoo et al., 2013) stimulation have established a causal role for the LH projection to the VTA in ICSS, several questions remain to be answered. First, what do VTA-projecting LH (LH-VTA) neurons do during reward-related behaviors? Second, what is the role of the LH-VTA projection in reward-seeking under different reinforcement contingencies? Third, what is the overall composition of fast transmission mediated by LH inputs to the VTA, and which VTA cells receive excitatory/inhibitory input? Finally, what do the excitatory and inhibitory components of the LH-VTA pathway each contribute towards orchestrating the pursuit of appetitive rewards?

To address these questions, we first combined in vivo electrophysiological recordings of LH neurons with a dual-virus strategy to allow for photoidentification of neurons that originate in the LH and provide monosynaptic input to VTA neurons. Further combinatorial optogenetic manipulations during in vivo electrophysiology allowed us to identify two populations of LH

neurons, those projecting to the VTA and those downstream of the VTA. Second, we recorded from LH neurons in freely-moving mice during a task where an operant response initiates a trial where cue presentation predicts subsequent sucrose delivery at an adjacent port and used optogenetic-mediated photoidentification to overlay information about the naturally-occurring neural computations during reward processing upon information about the connectivity of LH neurons. We found that VTA-projecting LH neurons predominantly encoded the act of reward retrieval following many conditioning sessions, while LH neurons receiving feedback from the VTA encoded both the conditioned stimulus and reward retrieval. To determine whether encoding of reward retrieval was due to conditioned responding or sucrose consumption itself, we omitted a portion of the expected rewards and observed that LH-VTA neurons were insensitive to unexpected reward omission, while LH neurons downstream of the VTA displayed significant changes in activity.

Based on our observation that LH-VTA neurons encoded conditioned responding independent of unexpected reward omission, and because phasic activity in these cells begins to ramp up before the mouse reaches the sucrose delivery port, we wondered if LH-VTA neurons might play a causal role in driving conditioned responding, perhaps by increasing motivation to seek sucrose. Two paradigms that have historically been used to characterize compulsive drug-seeking with relevance to rodent models of addiction include reward-seeking that persists 1) in periods of reward unavailability or 2) in the face of negative consequences (Belin et al., 2008; Deroche-Gamonet et al., 2004; Pelloux et al., 2007; Vanderschuren and Everitt, 2004). To test the hypothesis that LH-VTA neurons play a causal role in mediating conditioned responding, we manipulated the LH-VTA pathway to examine the effect on sucrose-seeking 1) in the face of a negative consequence (foot shock) and 2) during a period of reward unavailability (within-

session extinction). We tested whether optogenetic manipulations of the LH-VTA projection could alter sucrose-seeking in the presence of a negative consequence such as a foot shock. Indeed, we observed that photoactivation of the LH-VTA projection promoted sucrose-seeking in the face of a negative consequence, via increased feeding behavior, without altering pain sensitivity. We also found that photoinhibition of the LH-VTA pathway reduced sucrose-seeking in the presence of foot shock, but did not alter feeding behavior or pain sensitivity. Next, we investigated the composition of LH inputs to the VTA using *ex vivo* patch-clamp recordings in post-hoc identified DA and GABA neurons in the VTA. We observed a mixture of GABAergic and glutamatergic inputs onto both DA and GABA neurons within the VTA.

This previously undescribed heterogeneity prompted us to characterize the causal roles of the excitatory and inhibitory components of the LH-VTA pathway in isolation during a variety of behavioral tasks. Although previous studies probing the LH-VTA pathway in ICSS suggested that glutamatergic signaling via NMDARs promoted reward (Kempadoo et al., 2013), we found that the GABAergic, rather than the glutamatergic, component of the LH-VTA pathway was important in driving feeding behavior. However, photoactivation of the GABAergic input from LH to the VTA alone (LH^{GABA}-VTA) also produced aberrant feeding-related motor outputs that were not directed at appetitive stimuli. Specifically, we observed licking and biting of other objects, or in the case of being placed in an empty chamber, gnawing of the floor or empty space. Taken together, these data suggest that the LH^{glut}-VTA pathway regulates appetitive behaviors and that coordinated activation of the excitatory and inhibitory components of the LH-VTA pathway is critical for directing motivated behaviors to appropriate stimuli.

2.3 Results

2.3.1 Photoidentification of Distinct Components in the LH-VTA Circuit

In order to facilitate the identification of LH neurons that provide monosynaptic input to the VTA *in vivo* and observe their activity during freely-moving behaviors, we used a dual-virus strategy to selectively express channelrhodopsin-2 (ChR2) in LH neurons providing monosynaptic input to the VTA (Figure 1A and Figure S1; Senn et al., 2014; Tye and Deisseroth, 2012; Zhang et al., 2013). We injected an adeno-associated viral vector (AAV_5) carrying a ChR2-eYFP fusion protein under the control of a double inverted open-reading frame (DIO) into the LH to infect local somata and injected a retrogradely-travelling herpes simplex virus (HSV) carrying Cre-recombinase into the VTA. Subsequent recombination permitted opsin and fluorophore expression selectively in LH neurons providing monosynaptic input to the VTA. To confirm our approach, we performed ex vivo whole-cell patch-clamp recordings in horizontal brain slices containing the LH and recorded from neurons expressing ChR2-eYFP, as well as neighboring LH neurons that were ChR2-eYFP negative (Figure 1B). We found that all recorded ChR2-eYFP-expressing LH neurons (n=10) showed light-evoked excitation, and (n=8 of 10) reliably spiked upon 473 nm light illumination. Light-evoked spike latencies, measured from light pulse onset to the peak of the action potential, ranged from 3-8 ms (Figure 1C). We also found that none of the recorded non-expressing (ChR2-eYFP-negative) cells showed excitatory responses to photostimulation (n=14, Figure 1C), despite their proximity to ChR2-expressing cells.

In order to perform optogenetically-mediated photoidentification *in vivo*, an optrode was implanted into the LH to extracellularly record neuronal activity during a sucrose-seeking task.

Immediately following the continuous recording session, we provided several patterns of photostimulation to identify ChR2-expressing LH-VTA neurons (Figure 1D and Figure S1; Cohen et al., 2012; Zhang et al., 2013). We predicted that ChR2-expressing LH-VTA neurons would show time-locked responses to photostimulation with very short latencies (8 ms or less; Zhang et al., 2013). Indeed, we observed a population of neurons during *in vivo* recordings with latencies in a range identical to the ChR2-expressing LH-VTA neurons we recorded from *ex vivo*, 3-8 ms (Figure 1C and 1E). We also observed a population of cells that showed photoresponses with much longer latencies, ~100 ms. In order to calculate the time interval between light onset and neuronal firing ("photoresponse latency"), we determined the first time point (1 or 10 ms bins) at which the firing rate rose above 4 standard deviations from baseline (Figure 1D) followed by a standard non-parametric test (see Methods for details) to test for a significant change in firing rates.

We examined the distribution of photoresponse latencies across all LH neurons displaying a time-locked change in firing rate in response to illumination and observed a bimodal distribution (Figure 1E). We observed neurons with short latencies, consistent with ChR2 expression (Figure 1E and 1F), which we termed "Type 1" units and a distinct population of cells with ~100 ms photoresponse latencies (Figure 1E and 1G) which we termed "Type 2" units. We also observed a third population of neurons that were actually inhibited in response to photostimulation of ChR2-expressing LH-VTA neurons (Figure S2), which we termed "Type 3" units. We compared the action potential duration (as measured from peak to trough) and mean firing rates of Type 1 and Type 2 neurons as well as LH neurons that did not show a photoresponse (Figure 1H). The distribution of action potential durations of Type 1 (Figure 1I)

and Type 2 (Figure 1J) neurons shows that the majority of Type 1 units have an action potential duration less than 500 μs (16/19, binomial distribution, $p = 0.002$).

While Type 1 units fit standard criterion to be classified as ChR2-expressing (Cohen et al., 2012; Zhang et al., 2013), it was unclear whether the longer latency photoresponse of Type 2 units was indicative of ChR2-expressing neurons that responded more slowly to photostimulation, or whether this effect was due to network activity. Given that the ChR2-expressing (Type 1) LH neurons project directly to the VTA, one possibility was that Type 2 neurons were receiving feedback from the VTA (Figure 1K). Another possibility was that Type 2 neurons were activated by axon collaterals from Type 1 neurons (Figure 1L). Both of these models include the possibility that the activation of Type 2 neurons could be polysynaptic. To differentiate between these two possible circuit models, we performed manipulations of the VTA in conjunction with photoidentification in the LH.

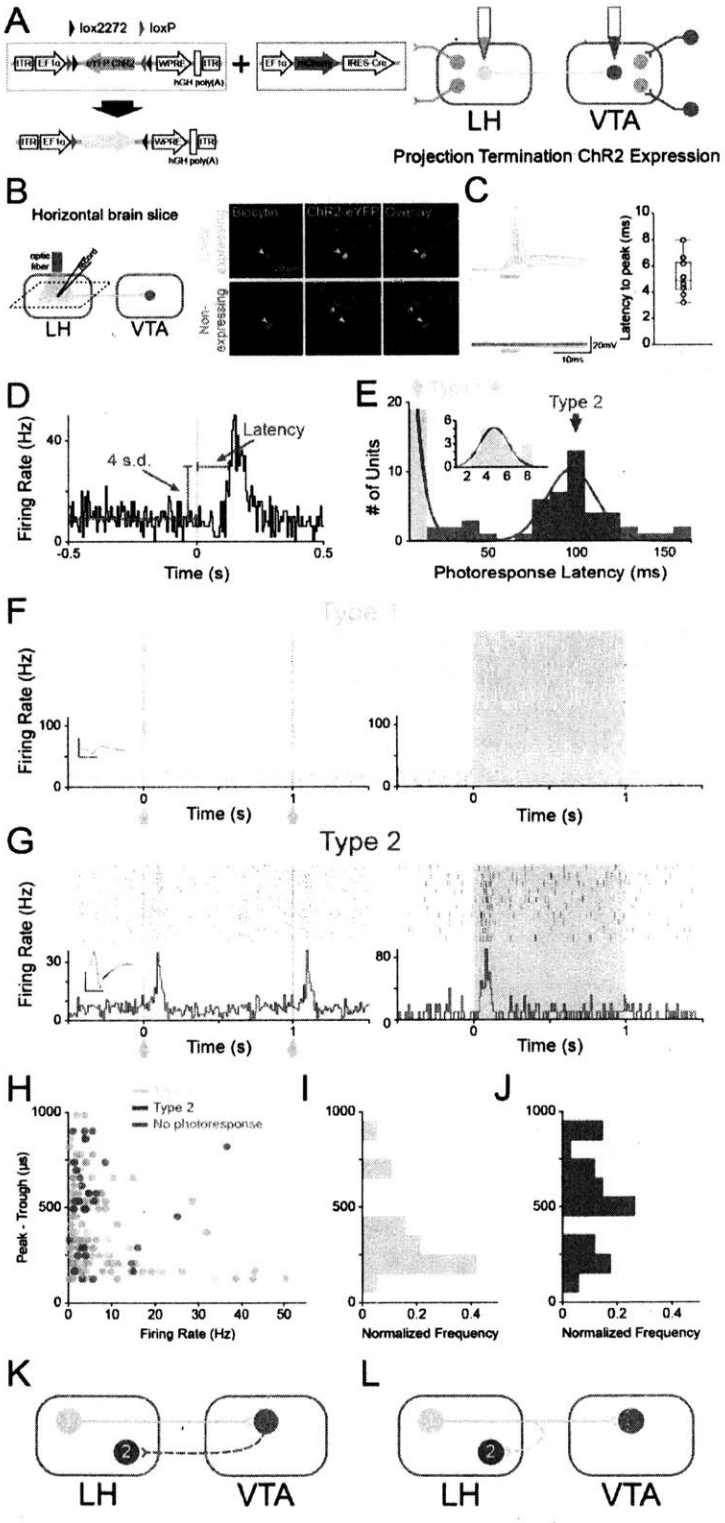
A
lox2272
loxP
LH
VTA
Projection Termination ChR2 Expression
B
Horizontal brain slice
LH
VTA
C
Latency to peak (ms)
D
Firing Rate (Hz)
4 s.d.
Latency
Time (s)
E
# of Units
Type 2
Photoresponse Latency (ms)
F
Type 1
Firing Rate (Hz)
Time (s)
G
Type 2
Firing Rate (Hz)
Time (s)
H
Type 2
No photoresponse
Peak - Trough (μs)
Firing Rate (Hz)
I
Normalized Frequency
J
Normalized Frequency
K
LH
VTA
L
LH
VTA

Figure 1. Phototagging LH-VTA Projections Reveals Two Populations of Neurons with Different Response Latencies to Photostimulation

(A) Wild-type mice (n = 12) were injected with AAV_5-DIO-ChR2-eYFP into the lateral hypothalamus (LH) and HSV-EF1α-IRES-Cre-mCherry into the ventral tegmental area (VTA).

(B) Horizontal brain slices containing the LH were prepared for whole-cell patch-clamp recordings in ChR2-expressing and non-expressing LH neurons.

(C) Individual traces recorded in current-clamp mode showing the response of ChR2-expressing (green, n = 10) and non-expressing (gray, n = 14) cells to a 5 ms pulse of 473 nm light are shown. The box and whisker plot shows the average response latency for each ChR2-expressing cell ex vivo.

(D) Photoresponse latencies in vivo were calculated by measuring the time from stimulation to 4 SD above the baseline firing rate.

(E) A bimodal distribution of excitatory photoresponse latencies was identified in recorded units (n = 198) and divided into Type 1 (green; n = 19) and Type 2 units (blue; n = 34).

(F) Type 1 units responded to photostimulation with fast excitation (3–8 ms latency). Inset shows the overlaid average traces for spontaneous spiking (black) and light-evoked spiking (blue) from a representative unit.

(G) Type 2 units responded to photostimulation with slower excitation (80-120 ms latency). Inset shows the overlaid average traces for spontaneous spiking (black) and light-evoked spiking (blue) from a representative unit.

(H) Scatterplot depicting the peak-trough duration of the waveform plotted against the average firing rate for each unit.

(I and J) Normalized histogram showing the distribution of peak-trough durations for (I) Type 1 units and (J) Type 2 units.

(K and L) Diagrams illustrating two possible circuit models. (K) Type 1 units project directly from the LH to the VTA, whereas Type 2 units represent a population in the LH that is receiving feedback from the VTA, or (L) Type 2 units represent a population in the LH that is receiving input from collaterals of Type 1 units. Dotted lines indicate uncertainty regarding whether the proposed connection is monosynaptic or polysynaptic.

Scale bar: y-axis, 0.2 mV; x-axis, 500 μs. See also Figure S1.

2.3.2 Long Latency Photoresponses in LH Neurons are Mediated by Feedback from the VTA

Based on our circuit models, we would expect distal inhibition to have no effect on the photoresponse of ChR2-expressing LH neurons. However, if photoresponsive, but non-expressing, LH neurons relied on feedback from the VTA to elicit a time-locked response to illumination, we would expect an attenuation of photoresponses in these neurons upon inhibition of the VTA. To initially probe this hypothesis, we delivered blue light stimulation to the LH before and after intra-VTA infusion of TTX (Figure S3A). We found that while the photoresponse of LH Type 1 units remained intact (Figure S3B), the photoresponses of Type 2 (n=4 of 4 cells) units were abolished (Figure S3C). This suggested that the photoresponses we observed in Type 2 neurons were mediated by a distributed network which includes the VTA.

However, because TTX infusion in the VTA would inhibit both cell bodies as well as axons of passage, we conducted additional experiments using halorhodopsin (NpHR)-mediated photoinhibition. We again expressed ChR2 in LH-VTA cells as above, but this time also expressed NpHR in the VTA and implanted optical fibers over both the LH and the VTA (Figure 2A). In these mice, we again recorded naturally-occurring activity during a sucrose-seeking task and immediately followed this with the delivery of blue light to facilitate photoidentification. During this recording session we delivered the same blue light illumination patterns in the LH for all three epochs, but also illuminated the VTA with amber light (593 nm) to inhibit VTA neurons in the second epoch (Figure 2A).

The photoresponse of Type 1 neurons to blue light illumination in the LH was unaffected by photoinhibition of the VTA, (0%; n=0 of 6) (Figure 2B), which is consistent with ChR2

expression in Type 1 LH-VTA neurons. In contrast, the majority of Type 2 neurons (87%; n=13 of 15, p=0.004, binomial distribution) showed a significant attenuation of their photoresponse to blue light pulses delivered in the LH upon photoinhibition of VTA neurons (Figure 2C). The responses of Type 1 and Type 2 units during VTA photoinhibition were significantly different (chi-square = 7.64, p = 0.0057; Figures 2B and 2C). These differences can also be seen in the max Z-scores during individual epochs (Figure 2D) and with the yellow-ON epoch normalized to the yellow-OFF epoch (Figure 2E). These data suggest that Type 2 LH neurons receive input (either directly or indirectly) from the VTA (Figure 1K) rather than via local axon collaterals (Figure 1L).

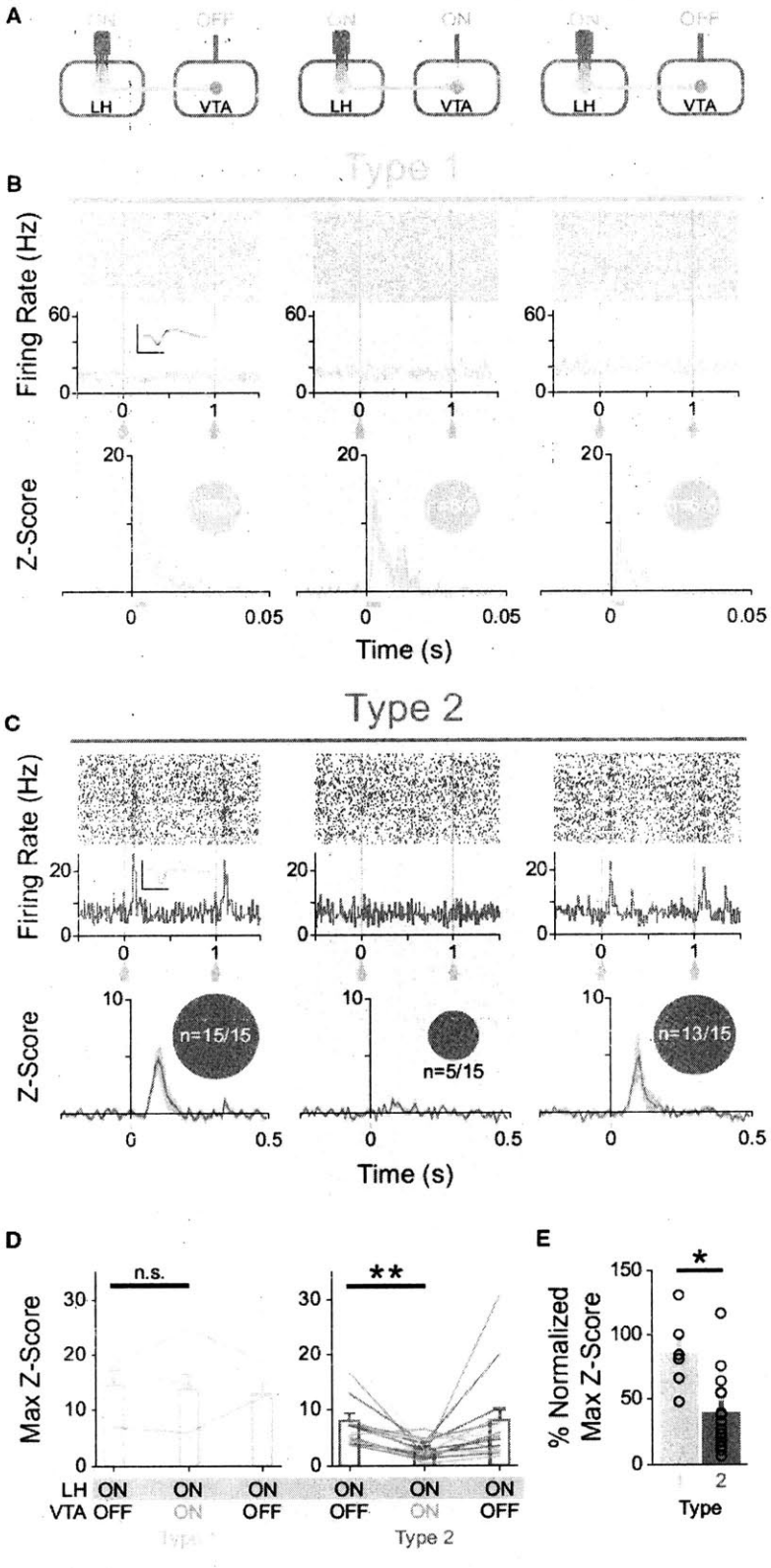
A
LH
VTA
B
Type 1
Firing Rate (Hz)
Z-Score
Time (s)
C
Type 2
n=15/15
n=5/15
n=13/15
D
n.s.
**
Max Z-Score
LH ON ON ON ON ON ON
VTA OFF ON OFF OFF ON OFF
Type 2
E
*
% Normalized Max Z-Score
Type

Figure 2. Inhibition of the VTA Attenuates the Photoresponse of Type 2 Units but Does Not Change the Photoresponse of Type 1 Units

(A) Mice expressing ChR2 in LH-VTA projections received an additional injection of AAV_5-CaMKIIα-eNpHR3.0-eYFP into the VTA to allow for transient inhibition of VTA neurons by yellow light. Three epochs of phototagging were conducted (LH photoactivation: ON-ON-ON, VTA photoinhibition: OFF-ON-OFF).

(B) Type 1 (n = 6/121 units, n = 6 animals) photoresponse properties were unaffected (0%; n = 0/6 attenuated or abolished) by VTA inhibition. Inset circles represent the number of units photoresponsive during each epoch. Inset shows the overlaid average traces for spontaneous spiking (black) and light-evoked spiking (blue) from a representative unit.

(C) Type 2 (n = 15/121 units, n = 6 animals) photoresponse properties were abolished (67%; n = 10/15) or attenuated (87%; n = 13/15) during NpHR-mediated VTA inhibition.

(D) No significant difference in max Z-score was detected between epochs with and without inhibition of the VTA for Type 1 units (two-tailed, paired Student's t-test, $p = 0.71$). The max Z-score was significantly lower in the ON (LH blue light illumination + VTA photoinhibition) epoch relative to the first OFF epoch (LH blue light illumination only) for Type 2 units (two-tailed, paired Student's t-test, $^{**}p = 0.0015$).

(E) There was a significant difference in max Z-score (normalized to the OFF epoch) during photoinhibition of the VTA between Type 1 units compared to Type 2 units (two-tailed, unpaired Student's t-test, $^{*}p = 0.014$).

Error bars indicate ±SEM. Scale bar: y-axis, 0.2 mV; x-axis, 500 μs. See also Figure S3.

2.3.3 Distinct Encoding Properties of LH Neurons Either Upstream or Downstream of the VTA

Having identified these two distinct types of LH neurons representing separate populations in the LH-VTA circuit, we wanted to examine naturally-occurring neural activity during a sucrose self-administration task (Figure 3A). In this task, mice were trained to perform nosepoke responses for a cue predicting sucrose delivery at an adjacent port (as in Tye et al., 2008). To allow us to differentiate neural responses to the nosepoke and the cue, the cue and sucrose were delivered on a partial reinforcement schedule, wherein 50% of nosepokes were paired with a cue and sucrose delivery. The recordings were performed during maintenance, after the animal had acquired the task (see Methods for acquisition criteria).

Type 1 neurons showed phasic responses to sucrose port entry, as seen by the response of a representative Type 1 neuron, shown in perievent raster histograms (Figure 3B), as well as the population data for all Type 1 neurons (Figure 3C). The phasic response of Type 2 neurons, however, mainly reflected responses to the reward-predictive cue (Figure 3D&E). The normalized firing pattern of all recorded neurons (n=198, divided into Type 1, 2, 3, and non-responsive neurons) are displayed for each task component: nosepokes paired with the cue, nosepokes in the absence of the cue, and sucrose port entry (Figure 3F).

All Type 1 neurons that showed task-relevant phasic changes in activity (n=12 of 19, 63%) encoded sucrose port entry (Figure 3B, C, and G). Both phasic excitations (64%) and inhibitions (36%) were observed in Type 1 neuron responses to port entry (Figure 3G). A small subset of Type 1 neurons also showed phasic inhibitions in response to the reward-predictive cue (n=2 of 19, 11%), but none of the Type 1 neurons selectively encoded the reward-predictive cue.

In contrast, Type 2 neurons were more heterogeneous (Figure 3D, E, and H), with task-responsive neurons encoding the cue selectively (n=12 of 34; 35%), the sucrose port entry selectively (n=9 of 34; 26%) or both the cue and port entry (n=4 of 34; 12%). To illustrate the relative distribution of responses of Type 1 and Type 2 neurons relative to the general LH population, in terms of the amplitude of phasic changes in firing in response to the major task components, we plotted each cell on a 3-dimensional plot according to Z-score (Figure 3I). To show the distribution of phasic changes in firing to multiple task-related events on a qualitative level, we also plot the number of cells within each photoresponse Type that fell into a given category (Figure 3J).

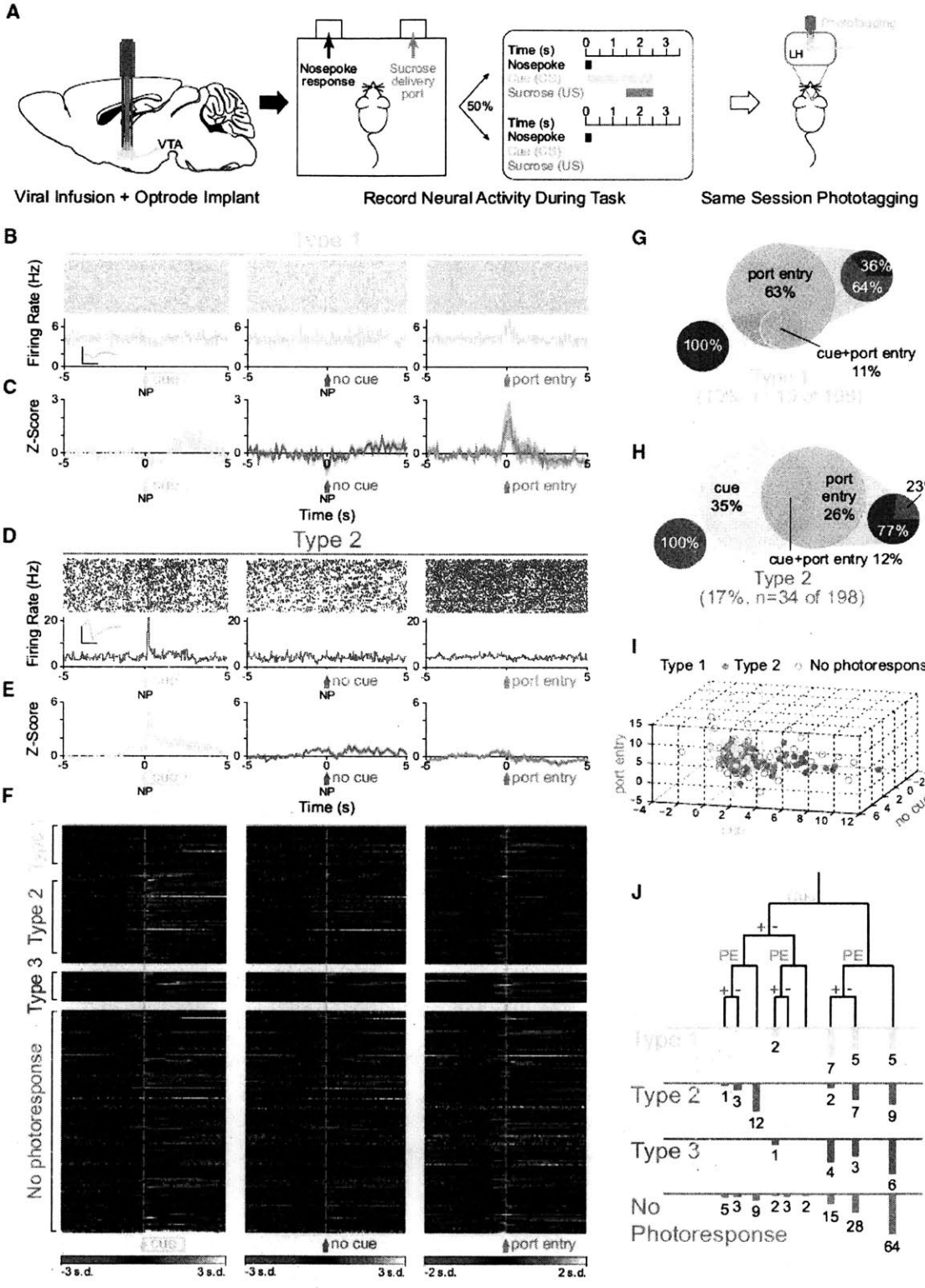
A
VTA
Nosepoke response
Sucrose delivery port
50%
Time (s)
Nosepoke
Sucrose (US)
LH
Viral Infusion + Optrode Implant
Record Neural Activity During Task
Same Session Phototagging
B
Type 1
Firing Rate (Hz)
C
Z-Score
NP
no cue
port entry
Time (s)
D
Type 2
E
F
Type 3
No photoresponse
-3 s.d.
3 s.d.
-2 s.d.
2 s.d.
G
port entry 63%
36%
64%
100%
cue+port entry 11%
H
cue 35%
port entry 26%
23%
77%
cue+port entry 12%
Type 2
(17%, n=34 of 198)
I
Type 1
Type 2
No photoresponse
port entry
no cue
J
PE
Type 2
Type 3
No Photoresponse

Figure 3. Type 1 Units Predominantly Respond to the Port Entry, While Type 2 Units Respond to Both the Conditioned Stimulus and the Port Entry

(A) Mice with optrodes implanted in the LH and expressing ChR2 in LH-VTA projections were trained on a task where 50% of nosepokes (NP) were followed by a cue (conditioned stimulus; CS) that predicts the delivery of sucrose (unconditioned stimulus; US) at the delivery port. In vivo electrophysiological recordings were performed during the behavioral task followed by phototagging in the same recording session to identify units by projection target.

(B) Perievent raster histograms for a representative Type 1 unit that responded to port entry, but not to the reward-predictive cue. Inset shows overlaid average traces for spontaneous spiking (black) and light-evoked spiking (blue) from a representative unit.

(C) Population Z-score plots showing the average responses of all Type 1 units (n = 19/198 units, n = 12 animals).

(D) Perievent raster histograms for a representative Type 2 unit that responded to the reward-predictive cue, but not to port entry.

(E) Population Z-score plots show the average responses of all Type 2 units (n = 34/198 units, n = 12 animals).

(F) Heatmap representation of the individual Z scores of all units.

(G) Of all Type 1 units, 63% responded exclusively to the port entry (n = 12/19), whereas 11% responded to both the port entry and the reward-predictive cue (n = 2/19). Within the Type 1 units that responded to the port entry, 64% (n = 9/14) were excited (red) upon port entry, whereas 36% (n = 5/14) were inhibited (blue), and within the units that responded to the reward-predictive cue, 100% (n = 2/2) were inhibited by the cue.

(H) Of all Type 2 units, 35% (n = 12/34) responded exclusively to the reward-predictive cue, 26% (n = 9/34) responded exclusively to the port entry, and 12% (n = 4/34) responded to both. Within the Type 2 units that responded to the cue, 100% (n = 16/16) were excited by the cue, whereas none were inhibited, and within the units that responded to port entry, 77% (n = 10/13) were inhibited upon port entry, whereas 23% (n = 3/13) were excited.

(I) Graphical representation of Z-scores during the experimental windows for cue, no cue, and port entry for Type 1, Type 2, and ''no photoresponse'' units.

(J) Diagram of recorded units demonstrating whether they responded to the cue or port entry (PE) and whether that response was with excitation (+) or inhibition (-).

Error bars indicate ±SEM. Scale bar: y-axis, 0.2 mV; x-axis, 500 μs. See also Figure S2.

2.3.4 Different Components of the LH-VTA Circuit Represent Distinct Aspects of Reward-Related Behavior

Given the well-defined role of the VTA in reward-prediction error, (e.g. the phasic reduction of dopamine neuron firing in response to the unexpected omission of an expected reward and the phasic excitation in response to unexpected reward delivery) (Cohen et al., 2012; Schultz et al., 1997), we investigated whether LH neurons would encode the unexpected omission of a sucrose reward. To do this, we recorded the neural activity of photoresponsive neurons during the same cue-reward task in well-trained animals, but in 30% of cue presentations (random intermingled trials) we omitted sucrose delivery (Figure 4A). We then compared the phasic responses of LH neurons to port entry when sucrose was present or unexpectedly omitted.

The majority of Type 1 units (88%; n = 15/17, binomial distribution, p = 0.001) were insensitive to reward omission (Figures 4B and 4D), whereas a large subset of Type 2 units (67%; n = 12/18) showed a significantly different response to reward-presented and reward-omitted trials (Figures 4C and 4D). We concluded that LH-VTA (Type 1) neurons encoded the action of entering the port, as these port-entry responses were persistent even upon reward omission (Figure 4D), in contrast to Type 2 units (chi-square = 10.9804, p = 0.0009).

To determine whether Type 1 responses to port entry were truly encoding conditioned responding, as opposed to general reward-seeking or exploratory behavior, we recorded in untrained mice that had not yet acquired the task. In these task-naïve mice, we delivered sucrose to the port in the absence of a predictive cue (unpredicted reward delivery) and found that Type 1 neurons did not show phasic responses to port entry (0%, 0 of 8 Type 1 cells; Figure 4E, 4F and

4I). This observation, combined with the persistent response of Type 1 neurons to port entry independent of sucrose presentation after overtraining (Figure 4B and 4D) are consistent with the model that Type 1 neurons encode the CR (Figure 4J).

Next, to determine whether Type 2 neuron activity is consistent with a reward-prediction error-like response profile we also recorded these neurons during unpredicted reward delivery (Figure 4G). We found that a subset of Type 2 neurons responded to unpredicted sucrose deliveries (Figure 4G-4I). Taken together, a subset of Type 2 neurons are sensitive to unexpected reward omission, as seen by decreases in phasic firing (Figure 4C and 4D), and a subset of Type 2 neurons show phasic excitation upon unpredicted reward delivery (Figure 4G-4I), consistent with a reward-prediction error-like response profile.

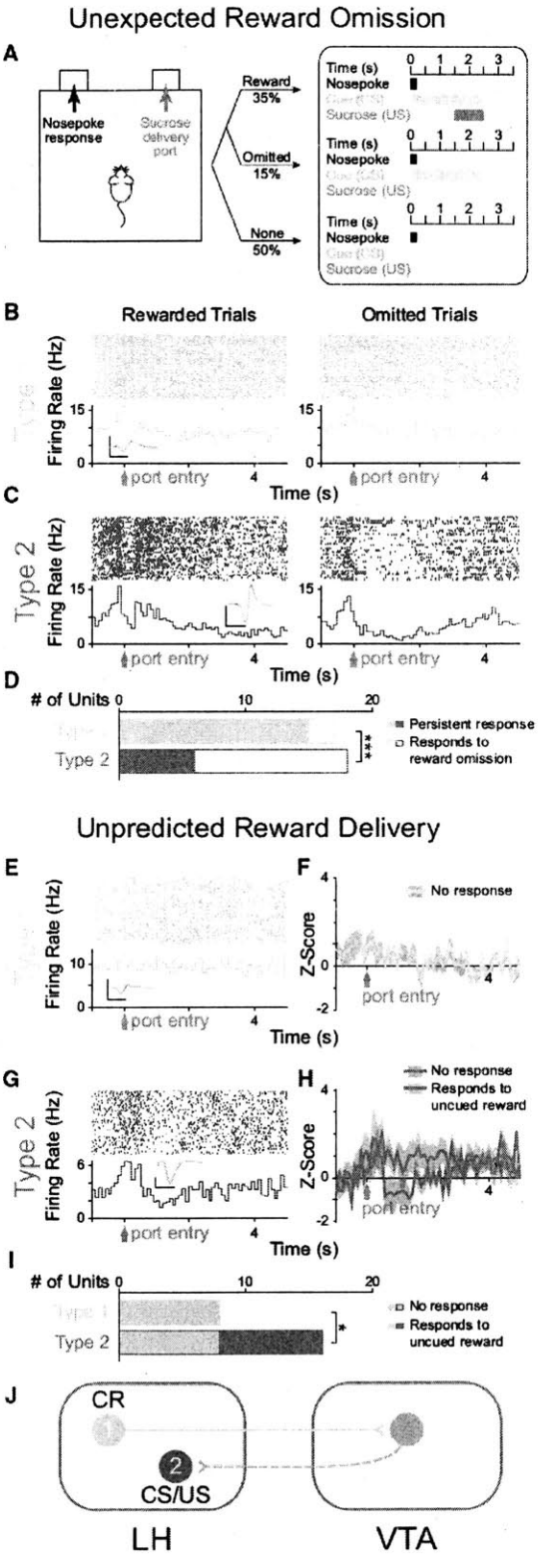
Unexpected Reward Omission
A
Nosepoke response
Sucrose delivery port
Reward 35%
Omitted 15%
None 50%
Time (s)
Nosepoke
Sucrose (US)
B
Rewarded Trials
Omitted Trials
Firing Rate (Hz)
port entry
Time (s)
C
Type 2
D
# of Units
Type 1
Type 2
Persistent response
Responds to reward omission
Unpredicted Reward Delivery
E
F
No response
Z-Score
G
H
Responds to uncued reward
I
No response
Responds to uncued reward
J
CR
CS/US
LH
VTA

Figure 4. LH-VTA Neurons Encode the Conditioned Response of Sucrose Seeking

(A) The original partial reinforcement sucrose self-administration task was modified so that in 30% of trials during which the reward-predictive cue was present, the expected sucrose delivery was omitted (15% of all trials).

(B) Perievent raster histograms of a Type 1 unit that showed no difference in response to port entry with reward omission. Inset shows overlaid average traces for spontaneous spiking (black) and light-evoked spiking (blue) from a representative unit.

(C) Perievent raster histograms of a Type 2 unit that showed a significantly different response to port entry upon omission of the expected reward.

(D) Of all Type 1 units recorded (n = 17/122 units, n = 6 animals), only 12% (n = 2/17) showed a significant difference in their responses when the expected reward was omitted. In contrast, of all Type 2 units recorded (n = 18/122 units, n = 6 animals), 67% (n = 12/18) showed a significant difference in their responses when the expected reward was omitted (chi-square = 10.9804, ***p = 0.0009).

(E) Unexpected sucrose delivery occurred in the absence of predictive cues. Perievent raster histogram of a Type 1 unit that did not respond to port entry following unpredicted reward delivery is shown.

(F) Population Z-score plot showing the average responses of all Type 1 units to the port entry following unpredicted reward delivery.

(G) Perievent raster histogram of a Type 2 unit that showed an increase in firing rate to port entry following unpredicted reward delivery.

(H) Population Z-score plot of Type 2 unit responses to port entry following unpredicted reward delivery, separated into those that showed a significant response and those that showed no significant response.

(I) Of all Type 1 units recorded (n = 8/105 units, n = 6 animals), 0% (n = 0/8) showed a significant response to the port entry following unpredicted reward delivery. In contrast, of all Type 2 units recorded (n = 16/105 units, n = 6 animals), 50% (n = 8/16) showed a significant response to the port entry following unpredicted reward delivery (chi-square = 6, *p = 0.0143).

(J) Schematic of the LH-VTA loop and the components of reward processing encoded by Type 1 and 2 cells. CR = conditioned response; CS = conditioned stimulus; US = unconditioned stimulus.

Error bars indicate ±SEM. Scale bar: y-axis, 0.2 mV; x-axis, 500 μs.

2.3.5 Photostimulation of the LH-VTA Projection Promotes Sucrose-Seeking in the Face of a Negative Consequence

As we have shown above, Type 1 units represent a neural correlate of CR. Importantly, the increase in firing rate begins prior to CR, ramping up until the CR has been completed (Figure 3B, 3C, and 4B). To determine whether activation of the LH-VTA pathway could promote CR, we wanted to test the ability of LH-VTA activation in driving CR in the face of a negative consequence. In wild-type mice, we expressed ChR2-eYFP or eYFP alone in LH cell bodies and implanted an optic fiber over the VTA (Figures 5A and S4). Conversely, to test the necessity of the LH-VTA pathway in mediating conditioned responding or feeding-related behaviors, we bilaterally expressed NpHR-eYFP or eYFP alone in LH cell bodies and implanted an optical fiber above the VTA (Figure 5A and Figure S4).

We designed a Pavlovian conditioning task in which food-deprived mice had to cross a shock grid to retrieve a sucrose reward (Figure 5B). In the first ('Baseline') epoch with the shock grid off, we verified that each mouse had acquired the Pavlovian conditioned approach task. In the second ('Shock') epoch, the shock grid delivered mild foot shocks every second. Finally, in the third epoch ('Shock+Light'), we continued to deliver regular foot shocks but also illuminated LH terminals in the VTA using 473 nm light (10 Hz) in mice expressing ChR2 and matched eYFP controls and 593 nm light (constant) for mice expressing NpHR and their eYFP controls (Figure 5B).

While ChR2 and eYFP groups performed similarly in the Baseline and Shock epochs, we observed a significantly higher number of port entries per cue during the Shock+Light epoch in ChR2 mice relative to eYFP mice (Figure 5C). Illumination of LH terminals in the VTA

produced a significantly higher difference score (Shock+Light epoch - Shock only epoch) in the ChR2 group relative to their eYFP controls (Figure 5C). In contrast, photoinhibition of the LH-VTA pathway resulted in a significant reduction in port entries per cue and difference scores in the NpHR group relative to their eYFP controls (Figure 5D). Within-session extinction experiments during which cue presentations were not followed by sucrose deliveries showed similar trends in effect (Figure S4).

Importantly, we wanted to determine whether the changes in sucrose seeking we had obtained were caused by changes in feeding-related behavior or sensitivity to pain. We observed that photoactivation of the LH-VTA projection significantly increased the time spent feeding in well-fed mice in the ChR2 group (Figure 5E). However, photoinhibition of the LH-VTA pathway did not significantly reduce feeding (Figure 5F), even though these animals were food deprived to enhance our ability to detect a reduction relative to the baseline epoch (compare to sated animals in Figure 5E). In neither the ChR2 (Figure 5G) nor NpHR group (Figure 5H) did we observe a difference in latency to tail withdrawal from hot water (Ben-Bassat et al., 1959; Grotto and Sulman, 1967), indicating that manipulating the LH-VTA projection was not altering analgesia.

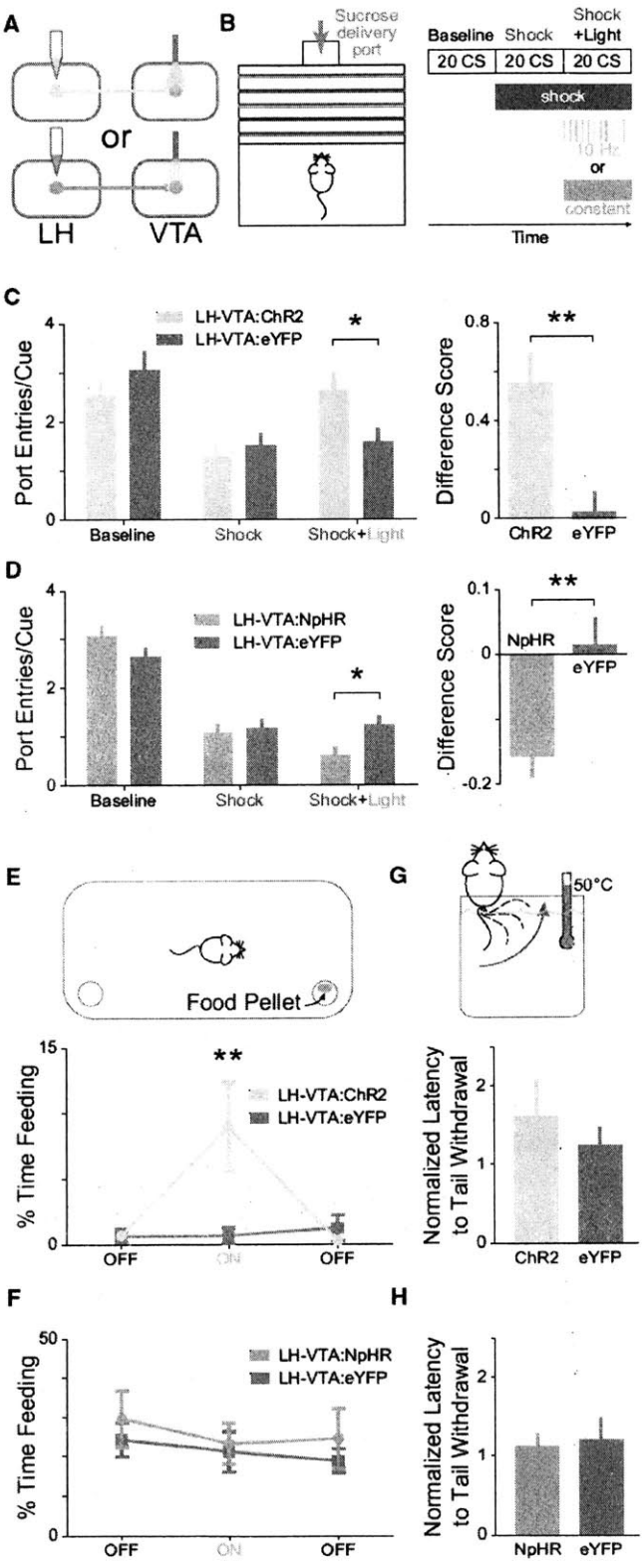
A
LH
or
VTA
B
Sucrose delivery port
Baseline
Shock
Shock +Light
20 CS
20 CS
20 CS
shock
10 Hz
or
constant
Time
C
LH-VTA:ChR2
LH-VTA:eYFP
Port Entries/Cue
Baseline
Shock
Shock+Light
Difference Score
ChR2
eYFP
D
LH-VTA:NpHR
LH-VTA:eYFP
Port Entries/Cue
Baseline
Shock
Shock+Light
Difference Score
NpHR
eYFP
E
Food Pellet
% Time Feeding
LH-VTA:ChR2
LH-VTA:eYFP
OFF
ON
OFF
G
50°C
Normalized Latency to Tail Withdrawal
ChR2
eYFP
F
% Time Feeding
LH-VTA:NpHR
LH-VTA:eYFP
OFF
ON
OFF
H
Normalized Latency to Tail Withdrawal
NpHR
eYFP

Figure 5. Excitation of LH-VTA Projections Promotes, whereas Inhibition Attenuates, Compulsive Sucrose-Seeking

(A) Mice received injections of AAV_5-CaMKIIα-ChR2-eYFP (n = 8), AAV_5-CaMKIIα-eNpHR3.0-eYFP (n = 14), or AAV_5-CaMKIIα-eYFP (n = 6 controls for ChR2, n = 8 controls for NpHR) into the LH, and an optic fiber was implanted above the VTA.

(B) Mice were trained on a Pavlovian conditioned approach task wherein a cue predicted sucrose delivery to a port located across a shock grid. On test day, mice were presented with 20 cues during a baseline period without shock, 20 cues when the shock grid was on, and 20 cues during which 10 Hz blue or constant yellow light was delivered while the shock floor remained on.

(C) Mice in the ChR2 group showed a significant increase in the number of port entries per cue during the ''Shock+Light'' epoch relative to eYFP controls (n = 8 ChR2, n = 6 eYFP; two-way ANOVA revealed a group x epoch interaction, $F_{2,24} = 20.47$, $p < 0.0001$; Bonferroni post-hoc analysis, $^{*}p < 0.05$). The difference between the number of port entries per cue during the ''Shock+Light'' epoch and ''Shock'' epoch was also significantly different between the ChR2 and eYFP control groups (two-tailed, unpaired Student's t-test, $^{**}p = 0.0090$).

(D) Mice in the NpHR group showed a significant decrease in the number of port entries per cue during the Shock+Light epoch relative to eYFP controls (n = 13 NpHR, n = 8 eYFP; two-way ANOVA revealed a group x epoch interaction, $F_{2,38} = 116.63$, $p < 0.0001$; Bonferroni post-hoc analysis, $^{*}p < 0.05$). The difference score was also significantly different between the NpHR-expressing and eYFP control mice (two-tailed, unpaired Student's t-test, $^{**}p = 0.0062$).

(E) Mice were placed into an open chamber with two cups, one containing food and the other without, and behavior in three experimental epochs was recorded (light OFF-ON-OFF). ChR2-expressing mice showed a significant increase in feeding (measured by time spent consuming food) compared with eYFP controls during the epoch paired with blue-light stimulation (n = 8 ChR2, n = 6 eYFP; two-way ANOVA revealed a group x epoch interaction, $F_{2,24} = 4.23$, $p = 0.0268$; Bonferroni post-hoc analysis, $^{**}p < 0.01$).

(F) NpHR-expressing mice showed no significant differences from eYFP control mice in time spent feeding in any of the epochs (n = 9 NpHR, n = 7 eYFP).

(G and H) To examine the effect of light stimulation on analgesia, mice had their tails placed into a heated water bath, and the latency-to-tail withdrawal was measured during two counterbalanced epochs (light ON-OFF). (G) ChR2-expressing mice showed no significant difference in tail-withdrawal latency (normalized to OFF epoch) during blue-light stimulation compared to eYFP controls (n = 8 ChR2, n = 6 eYFP), (H) nor did NpHR-expressing mice during yellow-light stimulation (n = 5 NpHR, n = 8 eYFP).

Error bars indicate ±SEM. See also Figure S4.

2.3.6 The LH Provides Both Glutamatergic and GABAergic Input onto VTA DA and GABA Neurons

To study the fast transmission components of LH inputs to the VTA, we performed whole-cell patch-clamp recordings from VTA neurons in an acute slice preparation while optically activating LH inputs expressing ChR2–eYFP (Figure 6A and Figure S5). Given that there is well-established heterogeneity within the VTA, including ~65% dopamine neurons, ~30% GABA neurons, and ~5% glutamate neurons (Dobi et al., 2010; Kawano et al., 2006; Lammel et al., 2008; Margolis et al., 2006; Nair-Roberts et al., 2008; Yamaguchi et al., 2007), we filled cells with biocytin while recording to allow for identification of cell type using post-hoc immunohistochemistry for tyrosine hydroxylase (TH; Figure 6B), in addition to recording the hyperpolarization-activated cation current (I_h) and mapping cell location (Figure 6B and S5).

First, to evaluate the net effect of LH input on VTA dopamine (DA) neurons, we recorded in current-clamp during photostimulation of ChR2-expressing LH inputs and observed that 23 of 27 neurons showed a time-locked response to photostimulation of LH inputs (Figure 6C). The majority of DA neurons sampled in the VTA received a net excitatory input from the LH, observed in 15 of 23 cells (65%), while another subset showed net inhibition (8 of 23; 34%; Figure 6C). The spatial distribution of these DA neurons is mapped onto an atlas for horizontal slices containing the VTA (Figure 6D).

Importantly the net effect of LH inputs did not preclude the contribution of polysynaptic mechanisms. For example, VTA DA neurons may receive inhibition from local GABA neurons, so the net effect measured may be partially mediated by feed-forward inhibition via GABAergic interneurons. Therefore, to establish the monosynaptic contribution of LH inputs to VTA DA

neurons, we used ChR2-assisted circuit mapping where voltage-clamp recordings were performed in the presence of tetrodotoxin (TTX), which eliminates polysynaptic network activity, and 4-aminopyridine (4AP), which enhances detection of monosynaptic transmission by blocking potassium-channel-mediated repolarization (Petreanu et al., 2007). AMPAR-mediated excitatory postsynaptic currents (EPSCs) and $GABA_A$-R mediated inhibitory postsynaptic currents (IPSCs), were isolated by holding the cell at -70 mV and 0 mV, respectively (Figure 6E, see Methods). Consistent with our observations from current-clamp recordings, we observed that a greater proportion of VTA DA neurons exclusively received excitatory monosynaptic input from the LH (67%, n=6 of 9; Chi-square = 5.8442, p = 0.015; Figure 6E), compared to VTA DA neurons that exclusively received inhibitory monosynaptic input from the LH (n=1 of 9). We also observed a small subset of cells that received both excitatory and inhibitory LH input (n=2 of 9; Figure 6E). Similar results were obtained when ChR2 was expressed in the LH under the control of the CaMKIIα promotor or the EF1α promoter to facilitate projection-specific Cre-mediated recombination (Figure S6).

We identified VTA GABA neurons by injecting a Cre-dependent fluorophore (AAV_5-DIO-mCherry) into the VTA of VGAT::Cre mice and utilizing mCherry expression to direct the recording of VTA GABA neurons (Figure 6F). In contrast to VTA DA neurons, all of the GABA neurons sampled showed a response to LH input activation (n=24 of 24 neurons).

A subset of VTA GABA neurons (n=11 of 24 cells, 46%) responded to photostimulation of ChR2-expressing LH axon terminals with net excitation, while the rest of the VTA GABA neurons sampled responded with net inhibition (n=13 of 24, 54%; Figure 6G). The spatial distribution of these cells is shown in Figure 6H. Upon examination of the monosynaptic input

from the LH (as described above), we found that 2 of 11 sampled GABA neurons showed exclusive excitation, and 1 of 11 showed exclusive inhibition (Figure 6I). However, relative to VTA DA neurons, we found that more VTA GABA neurons received both excitatory AMPAR-mediated and inhibitory $GABA_AR$-mediated monosynaptic input from the LH (n=8 of 11, 73%; Chi-square = 5.0505, p = 0.0246; Figure 6I). Additionally, we found that putative GABA neurons (TH-immunonegative) in wild-type mice showed a similar pattern of responses (Figure S6), suggesting that the input composition is comparable in VGAT::Cre mice. Given the mixed composition of the LH-VTA pathway, we next investigated the individual roles of the glutamatergic and GABAergic components of the LH-VTA projection when independently activated during behavior.

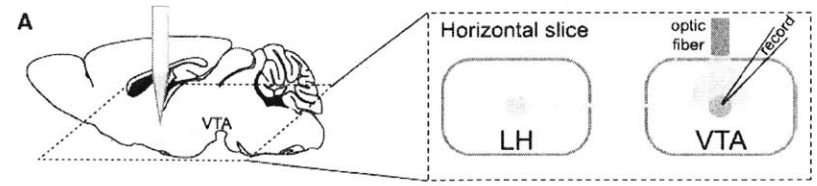

Dopamine neurons

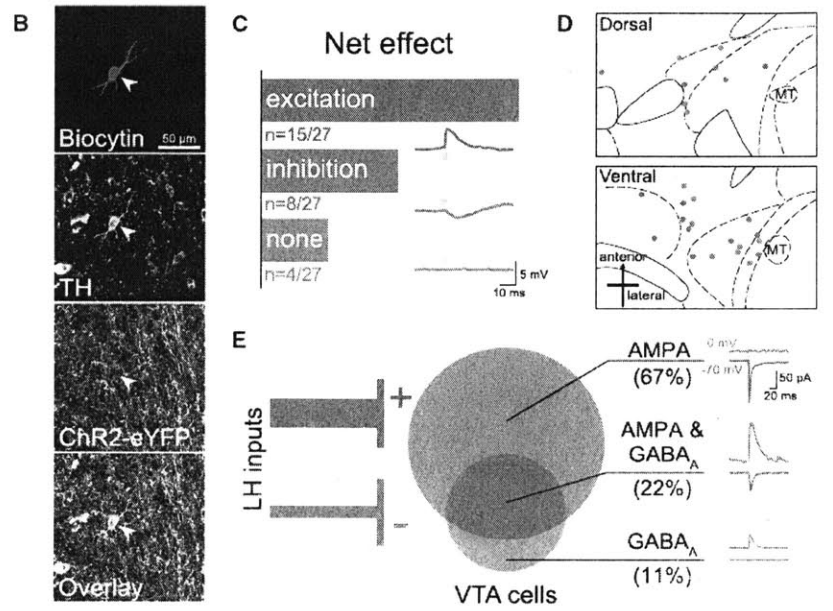

GABA neurons

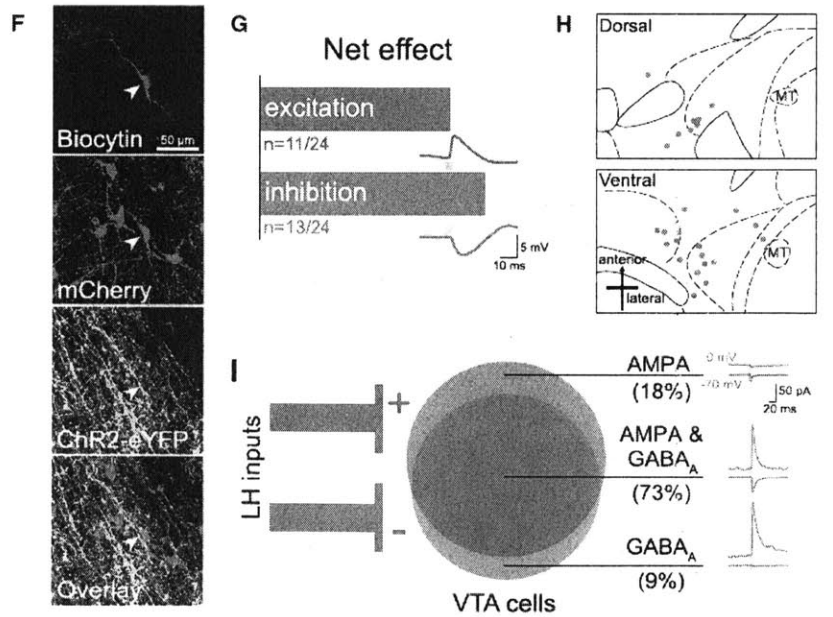

Figure 6. The Lateral Hypothalamus Sends a Mixture of Excitatory and Inhibitory Projections to Both Dopamine and GABA Neurons in the VTA

(A) AAV_5-CaMKIIα-ChR2-eYFP was injected into the LH, and at least 6 weeks later, 300 μm-thick horizontal brain slices were prepared containing the VTA. Whole-cell patch-clamp recordings were made in VTA neurons, and ChR2-expressing LH terminals were activated by illumination with 473 nm light via an optic fiber resting on the brain slice.

(B) Neurons were filled with biocytin during recording, and DA neurons were identified by immunohistochemistry for TH (n = 27).

(C) The net effect of optical stimulation of LH terminals was assessed in current-clamp mode, which revealed that 55% of DA neurons (n = 15/27) showed a net excitatory response, whereas 30% (n = 8/27) responded with net inhibition, and 15% (n = 4/27) showed no response. An example of an excitatory postsynaptic potential (EPSP, red trace), an inhibitory postsynaptic potential (IPSP, blue trace), and a non-responsive cell (gray trace) are shown below each bar.

(D) The distribution of all recorded TH+ neurons plotted on horizontal midbrain slices with colors indicating the response to LH terminal photostimulation.

(E) VTA DA neurons received only AMPAR-mediated input (67%, n = 6/9), only $GABA_A$R-mediated input (11%, n = 1/9), or both of these currents (22%, n = 2/9).

(F) VTA GABA neurons were identified by the presence of mCherry (n = 24), achieved by injection of Cre-dependent AAV_5-EF1α-DIO-mCherry into the VTA of VGAT::Cre mice.

(G) Optical stimulation of LH terminals in current-clamp mode showed that GABA neurons respond with either net excitation (46%, n = 11/24) or net inhibition (54%, n = 13/24) to LH input.

(H) The distribution of each recorded GABA neuron plotted on horizontal midbrain slices with colors indicating the response to LH terminal stimulation.

(I) GABA neurons received a mixture of AMPAR-mediated and $GABA_A$R-mediated input from the LH (AMPA only: 18%, n = 2/11; AMPA & $GABA_A$: 73%, n = 8/11; $GABA_A$: 9%, n = 1/11).

MT = medial terminal nucleus of the accessory optic tract. See also Figures S5 and S6.

2.3.7 Distinct Roles of Glutamatergic and GABAergic Components of the LH-VTA Pathway in Behavior

Given that our ex vivo recordings provided evidence supporting robust input from both GABAergic and glutamatergic LH projections to the VTA, we next probed the role of each component independently. To do this, we used transgenic mouse lines expressing Cre-recombinase in neurons that expressed either vesicular glutamate transporter 2 (VGLUT2) or vesicular GABA transporter (VGAT). We injected AAV_5-DIO-ChR2-eYFP or AAV_5-DIO-eYFP into the LH of VGLUT2::Cre and VGAT::Cre mice and implanted an optic fiber over the VTA (Figure S7). These animals were then run on each of the behavioral assays shown in Figure 5.

We did not observe any detectable differences in the number of port entries made per cue between mice expressing ChR2 or eYFP in the LH^{glut}-VTA projection (Figure 7A) or in the LH^{GABA}-VTA projection (Figure 7B). However upon video analysis, we noticed aberrant gnawing behaviors in the LH^{GABA}-VTA:ChR2 group upon blue-light illumination. In LH^{glut}-VTA mice, although there was a trend toward a reduction in feeding upon photostimulation in the ChR2 group compared to the eYFP group, this was not statistically significant (Figure 7C). In contrast, we observed a robust increase in the time spent feeding in sated mice upon illumination in the LH^{GABA}-VTA:ChR2 group relative to controls (Figure 7D). In neither group of animals was there an effect of light stimulation in the tail-withdrawal assay (Figures 7E and 7F).

During the feeding task, as we did during the sucrose-seeking task, we again noticed aberrant feeding-related motor sequences that were not directed at food. We filmed a representative mouse in the LH^{GABA}-VTA:ChR2 group in an empty transparent chamber, and

upon 20 Hz photostimulation, we observed unusual appetitive motor sequences such as licking and gnawing the floor or empty space. We quantified these "gnawing" behaviors during the feeding task in the wildtype LH-VTA (Figure 7G), LH^{glut}-VTA (Figure 7H), and LH^{GABA}-VTA (Figure 7I) groups and showed that LH^{GABA}-VTA:ChR2 mice gnawed more than wild-type or LH^{glut}-VTA:ChR2 mice when photostimulated, as compared to their respective eYFP groups (Figure 7J). We considered whether the aberrant feeding-related behaviors might be separated from appropriately directed feeding at lower frequencies. However, when we tested the LH^{GABA}-VTA:ChR2 group with 5 Hz and 10 Hz trains of blue light, we observed a proportional relationship between stimulation frequency and both feeding and gnawing (Figure 7K).

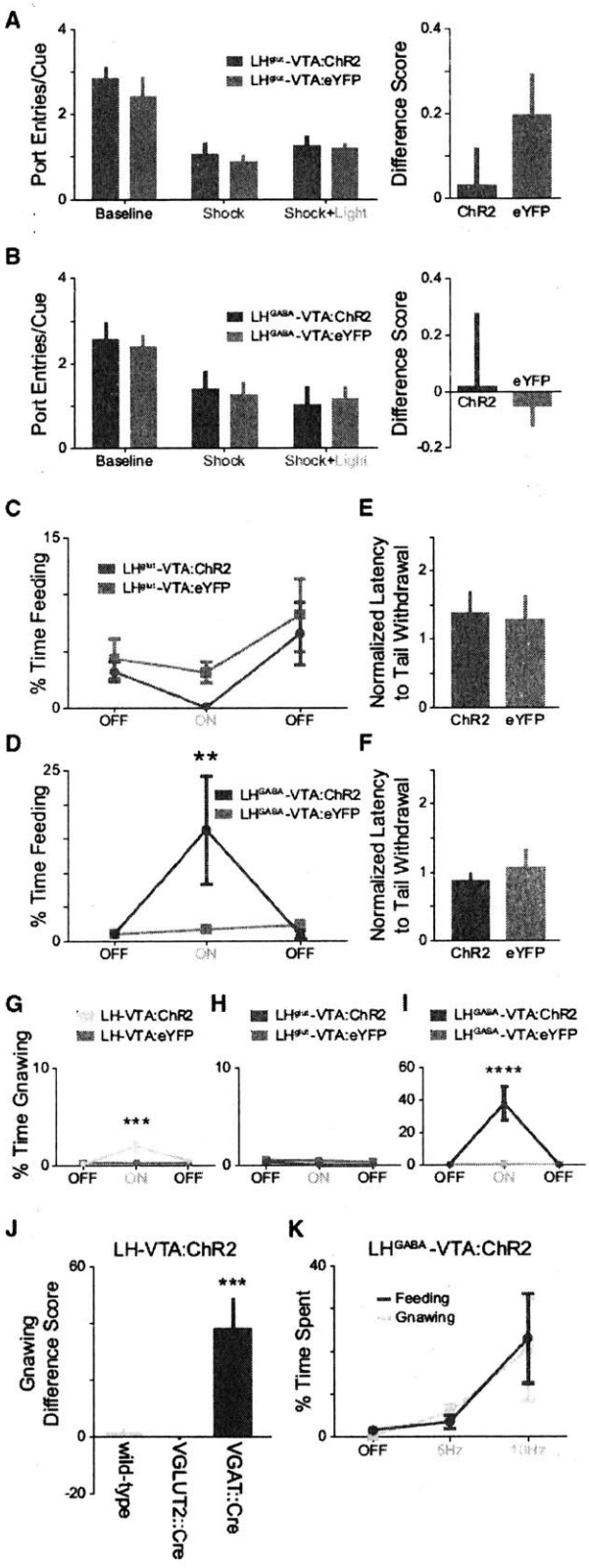
A
Port Entries/Cue
LHgat-VTA:ChR2
LHgat-VTA:eYFP
Baseline
Shock
Shock+Light
Difference Score
ChR2
eYFP
B
Port Entries/Cue
LHGABA-VTA:ChR2
LHGABA-VTA:eYFP
Baseline
Shock
Shock+Light
Difference Score
ChR2
eYFP
C
% Time Feeding
LHvglut-VTA:ChR2
LHvglut-VTA:eYFP
OFF
ON
OFF
D
**
% Time Feeding
LHGABA-VTA:ChR2
LHGABA-VTA:eYFP
OFF
ON
OFF
E
Normalized Latency to Tail Withdrawal
ChR2
eYFP
F
Normalized Latency to Tail Withdrawal
ChR2
eYFP
G
LH-VTA:ChR2
LH-VTA:eYFP
% Time Gnawing
***
OFF
ON
OFF
H
LHgat-VTA:ChR2
LHgat-VTA:eYFP
OFF
ON
OFF
I
LHGABA-VTA:ChR2
LHGABA-VTA:eYFP
****
OFF
ON
OFF
J
LH-VTA:ChR2
Gnawing Difference Score
***
wild-type
VGLUT2::Cre
VGAT::Cre
K
LHGABA-VTA:ChR2
Feeding
Gnawing
% Time Spent
OFF
5Hz
10Hz

Figure 7. Photoactivation of the GABAergic, but Not the Glutamatergic, Component of the LH-VTA Projection Increased Feeding Behaviors

(A and B) In order to selectively activate glutamatergic or GABAergic LH-VTA projections, VGLUT2::Cre and VGAT::Cre mice received an injection of AAV_5-DIO-ChR2-eYFP or AAV_5-DIO-eYFP into the LH and had an optic fiber implanted over the VTA. (A) In the sucrose-seeking task, there were no significant differences in the numbers of port entries per cue in any epoch for LH^{glut}-VTA:ChR2 mice (n = 7) compared to LH^{glut}-VTA:eYFP control mice (n = 6), (B) nor in those of LH^{GABA}-VTA:ChR2 mice (n = 6) compared to LH^{GABA}-VTA:eYFP mice (n = 8).

(C) There was no significant difference between LH^{glut}-VTA:ChR2 mice and eYFP controls in feeding behavior.

(D) However, LH^{GABA}-VTA:ChR2 mice showed a significant increase in time spent feeding during light stimulation compared to LH^{GABA}-VTA:eYFP controls (two-way ANOVA revealed a group x epoch interaction, $F_{2,24} = 4.78$, $p = 0.0178$; Bonferroni post-hoc analysis, $^{**}p < 0.01$).

(E and F) (E) Neither LH^{glut}-VTA:ChR2 mice nor (F) LH^{GABA}-VTA:ChR2 mice showed a difference in tail withdrawal latency compared to their respective controls.

(G) LH-VTA:ChR2 mice showed a significant increase in time spent gnawing during the light ON epoch compared to eYFP controls (two-way ANOVA revealed a group x epoch interaction, $F_{2,24} = 4.78$, $p = 0.0179$; Bonferroni posthoc analysis, ***$p < 0.001$).

(H) There was no significant difference between LH^{glut}-VTA:ChR2 and LH^{glut}-VTA:eYFP controls in gnawing behavior.

(I) However, LH^{GABA}-VTA:ChR2 animals also showed a significant increase in time spent gnawing during the light ON epoch compared to LH^{GABA}-VTA:eYFP controls (two-way ANOVA revealed a group x epoch interaction, $F_{2,24} = 18.91$, $p < 0.0001$; Bonferroni post-hoc analysis, ****$p < 0.0001$).

(J) The difference score for gnawing behavior between the ON and OFF epochs was significantly greater in LH^{GABA}-VTA:ChR2 animals in comparison with either wild-type LH-VTA:ChR2 or LH^{glut}-VTA:ChR2 animals (one-way ANOVA, $F_{2,18} = 16.76$, $p < 0.0001$; Bonferroni post-hoc analysis, ***$p < 0.001$).

(K) Frequency-response curve showing the effect of different blue-light stimulation frequencies (OFF, 5 Hz, 10 Hz) on behavior in LH^{GABA}-VTA:ChR2 animals.

Error bars indicate ±SEM. See also Figure S7.

2.4 Discussion

2.4.1 Functional Components of the LH-VTA Loop

The LH projection to the VTA has been explored with electrical stimulation collision studies (Bielajew and Shizgal, 1986; Murray and Shizgal, 1996a, 1996b), and has long been hypothesized to play a role in reward processing (Hoebel and Teitelbaum, 1962; Margules and Olds, 1962; Olds and Milner, 1954), yet pinpointing this role has been a challenge. Here, for the first time, we are providing a detailed dissection of how individual components of the LH-VTA loop process different aspects of a reward-related task and thereby overlay information regarding function and connectivity.

Through the use of optogenetic-mediated phototagging (Figure 1), we have identified two separate populations of LH neurons: one that sends projections to the VTA, and another that receives feedback from the VTA (Figure 2). In this study, we have prioritized specificity over penetrance and acknowledge that there are likely LH-VTA neurons that did not express ChR2 or that expressed ChR2 but were not "phototagged" due to distance from the light cone. There are also sampling biases introduced by recording over multiple sessions and selecting sessions with more photoresponsive units, as well as implanting the electrode in locations where photoresponsive neurons were detected, and as with any *in vivo* electrophysiology recordings, there is a sampling bias against very low-firing neurons. However, the positive results we report can be interpreted with confidence.

We show that LH-VTA neurons encode a motivational signal during conditioned responding for an appetitive reinforcer, while LH neurons downstream of the VTA encode the

reward-predictive cue (conditioned stimulus), the sucrose itself (the unconditioned stimulus), or both (Figures 3 and 4). All Type 1 neurons sampled that were task responsive encoded the action of port entry (Figure 3), but only after conditioning. The relative functional homogeneity of photoidentified LH-VTA (Type 1) neurons is consistent with the specific connectivity of this population, though some type 1 neurons do respond with excitation to port entry while others respond with inhibition, possibly representing the separate GABAergic and glutamatergic projections. However, it is not clear whether the heterogeneity in behavioral responses of Type 2 neurons (Figure 3) is due to heterogeneity in connectivity, or if this reliably reflects the input of VTA neurons which is thought to respond to both the CS and US in intermediate phases of conditioning (Day et al., 2007; Flagel et al., 2011).

We detected relatively few photoresponsive neurons that fell outside the bimodal distribution encapsulating Type 1 and Type 2 neurons (Figure S2B and Figure 1E). Given this, in combination with the long latency delay in Type 2 photoresponses (~100 ms), we speculate that there may be one dominant path representing an important component in reinforcement learning that has not previously been characterized. Additionally, this long duration photoresponse latency cannot be easily explained by disynaptic feed-forward excitation mediated by ionotropic receptors. However, because dopamine binds to G-protein-coupled receptors, the kinetics are significantly slower than most glutamatergic synapses (Girault J and Greengard P, 2004) and could, at least in part, explain this cluster of 100ms latency photoresponsive units. .In addition, the VTA may provide indirect feedback through other distal regions, for example, via excitatory intermediate regions such as the amygdala or with disinhibition via the nucleus accumbens (NAc) or bed nucleus of the stria terminalis (BNST).

The presence of the Type 3 neurons, which were inhibited upon photostimulation of LH-VTA neurons (Figure S2) represents a categorically different population from Type 1 and Type 2 neurons. These units show a qualitatively similar response profile to that of Type 1 units (Figure S2F and Figure 3G), and we speculate that Type 3 units are either inhibited directly by GABAergic Type 1 neurons, which have local axonal collaterals, or via feed-forward inhibition by VTA GABA neurons. Alternatively, these responses could be mediated by another polysynaptic feed-forward inhibitory circuit, such as the NAc.

Interestingly, while photostimulation of Type 1 neurons evokes excitatory responses in Type 2 neurons, Type 1 and 2 neurons show distinct behavioral encoding properties, for example, Type 1 and Type 2 neurons show robust differences in neurons that selectively encode the reward-predictive cue, (0/19 Type 1 vs 12/34 Type 2: $P = 0.003$, chi-square test). This paradoxical response pattern could be due to computational processes at an intermediate circuit element downstream of Type 1 neurons and upstream of Type 2 neurons, such as the VTA. Additionally, the behavioral state of the animal could influence how these data are processed, as animals are hungry and active during the performance of the reward-related task and they are sated and resting during the subsequent phototagging session.

2.4.2 Decoding Circuit Components in Reward Processing

Our model proposes a new way of conceptualizing how different components of a reward-related task might be represented in this LH-VTA loop (Figure 4J). Previous studies have used optogenetics to demonstrate that the LH-VTA pathway could support ICSS (Kempadoo et

al., 2013), implicating it in reward processing, but until now we had not uncovered the naturally-occurring activity in this pathway.

Our reward omission experiments allowed us to distinguish between LH neural encoding of the conditioned response (CR) and the consumption of the unconditioned stimulus (US). In these experiments, a subset of Type 2 neurons responded to the reward-predictive cue (CS) and the unconditioned stimulus (US) and also showed a decrease in firing rate when expected rewards were omitted. Furthermore, a subset of Type 2 neurons also showed phasic excitation upon unexpected reward delivery (Figure 4G and 4H). These data are reminiscent of the way DA neurons in the VTA encode reward-prediction error (Cohen et al., 2012; Schultz et al., 1997). Indeed, our VTA inhibition experiments have shown that Type 2 LH neurons are downstream of the VTA. We speculate that VTA neurons may transmit reward prediction error signals to a subset of LH neurons, which are well-positioned to integrate these signals for the determination of an appropriate behavioral output. Specifically, the LH is robustly interconnected with a multitude of other brain areas (Berthoud and Münzberg, 2011) and has been causally linked to homeostatic states such as sleep/arousal and hunger/satiety (Carter et al., 2009; Gutierrez et al., 2011; Jennings et al., 2013; Kempadoo et al., 2013).

2.4.3 A Causal Role for the LH-VTA Pathway in Compulsive Sucrose Seeking?

Compulsive reward-seeking behavior has primarily been discussed in the context of drug addiction wherein a classic paradigm for compulsive drug-seeking has been to examine the degree to which drug-seeking behavior persists in the face of a negative consequence, such as a

foot shock (Belin et al., 2008; Chen et al., 2013a; Deroche-Gamonet et al., 2004; Pelloux et al., 2007; Vanderschuren and Everitt, 2004). We adapted this task for sucrose-seeking to allow us to investigate whether activation of the LH-VTA pathway was sufficient to promote compulsive sucrose-seeking. Given that a distinct difference between drug and natural rewards is that drugs rewards are not necessary for survival, there is controversy as to what behaviors would constitute compulsive sucrose or food-seeking behavior. An alternative interpretation of our data is that activation of the LH-VTA pathway simply increases motivational drive or the urge to seek appetitive reinforcers. As the rates of obesity have increased in recent decades (Mietus-Snyder and Lustig, 2008), compulsive overeating and sugar addiction are prevalent conditions that are a major threat to human health (Avena, 2007; Avena et al., 2008; Benton, 2010; Corsica and Pelchat, 2010) and deserve equal attention in terms of elucidating the underlying pathology. Our findings that activation of the LH-VTA pathway increased feeding behavior in sated (fully-fed) mice is comparable to humans diagnosed with compulsive overeating disorder (or binge eating disorder) (DSM-V).

Furthermore, it has been proposed that actions which are repeated lead to the formation of habits, which themselves lead to the compulsive reward-seeking that characterizes addiction (Everitt and Robbins, 2005). Our finding that LH-VTA neurons only encode port entry after many repetitions across conditioning implies that this pathway is selectively encoding a conditioned response, not just any action. This is consistent with our observations that optically activating this projection can promote compulsive reward-seeking, in the face of a negative consequence (Figure 5C) as well as in the absence of need (as seen in sated mice, Figure 5E). This interpretation is further substantiated by our finding that photoinhibition of the LH-VTA

pathway selectively reduces compulsive sucrose-seeking (Figure 5D), but does not reduce feeding in food-restricted mice (Figure 5F).

Here, we report that LH-VTA neurons selectively encode the action of conditioned responding in the form of approaching the sucrose delivery port (Figure 4) and provide the first evidence that photostimulation of this pathway triggers compulsive sucrose-seeking in the face of a negative consequence (Figure 5). Notably, we did not observe a change in analgesia upon photostimulation of the LH-VTA pathway, despite the implication of the LH in pain modulation and analgesia by previous studies (Basbaum and Fields, 1979; Dafny et al., 1996; Mayer et al., 1971; Tasker et al., 1987). Consistent with previous reports of LH involvement in feeding behavior (Burton et al., 1976; Gutierrez et al., 2011; Hoebel and Teitelbaum, 1962; Jennings et al., 2013; Margules and Olds, 1962), we also observed a causal role for the LH-VTA pathway in feeding (Figure 5E). Feeding can be mediated through many parallel processing streams: by increasing hunger, by increasing the value of food rewards, or by increasing general arousal (Sternson, 2013). Many studies have established causal relationships between neural substrates and feeding behavior (Aponte et al., 2011; Atasoy et al., 2012; Betley et al., 2013; Carter et al., 2013; Jennings et al., 2013; Krashes et al., 2011, 2014; Land et al., 2014). While it may be evolutionarily adaptive to have considerable redundancy in these circuits, additional studies are required to determine which of these parallel circuits are truly redundant and which encode distinct aspects of these critical processes necessary for survival.

Remarkably, photoinhibition of the LH-VTA pathway in food-restricted mice reduced compulsive sucrose-seeking without reducing feeding on standard diet (regular mouse chow). One of the greatest challenges in treating compulsive overeating or binge eating disorders is the

risk of impairing feeding behaviors in general. However, our results suggest that we have identified a specific neural circuit element that can selectively reduce compulsive sucrose-seeking without sacrificing adaptive feeding behaviors critical for survival. From a translational perspective, we may have identified a specific neural circuit as a potential target that could facilitate the development of therapeutic interventions for compulsive overeating or sugar addiction.

2.4.4 Composition of LH Input to the VTA

The role of neuropeptides in the LH is well known (Berthoud and Münzberg, 2011; DiLeone et al., 2003). Indeed, several elegant studies have already investigated the role of specific neuropeptidergic LH input to the VTA (Harris et al., 2005; Kempadoo et al., 2013) and it has also been shown that the LH provides glutamatergic input onto putative VTA DA neurons (Kempadoo et al., 2013). However, the monosynaptic fast transmission contribution of the LH to the VTA was poorly understood. Here, for the first time, we show that there is also a significant GABAergic component in the projection from the LH to the VTA, and that LH neurons synapse directly onto both DA and GABA neurons in the VTA (Figure 6). However, there is a difference in the balance of the excitatory/inhibitory input onto VTA DA and GABA neurons, as seen by the proportionally greater number of VTA DA neurons receiving exclusively excitatory input compared to VTA GABA neurons (Chi-square = 4.8485, $p = 0.02767$).

There are several important caveats to consider in our experiments. First, VTA neurons that did not show a response to photostimulation do not necessarily lack input from the LH as it is possible that due to the limitations of viral penetrance or general opsin expression an existing

synaptic input was not detected. A sampling bias in the other direction may arise from experimenter selection of VTA neurons that are near axonal processes that express eYFP, though this does not necessarily reflect the density of functional synapses. Additionally, acute slice preparation severs much of the distal circuitry which certainly plays a huge role in determining VTA responses *in vivo*.

While we used immunohistochemical processing to verify the identity of VTA neurons, we also measured I_h, a hyperpolarization-activated inwardly rectifying non-specific cation current (Lacey et al., 1989; Ungless and Grace, 2012). The presence of this current has been widely used in electrophysiological studies to identify dopamine neurons, but it has been shown to be present only in subpopulations of dopamine neurons, delineated by projection target (Lammel et al., 2011). Although it has previously been proposed in a review by Fields and colleagues that "LH neurons synapse onto VTA projections to the PFC, but not those projecting to the NAc" (Fields et al., 2007) our data suggest that this controversy be reopened for further investigation. Even though we did observe a subset of DA neurons receiving net excitation from the LH which possessed a very small *Ih* (consistent with mPFC- or NAc medial shell-projecting DA neurons (Lammel et al., 2011), we also observed a subset of DA neurons receiving net excitatory input which showed a large I_h (Figure S5), consistent with characteristics of DA neurons projecting to the lateral shell of the NAc (Lammel et al., 2011). Conversely, VTA DA neurons that received a net inhibitory input showed a very small I_h, or lacked this current, which is consistent with the notion that the LH sends predominantly inhibitory input onto VTA DA neurons projecting to the mPFC or the medial shell of the NAc. We also show that LH inputs can be observed in both medial and lateral VTA, suggesting that the LH provides inputs onto VTA neurons with diverse projection targets, as it is known that VTA projection target

corresponds somewhat to spatial location along a medial-lateral axis (Lammel et al., 2008). However, these neurons might also represent populations of VTA neurons projecting to other regions that have not yet been characterized.

2.4.5 Excitation/Inhibition Balance in the LH-VTA pathway

The role of the LH-VTA pathway in promoting reward has previously been ascribed to glutamatergic transmission in the VTA (Kempadoo et al., 2013), as the CaMKIIα promoter is often thought to be selective for excitatory projection neurons. While the specificity of expression of ChR2 under the CaMKIIα promoter has been clearly demonstrated and characterized in some brain regions such as the basolateral amygdala (Tye et al., 2011), our data clearly show that expressing ChR2 under the control of the CaMKIIα promoter also targets GABAergic, in addition to glutamatergic projection neurons in the LH (Figure 6). In contrast to the glutamatergic component of the LH-VTA pathway, the GABAergic component has been largely ignored.

The behavior elicited by photostimulation of the LH^{GABA}-VTA pathway was frenzied, misdirected, and maladaptive. One interpretation is that activation of the LH^{GABA}-VTA pathway sends a signal to the mouse that causes the recognition of an appetitive reinforcer. In the absence of food this is aberrantly directed at non-food objects (gnawing), and in the absence of any object the signal is falsely interpreted such that the mouse perceives the presence of a consumable object. An alternative interpretation is that the LH^{GABA}-VTA pathway might drive incentive salience or an intense "wanting", consistent with a signal underlying conditioned approach, but

at a non-physiological level that produces this aberrant feeding-related behavior (Berridge and Robinson, 2003). Consistent with this, it is possible that activation of the LH^{GABA}-VTA projection actually produces intense sensations of craving, or urges to feed, which may support compulsive sucrose-seeking. However, activation of LH^{GABA}-VTA did not produce an increase in compulsive sucrose-seeking due to the excessive gnawing and aberrant appetitive behaviors. While it is difficult to determine the experience of the mouse during this manipulation, it is clear that appropriately directed feeding-related behaviors require the coordinated activation of the GABAergic and glutamatergic components of the LH-VTA pathway.

In stark contrast, activation of the LH^{glut}-VTA pathway may actually have reduced feeding in sated animals (Figure 7C) and time spent gnawing (Figure 7H), though in both cases, the control groups were so close to zero that statistical significance may have been occluded by a floor effect. Our study provides exciting data that beg for the attribution of more attention to these circuit components.

Taking the behavioral and recording data together, and given the qualitative similarities between Type 1 and Type 3 neurons (Figure 3G and Figure S2) in terms of the profile of responses to task-related events, this raises the possibility that the coordinated activation of the glutamatergic and GABAergic components may be driven by feed-forward or direct inhibition by LH GABA neurons onto neighboring GABA neurons. Indeed, given the caveats discussed above, we speculate that Type 1 and Type 3 neurons could be at least partially overlapping, as the LH^{GABA}-VTA neurons require a means to regulate their own activity and Type 3 neurons might be LH-VTA neurons that were not expressing ChR2. However, it is equally likely that Type 3 neurons have completely unrelated connectivity. We also note that almost all of the LH

neurons showing an excitatory photoresponse were either ChR2-expressing or the photoresponse was dependent on input from the VTA – indicating sparse or non-existent local feed-forward excitation driven by Type 1 neurons.

2.5 Conclusion

Optogenetic and pharmacogenetic manipulations are powerful tools for establishing causal relationships, yet they do not reveal the endogenous, physiological properties of neural circuit elements. Our study unifies information about the synaptic connectivity, the naturally occurring endogenous function, and the causal role of the LH-VTA pathway, providing a new level of insight toward how information is integrated in this circuit. These results highlight the importance of examining the functional role of neurons by connectivity, in addition to genetic markers. LH-VTA neurons selectively encoded the action of reward seeking but did not encode environmental stimuli, whereas rewarding stimuli and reward-predictive cues were encoded by a discrete population of LH neurons downstream of the VTA. Furthermore, we have identified a specific projection that is causally linked to compulsive sucrose-seeking and feeding behavior. The heterogeneity in the LH-VTA projection is necessary for providing an adaptive balance between driving motivation and regulating appropriately directed appetitive behaviors. These findings provide insights relevant to pathological conditions such as compulsive overeating disorder, sugar addiction, and obesity.

2.6 Methods and Materials

2.6.1 Animals and Stereotaxic Surgery

Animals were housed in a reverse 12 hr light-dark cycle room with ad libitum food and water. All procedures involving the handling of animals were in accordance with the guidelines from the NIH and with approval of the MIT Institutional Animal Care and Use Committee. Surgeries were conducted under aseptic conditions using a digital small animal stereotaxic instrument (David Kopf Instruments, Tujunga, CA, USA). For all surgeries mice were anaesthetized with isoflurane (5% for induction, 1.5%–2.0% thereafter) in a stereotaxic frame, and body temperature was maintained with a heating pad. Injections were performed using a beveled 33 gauge microinjection needle. A 10 ml microsyringe (nanofil; WPI, Sarasotam FL, USA) was used to deliver the virus at a rate of 0.1 ml per min using a microsyringe pump (UMP3; WPI) and controller (Micro4; WPI). After completion of the injection, 2 min were allowed to pass before withdrawing the needle 50 mm and leaving it for an additional 15 min to allow for diffusion of the virus, after which the needle was then slowly withdrawn. Following surgery, animals were allowed to recover from anesthesia under a heat lamp.

2.6.1.1 Surgeries for Experiments in Figures 1-4 and S1-S3 (*In Vivo* Electrophysiological Recording)

Male C57BL/6 mice used for *in vivo* electrophysiological recordings (Figures 1-4, S1-S3), received a unilateral injection of 1 μL of an anterogradely travelling adeno-associated virus, serotype 5 (AAV_5), carrying ChR2-eYFP under a double-floxed inverted open-reading frame

construct (DIO) (AAV_5-DIO-ChR2-eYFP) into the LH (-0.4 to -0.6 mm anteroposterior (AP); 1.0 mm mediolateral (ML); -4.9 to -5.25 mm dorsoventral (DV) and 1 μL of a retrogradely travelling herpes simplex virus (HSV) carrying Cre-recombinase (HSV-EF1α-mCherry-IRES-Cre) into the VTA (-3.1 to -3.5 mm AP; 0.65 mm ML; -4.3 to -4.6 mm DV). These injections ensure that only cells in the LH that project to the VTA express ChR2-eYFP.

After animals had been trained on a partial reinforcement sucrose self-administration task (as described below), a second surgery was performed (6-12 months after the initial surgery) to implant an optrode (construction described below). Using the same conditions for surgery and anesthesia as previously described, one craniotomy was drilled over the LH (-0.6 mm AP; 1.0 mm ML), and four skull screws were implanted around the site of the craniotomy. The optrode was connected to the head-stage of the RZ5 recording system (Tucker-Davis Technologies, Alachua, FL) and then driven down while the system recorded electrical activity. After the optrode had been stereotaxically lowered down to -2.0 mm DV, the ground wire was implanted at a depth of approximately 1.5 mm into the posterior ipsilateral hemisphere. The optrode was lowered at approximately 0.01 mm/s until -4.5 mm DV. At this point, blue light (473 nm, 20 mW, 1 s constant pulse) was delivered through the optic fiber of the optrode to identify photoresponsive units (neurons that showed time-locked action potentials in response to illumination). If no units were visually identified, the optrode was driven down another ~0.05 mm, and blue light was delivered again. This process was repeated until photoresponsive units were found, indicating that the optrode was now in the correct location, or until a maximum depth of approximately -5.5 mm. If the maximum depth was reached and no photoresponsive units were found, the optrode was retracted slowly at approximately 0.01 mm/s and then re-implanted in a location approximately -0.2 mm AP from the previous implant site. This was

repeated until phototagged units were discovered. If no phototagged units were found after five attempts, the optrode was implanted at: -0.6 mm AP, 1.0 mm ML, -5.0 DV. One layer of adhesive cement (C&B Metabond; Parkell, Edgewood, NY) followed by cranioplastic cement (Dental cement; Ortho-Jet, Lang Dental, Wheeling, IL) was used to affix the optrode to the skull. Once the cement was dry, the incision was closed with nylon sutures.

2.6.1.2 Surgeries for Experiments in Figure 2 and S3 (Inhibition of VTA During Phototagging)

In a subset of animals used for *in vivo* electrophysiological recordings, we also expressed enhanced halorhodopsin 3.0 (NpHR) in the VTA to allow for transient inhibition (Figure 2). In these animals, 1 μL of AAV_5-DIO-ChR2-eYFP was unilaterally injected into the LH (-0.4 to -0.6 mm AP; 1.0 mm ML; -4.9 to -5.25 mm DV). In addition, 1.0-1.5 μL of a 1:1 mix of HSV-EF1α-mCherry-IRES-Cre and AAV_5-CaMKIIα-NpHR-eYFP was injected into two sites in the VTA (-3.2 to -3.5 mm AP; 0.65 mm ML; -4.6 and -4.4 DV, with 0.5-0.75 μL at each site). An optrode was implanted over the LH (as described above) and an optic fiber (400 μm core, 0.48 numerical aperture (NA), Thorlabs, Newton, NJ) held in a 1.25 mm ferrule (Precision Fiber Products, Milpitas, CA) was implanted above the VTA (-3.1 to -3.5 mm AP; 0.0 mm ML; -2.0 to -2.5 mm DV).

In order to inhibit the VTA by infusion of tetrodotoxin (TTX) (Figure S3), in a subset of animals, we injected AAV_5-DIO-ChR2-eYFP into the LH (-0.4 to -0.6 mm AP; 1.0 mm ML; -4.9 to -5.25 mm DV) and HSV-EF1α-mCherry-IRES-Cre into the VTA (-3.1 to -3.5 mm AP; 0.65

mm ML; -4.3 to -4.6 mm DV) and implanted a cannula (PlasticsOne, Roanoke, VA) above the VTA (-3.3 to -3.5 mm AP; 0.65 mm ML; -3.1 mm DV).

2.6.1.3 Surgeries for Experiments in Figure 5 and S4 (Optogenetic Behavioral Manipulations)

For ChR2 activation experiments, male C57BL/6 mice used in the behavioral tasks in Figure 5 and S4 were injected with 300-500 nL of AAV_5-CaMKIIα-ChR2-eYFP (experimental animals) or AAV_5-CaMKIIα-eYFP (control animals) unilaterally into the LH at either one or two injection sites (-0.4 to -0.6 mm AP and/or -1.2 to -1.4 mm AP; 1.0 mm ML; -4.9 to -5.25 mm DV). In addition, an optic fiber (300 μm core, 0.37 NA) held in a 1.25 mm ferrule was implanted above the VTA (-3.1 to -3.5 mm AP; 0.65 mm ML; -3.7 to -3.9 mm DV).

For NpHR inhibition experiments, male C57BL/6 mice were injected with 300-500 nL of AAV_5-CaMKIIα-NpHR-eYFP (experimental animals) or AAV_5-CaMKIIα-eYFP (control animals) bilaterally into the LH at either two or four injection sites (-0.4 to -0.6 mm AP and also -1.2 to -1.4 mm AP if four injections; 1.0 mm ML; -4.9 to -5.25 mm DV). In addition, an optic fiber (300 μm core, 0.37 NA) held in a 2.5 mm ferrule was implanted above the VTA (-3.1 to -3.5 mm AP; 0.65 mm ML; -2.0 to -2.5 mm DV).

2.6.1.4 Surgeries for Experiments in Figure 6 and S5-S6 (Patch-Clamp Recordings)

For *ex vivo* recording from VTA dopamine and GABA neurons (Figure 6 and S5-S6), adult wild-type male C57BL/6 mice and VGAT::IRES-Cre mice (Jackson Laboratory, Bar Harbor, ME) were used, respectively. For all animals, ChR2 was expressed unilaterally in the LH. In a subset of animals, this was achieved by injecting 300-500 nL of AAV_5-CaMKIIα-ChR2-eYFP into the LH (-0.4 to -0.6 mm AP; 1.0 mm ML; -4.9 to -5.25 mm DV). In a second subset, this was achieved by injecting 1 μL of AAV_5-DIO-ChR2-eYFP into the LH (-0.4 to -0.6 mm AP; 1.0 mm ML; -4.9 to -5.25 mm DV) and 1 μL of HSV-EF1α-mCherry-IRES-Cre into the VTA (-3.3 to -3.5 mm AP; 0.65 mm ML; -4.3 to -4.6 mm DV). In VGAT::IRES-Cre animals (n=4), 300-500 nL of AAV_5-DIO-mCherry was also injected into the VTA (-3.3 to -3.5 mm AP; 0.65 mm ML; -4.3 to -4.6 mm DV) to aid the identification of GABA neurons in the VTA.

2.6.1.5 Surgeries for Experiments in Figure 7 and S7 (Optogenetic Behavioral Manipulations in Transgenic Animals)

In male VGAT::IRES-Cre mice or male VGLUT2::IRES-Cre mice (Jackson Laboratory, Bar Harbor, ME), 300-500 nL of AAV_5-DIO-ChR2-eYFP (experimental animals) or AAV_5-DIO-eYFP (control animals) was injected into the LH (-0.4 to -0.8 mm AP; 1.0 mm ML; -4.9 to -5.25 mm DV). In addition, an optic fiber (300 μm core, 0.37 NA) held in a 2.5 mm ferrule was implanted above the VTA (-3.1 to -3.5 mm AP; 1.0 mm ML; -3.5 to -3.9 mm DV).

2.6.1.6 Viral Constructs

The recombinant AAV vectors were serotyped with AAV_5 coat proteins and packaged by the University of North Carolina Vector Core (Chapel Hill, NC). The HSV vectors were packaged by the Massachusetts Institute of Technology Viral Gene Transfer Core (Cambridge, MA).

2.6.2 Optrode Construction

Optrodes were built in the lab by cementing a 300 μm core, 0.37 NA, optic fiber held in a 1.25 mm ferrule to a 16-channel multielectrode array (Innovative Neurophysiology, Durham, NC). These two components were cemented in a way that allowed the optic fiber and electrode tips to meet at an approximately 10 degree angle with a distance of 500 μm to 1500 μm between the end of the optic fiber and the electrode tips. These criteria were used to maximize the amount of light that reached the electrode tips from the light cone generated at the end of the optic fiber.

2.6.3 Partial Reinforcement Sucrose Self-Administration Task, Unexpected Reward Omission, and Unpredicted Reward Delivery

Animals used in Figures 1-4 were taken off *ad libitum* water for 12-24 h prior to behavioral training. The mice were placed in a sound-proofed conditioning chamber (MedAssociates, St Albans, VT). Each chamber included a modified nose-poke port, a sucrose delivery port, a house light, as well as speakers to play tones for the reward-predictive cue and

white noise. The animals learned that randomly following 50% of nosepoke responses, a compound sound (1 kHz) and light cue would play (2.45 s). The compound cue indicated that a small volume of sucrose solution (15%, 0.73 mL) was delivered at the sucrose delivery port. For reward omission experiments in Figure 4, in 30% of the trials in which the cue was played, no sucrose would be delivered. Once the animal made a port entry into the sucrose delivery port, the next time the animal nosepoked, there would be another 50% probability that a cue would play and sucrose would be delivered. However, if the mouse continued to nosepoke after a cue had been given, the cue would be given again for each nosepoke, and no extra sucrose would be delivered until the previous delivery had been collected. The animal would be allowed to continue performing the task for 30 minutes or for at least 60 sucrose deliveries. Performance of the mouse was assessed by computing the sensitivity and specificity of each session. Sensitivity was defined as the number of true positives (port entry within 10 s following cue) divided by the sum of the number of true positives and false negatives (no port entry within 10 s following cue). Specificity was defined as the number of true negatives (no port entry following no cue) divided by the sum of the number of true negatives and false positives (port entry following no cue). Animals were considered to have met training criterion when they reached 80% sensitivity and 60% specificity for two continuous days, and all recordings included in this study were performed during the maintenance phase (following training criterion).

For unpredicted reward delivery experiments, both naïve and well-trained animals who had met criterion were used. Animals were placed into the same chamber, where random sucrose deliveries would be made at the delivery port without any predictive cues.

2.6.4 Optogenetic Stimulation

For optogenetic stimulation during phototagging and behavioral experiments, a 473 nm DPSS laser (OEM Laser Systems, Draper, UT) was connected to a patch cord with a pair of FC/PC connectors in each end (Doric, Québec, Canada). For optical inhibition during phototagging experiments, a 589 nm or 593 nm DPSS Laser (OEM Laser Systems, Draper, UT) was used. This patch cord was either connected to the mechanical/optical commutator (Tucker-Davis Technologies, Alachua, FL) during phototagging experiments (Figures 1-4) or connected through a fiber-optic rotary joint (Doric, Québec, Canada) during behavioral experiments (Figure 5 and 7). Another patch cable with a FC/PC connector on one side and a ferrule connection on the other side was then connected to the commutator and to the ferrule on the animal using a ceramic mating sleeve (PFP, Milpitas, CA).

2.6.5 *In Vivo* Electrophysiological Recordings and Phototagging with ChR2 and NpHR

Once mice had been implanted with an optrode, they were allowed one week for recovery. The mice were then trained on the partial reinforcement sucrose self-administration task again, but with the head-stage attached to the recording system to record electrical activity and to trigger light pulses. The animals performed the task once per day (between 3 and 40 sessions) over a period of 1-6 months. Following completion of the task, a phototagging session using a 473 nm laser (30-40 mW) was conducted within the same recording session, during which pseudorandomly dispersed stimulations of 1 s constant light or 10 s of 1 Hz light (5 ms pulse duration) were delivered, with at least 10 iterations of each. During NpHR inhibition trials, after

the first phototagging session, yellow light was delivered to the VTA (593 nm, 10-15 mW, constant), and a second phototagging session was conducted. Following the second phototagging session, the yellow light was turned off, and a third and final phototagging session was conducted. During TTX inhibition trials (Figure S3), after the first phototagging session, 0.4 μL of 20 μM TTX was infused using a microsyringe pump (UMP3; WPI, Sarasota, FL) at 0.1 μL per min into the VTA via the implanted cannula. After 15 minutes, the second phototagging session was conducted.

Reward omission and unexpected reward experiments (Figure 4) were conducted on the day following a day with a large number of photoresponsive units to maximize the data collected.

2.6.6 Analysis of *In Vivo* Awake-Behaving LH Electrophysiological Recordings

Recording sessions were exported from the TDT system to Plexon offline sorter using OpenBridge. Offline sorter (Plexon) was used for sorting, and analyses were performed using NeuroExplorer and MATLAB. Due to the wide range of observed latencies in response to light stimulation in recorded units, we first used custom-written MATLAB scripts to calculate the latency from the time of photostimulation onset to the first 10 ms bin (within 500 ms) with a 4 standard deviation (SD) increase over the baseline firing rate (-0.5 to 0 s) during the 1 Hz or constant phototagging trials (Figure 1). For units in which a response was detected within the first 10 ms bin, a second latency was calculated using 1 ms bins. Following the identification of this latency, we used a nonparametric Wilcoxon rank-sum test to determine if the firing rate within an experimental window encompassing the detected latency (±2 ms for detections at 1 ms

bins, ±20 ms for detections at 10 ms bins) was significantly different than the baseline firing rate (window: -4 ms to 0 ms, -40 ms to 0 ms, respectively). The histograms of photoresponse latencies were fitted with a Gaussian function composed of multiple peaks (Figure 1). Units were defined as Type 1 units if they had latencies between 3-8 ms and a significant difference in the rank-sum analysis ($p<0.05$), while units were defined as Type 2 units if they had latencies between 80-120 ms and a significant difference in the rank-sum analysis ($p<0.05$). For each set of experiments, only one session from each animal was used, which was determined by the best recording quality, greatest number of phototagged units, and behavioral performance. This was in order to eliminate the possibility of counting the same unit across multiple days.

In order to analyze the response of units to various behavioral events, a Wilcoxon rank-sum test was performed on the activity of each unit in response to the presence of the cue following nosepoke, the absence of the cue following nosepoke, and the beam-break for port entry ($p<0.001$). Baseline windows of -4 to -2 s (before the event) were used, and the experimental window was set to 0 to 0.5 s for the presence or absence of the cue and from -0.25 to 0.25 s for the port entry. A unit was considered to be responsive to the cue only if the response during the absence of the cue was not significantly different to baseline. If there was a change in firing rate in response to both the presence and absence of the cue, this could represent encoding of the motor action of nosepoking.

For both NpHR and TTX inhibition experiments (Figure 2 and Figure S3), a Wilcoxon rank-sum test was also used to calculate whether the units were responding to light stimulation ($p<0.05$). For identified Type 1 units, the baseline used was from -0.004 to 0 s, while the experimental window was set to be ±2 ms from the identified photoresponse latency. For

identified Type 2 units, the baseline used was -0.04 to 0 s, while the experimental window was set to be ±20 ms from the identified photoresponse latency.

For reward omission experiments (Figure 4), port entries during reward trials were considered to be the first port entry within 10 s of rewarded trials, while port entries during omission trials were considered to be the first port entry within 10 s of omitted trials. The Wilcoxon test was used to compare the experimental window from 0 to 2 s in rewarded trials versus omitted trials. Units were considered to encode reward omission if $p<0.05$. For unpredicted reward delivery experiments, analysis was performed using only the first port entry made after each unpredicted delivery of sucrose in order to ensure that sucrose was present during the port entries being analyzed. Units were considered to encode the port entry if $p<0.001$.

For units that appeared to be inhibited by the blue light (Figure S2), we calculated firing rates for 100 ms bins during the 1 s constant light phototagging trials. Units were identified as inhibited to the blue light if they had firing rates less than half of the baseline firing rate (-0.5 s to 0 s) for two consecutive bins in the first 300 ms after the light was given and a Wilcoxon rank-sum test found their firing rates during the experimental window (0 to 1 s) to be significantly different than the baseline firing rate (-1 to 0 s; $p<0.05$).

2.6.7 *Ex Vivo* Electrophysiology

In order to activate LH inputs to the VTA, we expressed ChR2 in the LH and recorded from VTA neurons in brain slices *ex vivo* (Figure 6). To identify dopamine neurons, we recorded in wild-type mice with an internal solution containing biocytin and subsequently stained for

tyrosine hydroxylase (TH). To identify GABA neurons, we injected a Cre-dependent virus carrying an mCherry fluorophore into the VTA of VGAT::IRES-Cre mice to visually guide recordings. Additionally, putative GABA neurons in wild-type mice were identified by the absence of TH staining (Figure S6).

For *ex vivo* VTA recordings, horizontal 300 μm brain slices containing the VTA were prepared from wild-type C57BL/6 or VGAT::IRES-Cre mice. Mice were anaesthetized with an intraperitoneal (i.p.) injection of sodium pentobarbital (200 mg/kg) then transcardially perfused with 20 mL ice-cold modified artificial cerebrospinal fluid (ACSF; composition in mM: NaCl 87, KCl 2.5, NaH2PO4*H20 1.3, MgCl2*6H2O 7, NaHCO3 25, sucrose 75, ascorbate 5, CaCl2*2H2O 0.5, in ddH20; osmolarity 323-328 mOsm, pH 7.30-7.40) saturated with carbogen gas (95 % oxygen, 5 % carbon dioxide). The brain was rapidly dissected from the cranial cavity and sectioned on a vibrating-blade microtome (Leica VT1000S, Leica Microsystems, Germany). Slices were then transferred to a holding chamber containing ACSF (composition in mM: NaCl 126, KCl 2.5; NaH2PO4*H20 1.25, MgCl2*6H2O 1, NaHCO3 26, glucose 10, CaCl2*2H2O 2.4, in ddH20; osmolarity 299-301 mOsm; pH 7.35-7.45) saturated with carbogen gas at 32 °C, and allowed to recover for at least 90 minutes. For electrophysiological recordings, slices were placed in a recording chamber, where they were continuously perfused using a peristaltic pump (MINIPULS 3; Gilson, WI, USA) at a rate of 2 mL/min with fully oxygenated ACSF at 32 °C. Cells were visualized through a 40X water-immersion objective on an upright microscope (BX51; Olympus, PA, USA) equipped with infra-red (IR) differential interference contrast (DIC) optics and a Hamamatsu camera. Additionally, in VGAT::IRES-Cre mice, which had received an injection of AAV_5-DIO-mCherry in the VTA, brief illumination through a 595 nm LED light

source (pE-100; CoolLED, NY, USA) was used to identify mCherry-expressing cells prior to recording.

Whole-cell patch-clamp recordings were made using a Multiclamp 700B amplifier and Clampfit software (Molecular Devices, CA, USA). Signals were low-pass filtered at 1 Hz and digitized at 10 kHz using a Digidata 1440 (Molecular Devices, CA, USA). Electrodes were pulled from thin-walled borosilicate glass capillary tubing using a P-97 puller (Sutter Instrument, CA, USA) and had resistances of 4-6 MΩ when filled with internal solution (composition in mM: potassium gluconate 125, NaCl 10, HEPES 20, Mg-ATP 3, Na-GTP 0.4, and 0.5% biocytin, in ddH20; osmolarity 289 mOsm; pH 7.31). Capacitance, series resistance, and input resistance were frequently measured to monitor cell health. The hyperpolarization-activated cation current (I_h) was activated by holding the cell in voltage-clamp at -50 mV and delivering a 1 s hyperpolarizing step to -120 mV. The amplitude of the I_h was measured as the difference between the peak instantaneous and steady-state current achieved across the voltage step. ChR2 was activated by blue light generated by a 100 mW 473 nm DPSS laser (OEM Laser Systems, UT, USA), controlled by a Master-8 pulse stimulator (A.M.P.I., Jerusalem, Israel) and delivered via an optic fiber resting on the brain slice (Figure S5A). To assess the net effect of optical stimulation, neurons were recorded in current-clamp mode, with slow current injected to maintain cells at their resting potential (-50 to -60 mV). 5 ms light pulses were delivered at 1 Hz for 10 s and the predominant effect of optical stimulation was determined across 30 light pulses. To assess the composition of the optically-evoked current, neurons were recorded in voltage-clamp mode, and a 5 ms light pulse was delivered every 20 s at a holding potential of -70 mV or 0 mV to elicit AMPAR-mediated EPSCs or $GABA_AR$-mediated IPSCs, respectively. The optically-evoked current was recorded in the presence of tetrodotoxin (TTX; 1 μM) and 4-

aminopyridine (4AP; 0.1-0.6 mM) to confirm the existence of a monosynaptic connection (Petreanu et al., 2007). AMPAR-mediated EPSCs were blocked by NBQX (20 μM; Sigma, n = 6), and $GABA_AR$-mediated IPSCs were blocked by picrotoxin (100 μM; Sigma, n = 5). Additionally, a 1 s constant light pulse was used to confirm that the cell itself was not expressing ChR2. Analysis was performed using Clampfit software (Molecular Devices, CA, USA). DIC images were taken of the position of the recording electrode in the brain slice and used to map the location of recorded neurons onto horizontal midbrain slices from the mouse brain atlas (Paxinos & Franklin, 2001).

For *ex vivo* LH recordings, 300 μm horizontal brain slices were prepared (as described above) from wild-type mice which had received an injection of AAV_5-DIO-ChR2-eYFP into the LH and HSV-EF1α-mCherry-IRES-Cre into the VTA. ChR2-expressing and non-expressing LH neurons were visually identified in the brain slice by brief illumination through a 470 nm LED light source (pE-100; CoolLED, NY, USA). Whole-cell capacitance was estimated using pClamp (Molecular Devices, CA, USA) and the resting membrane potential was measured across the first 60 s of recording in current-clamp mode. ChR2 was activated by 473 nm light delivered via an optic fiber resting on the brain slice directed at the LH. The average latency to action potential peak in ChR2-expressing LH neurons was measured across 30 sweeps and taken as the duration from the start of the light pulse to the peak amplitude of the action potential. A sustained depolarizing response to a 1 s constant light pulse at a holding potential of -50 mV in voltage-clamp was used to confirm ChR2-expression in the recorded neuron.

2.6.7.1 Identification of Cell Type Following Whole-Cell Patch-Clamp Recordings

Cells were filled with biocytin during recording. Brain slices were subsequently fixed in 4% paraformaldehyde (PFA) overnight at 4 °C and then washed in PBS. They were then blocked for 1 h at room temperature in PBS containing 5% (v/v) normal donkey serum (NDS) and 0.3% Triton, followed by incubation with primary chicken anti-TH (1:1000; Millipore) overnight at 4 °C. Slices were washed in PBS and then incubated with AlexaFluor 647-conjugated donkey anti-chicken (1:1000; Jackson ImmunoResearch Laboratories, Inc, West Grove, PA) and CF405-conjugated streptavidin (1:1000; Biotum, CA, USA), to reveal biocytin labelling, in PBS containing 3% (v/v) NDS and 0.1% Triton, for 2 h at room temperature. Slices were subsequently washed in PBS, mounted on glass slides, and cover-slipped using polyvinyl alcohol mounting medium with DABCO (PVA-DABCO).

2.6.8 Optogenetic Behavioral Manipulations

2.6.8.1 Sucrose-Seeking Task

Animals were taken off *ad libitum* food 12-24 h prior to training. They were placed in behavioral chambers that each included a sucrose delivery port, a house light, as well as speakers to play tones for the reward-predictive cue and white noise. In addition, the half of the chamber that contained the sucrose port had an exposed shock grid, while the other half was covered with a plastic floor. Mice were trained on a task in which a light and tone cue (1.5 kHz, 3 s) signaled the delivery of 30% sucrose (0.73 mL) to the sucrose delivery port in the chamber. Mice were trained until they retrieved 70% of the sucrose deliveries before the onset of the next cue. After

reaching criteria, on the first test day, animals perform the task for 20 cues during the baseline epoch. In the second epoch, the shock floor was then turned on so that shock (0.06 mA, 0.5 s every 1 s) was delivered, 20 cues were given, and animals would continue to perform the task. If the animal retrieved as many cues as during the baseline epoch or made more than 80% of the number of port entries in the baseline period, the third epoch would not be given. Instead, the animal would perform the task again on the next day, and the shock would be increased by 0.02 mA. This would be repeated each day until the first day that an animal collected fewer rewards and made less than 80% the number of port entries during the baseline period. If necessary, smaller adjustments of 0.01 mA increases or decreases were made to find an optical shock level. Once these criteria were met, the shock was determined to be sufficiently strong enough to deter the animal from retrieving sucrose regularly, but weak enough not to deter all future retrieval attempts. In the third epoch, LH-VTA projections were activated by 473 nm light stimulation (20 mW, 10 Hz, 5 ms duration) or inhibited by 589/593 nm constant light, 20 more cues were given, and the animal continued performing the task. A reward-seeking index (port entries/cue presentation) for each animal was calculated for each epoch (Figure 5 and 7). Port entries within 1 s of a previous port entry were not counted.

2.6.8.2 Extinction Resistance Task

Once trained mice had completed testing on the sucrose seeking task they were re-trained for a single session before undergoing the extinction resistance task. The mice were placed into the same chamber and exposed to 20 cues paired with 30% sucrose delivery. Following this, 315 cues continued to play for the next 3 h, but in the absence of sucrose delivery into the port. LH-

VTA projections were activated or inhibited during the 3 hour extinction session using either blue (20 mW, 10 Hz, 5 ms duration) or yellow (589/593 nm, 5 mW, constant) light stimulation, respectively.

2.6.8.3 Feeding Task

Mice were allowed to explore a chamber with two empty plastic cups placed in opposite corners for a period of 10 min (habituation). A moist pellet of food was then placed into one of the cups (side placement of the pellet was counterbalanced between each animal), and mice were allowed to freely explore for 15 min (pre-stimulation). Following this, mice received either blue (473 nm, 20 mW, 20 Hz, 5 ms duration) or yellow (589/593 nm, 5 mW, constant) light for 15 minutes, while continuing to explore the cage (stimulation), depending on if they were expressing ChR2 or NpHR. The light was then turned off for another 15 minutes, and the animals were allowed to continue to explore (post-stimulation). The entire session was recorded, and the time spent eating during each epoch was analyzed manually. During this task, certain animals also exhibited oral stereotypies that were unrelated to the direct consumption of the freely available food in the task. We classified these behaviors as "gnawing" and used the recorded video to score them separately from feeding.

2.6.8.4 Dose-Dependent Feeding

Male VGAT::Cre mice which had received an injection of AAV_5-DIO-ChR2-eYFP in the LH and had an optic fiber implanted above the VTA were placed into the same chamber used for the feeding task. Mice were allowed to freely explore the chamber for 10 minutes (habituation). Following habituation, a moist pellet of food was placed into one of the two food containers (side placement was counterbalanced between each animal). Mice were allowed to explore the box with free access to the food for 10 min. Following this epoch, animals continued to explore the chamber while being stimulated with blue light (473 nm, 20 mW) at 5 Hz for 10 min. This second epoch was followed by a third epoch where animals were further stimulated at 10 Hz for 10 min while continuing to explore the chamber. The entire session was recorded and the time spent feeding and gnawing was manually scored.

2.6.8.5 Tail Withdrawal Assay

Animals were placed in a tail vein restrainer. The tail of each mouse was immersed 3 to 5 cm into 50 °C water until the mouse removed its tail due to a withdrawal reflex. If no reflex occurred, the tail would be withdrawn by the experimenter after 10 s. 15 s after the completion of the first immersion, another trial occurred, and the tail was again immersed. One hour later, each animal was tested again over two trials with either blue or yellow light stimulation starting 15 s prior to tail dipping (blue: 473 nm, 20 mW, 10 Hz, 5 ms duration; yellow: 589/593 nm, 5 mW, constant). The order in which animals were tested for light and non-light stimulation epochs was counter-balanced across trials. Each trial was recorded and manually analyzed in a frame-by-

frame manner to determine the time elapsed from tail immersion to the start of the withdrawal reflex.

2.6.8.6 Open Field Task

The open field arena was a 50 x 53 cm chamber composed of four transparent plastic walls that enclosed the mouse. Mice were connected to the patch cable, placed in the open field, and given 1 to 5 min to recover from handling before the trial was started. The duration of the behavioral test was 15 min, divided into three alternating 5-minute epochs (OFF-ON-OFF) of either blue (473 nm, 20 mW, 20 Hz, 5 ms duration) or yellow (589/593 nm, 5 mW, constant) light stimulation. A video camera positioned above the chamber recorded each trial, and mouse location and velocity, relative to body center, were tracked using EthoVision XT (Noldus, Wageningen, Netherlands). For analysis of anxiety-like behavior the chamber was divided into a center (36 x 36 cm) and a periphery region.

2.6.9 Histology

Sodium pentobarbital (200 mg/kg i.p.) was used to anesthetize all mice prior to transcardial perfusion with ice-cold saline, followed by ice-cold 4% PFA in PBS (pH 7.3). Extracted brains were fixed in 4% PFA overnight and then equilibrated in 30% sucrose in PBS. A sliding microtome (HM430; Thermo Fisher Scientific, Waltham, MA) was used to section the brains. Brains from recording experiments were sectioned into 60 μm-thick coronal sections and

were stored at 4 °C until processing using immunohistochemistry. All other brains were sectioned into 50 μm-thick coronal sections and stored under the same conditions.

For animals used for *in vivo* recording experiments, electrolytic lesions were created prior to sacrifice in order to histologically confirm electrode-tip location. After animals were anesthetized, a 19.6 μA current (15 s) was injected into each channel from which phototagged units had been obtained. The animals were perfused after a 30 minute waiting period to allow for gliosis around the lesion sites.

For immunohistochemistry, sections were incubated in 3% NDS in Triton 0.3% in PBS for 1 h at room temperature. LH sections were incubated in a DNA-specific fluorescent probe (DAPI : 4',6-Diamidino-2-Phenylindole (1:50,000 in PBS)) for 30 min, washed 4 times for 10 min each in PBS, and mounted on glass microscope slides with PVA-DABCO. VTA sections were incubated for 17-20 h at 4 °C in a solution containing chicken anti-TH (Millipore; 1:500) in 3% NDS in Triton 0.1% in PBS. VTA sections were then washed 4 times for 10 min each in PBS before 2 h incubation at room temperature in a solution containing AlexaFluor 647 anti-chicken (Jackson ImmunoResearch Laboratories, Inc., West Grove, PA; 1:500) and DAPI (1:50,000) in 3% NDS in PBS. Sections were then washed 4 times for 10 min each in PBS and mounted on glass microscope slides with PVA-DABCO.

2.6.10 Confocal Microscopy

Fluorescence images were acquired using an Olympus FV1000 confocal laser scanning microscope with a 10x/0.40NA or a 40x/1.30NA oil immersion objective. Images were acquired

using FluoView software (Olympus, Center Valley, PA) to confirm viral expression and optrode/fiber placements (Figure S1, S4, S7). The center of the viral injection site was located by the presence of eYFP-expressing cell bodies. The tip of the fiber was determined by the presence of a lesion in the brain from the fiber tract. The tips of the electrodes were determined by the gliosis present around the electrolytic lesion sites.

2.6.11 Statistical Analysis

Statistical analyses were performed using commercial software (GraphPad Prism; GraphPad Software, Inc, La Jolla, CA; MATLAB, Mathworks, Natick, MA). Group comparisons were made using one-way or two-way ANOVA followed by Bonferroni post-hoc tests. Single variable comparisons were made with two-tailed paired or unpaired Student t-tests. Chi-squared analyses were used to compare populations. Tests for a binomial distribution were also used on single populations. Non-parametric Wilcoxon rank-sum tests were used to determine whether changes in firing rates were statistically significant in *in vivo* electrophysiological recordings (MATLAB) (see the section named *Analysis of in vivo awake-behaving lateral hypothalamic electrophysiological recordings* for details). Multiple comparisons were corrected for by adjusting p-values.

2.7 Supplemental Figures

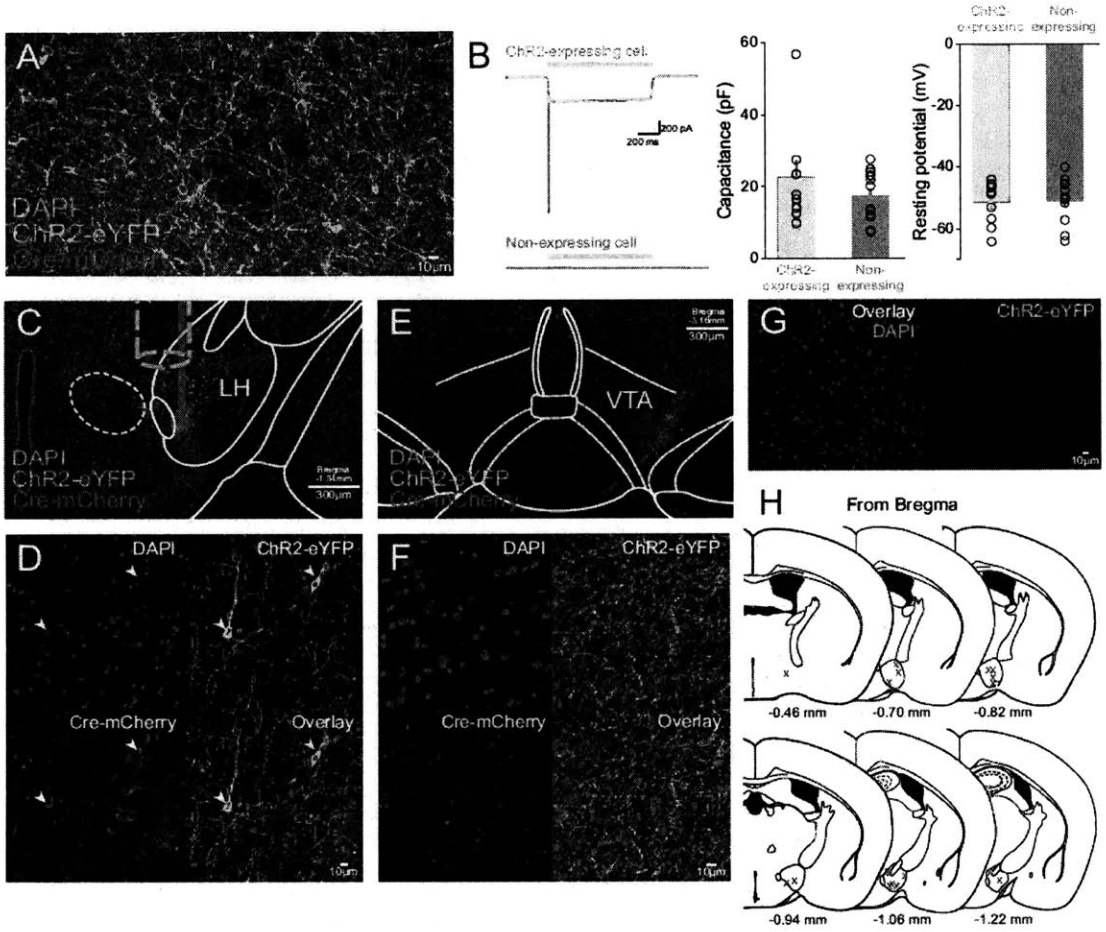

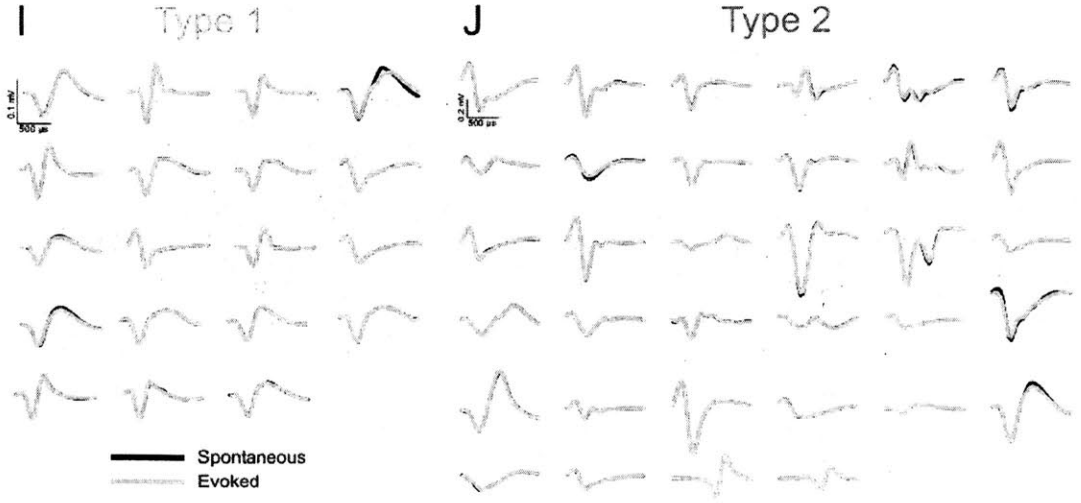

Figure S1. Related to Figures 1 and 2

Channelrhodopsin-2 (ChR2) expression in VTA-projecting LH neurons was achieved by injection of AAV_5-DIO-ChR2-eYFP into the LH and HSV-EF1α-mCherry-IRES-Cre into the VTA.

(A) High-magnification image of ChR2-expressing cell bodies in the LH.

(B) Horizontal brain slices were prepared and recordings were made from ChR2-expressing and non-expressing LH neurons using whole-cell patch-clamp electrophysiology. Example traces from a ChR2-expressing LH neuron (green) which responds to a 1 s constant 473 nm light pulse in voltage-clamp with a sustained inward photocurrent, and a non-expressing LH neuron (grey) which shows no response. Bar charts showing the whole-cell capacitance and resting membrane potential of all recorded ChR2-expressing (n=9) and non-expressing (n=14) LH neurons, which were not significantly different.

(C) Confocal image of the LH from a mouse implanted with an optrode (optical fiber surrounded by electrodes) and expressing ChR2 in LH-VTA projections. The location of both the optic fiber and the electrode tips from the optrode can be identified.

(D) High-magnification image of ChR2-expressing cell bodies within the LH in the vicinity of the electrode tip.

(E and F) (E) Low- and (F) high-magnification images of ChR2-expressing axon terminals located in the ipsilateral VTA.

(G) Injection of AAV_5-DIO-ChR2-eYFP in the LH without injection of HSV-EF1α-mCherry-IRES-Cre in the VTA leads to the absence of ChR2 expression in the LH.

(H) Placement of electrode tips of optrodes in animals used for *in vivo* electrophysiological recordings (Figures 1-4).

(I and J) All averaged waveforms of (I) Type 1 units and (J) Type 2 units recorded showing both spontaneous (black) and light-evoked (blue) action potential waveforms.

Error bars indicate ±SEM.

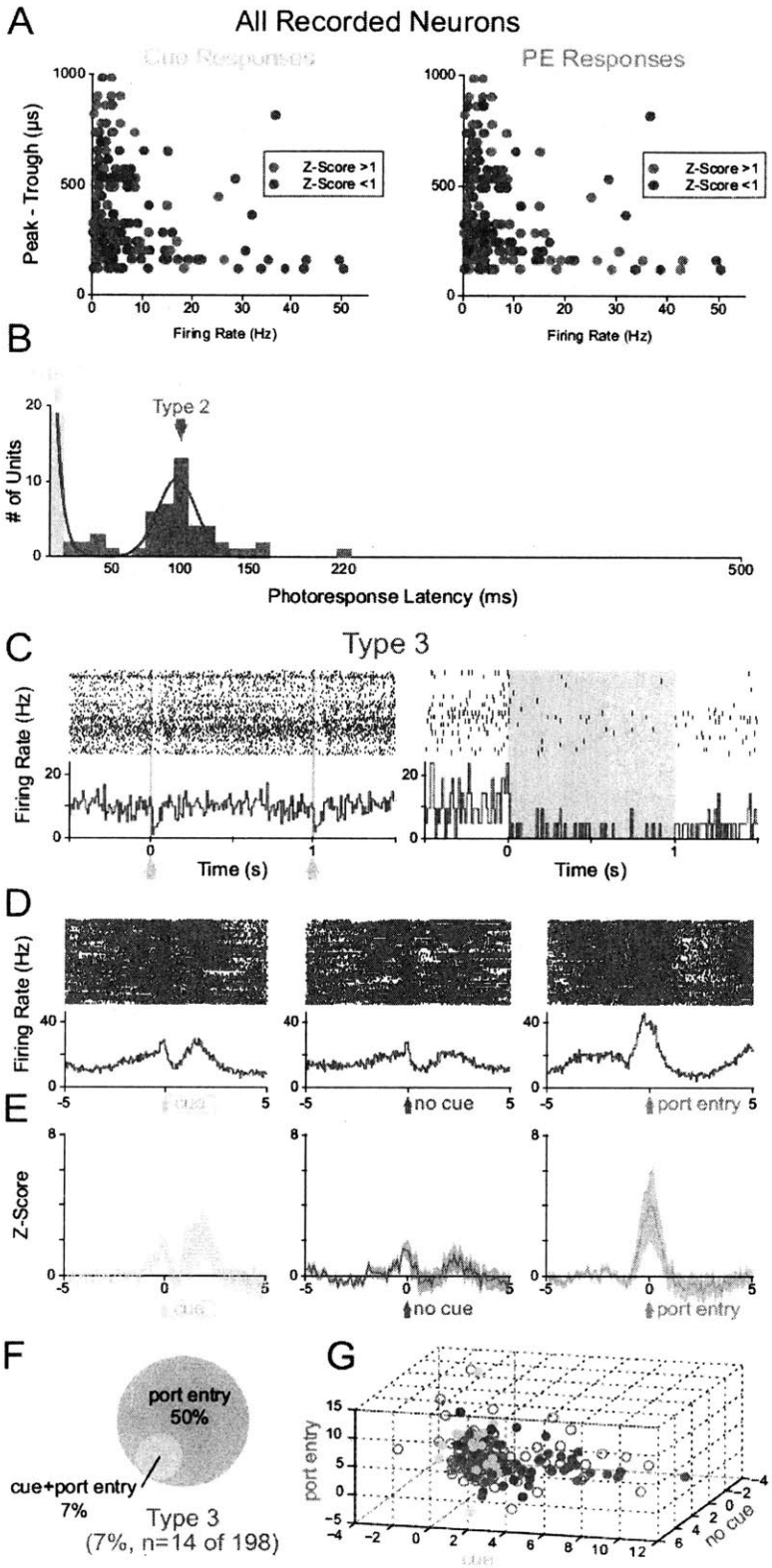
A
All Recorded Neurons
Cue Responses
PE Responses
Peak - Trough (µs)
Z-Score >1
Z-Score <1
Firing Rate (Hz)
B
Type 2
# of Units
Photoresponse Latency (ms)
C
Type 3
Firing Rate (Hz)
Time (s)
D
Firing Rate (Hz)
no cue
port entry
E
Z-Score
F
port entry
50%
cue+port entry
7%
Type 3
(7%, n=14 of 198)
G
port entry
no cue

Figure S2. Related to Figure 3

(A) Scatter plots showing peak-trough duration plotted against firing rate for all recorded neurons. Red indicates a Z-score greater than 1 and blue indicates a Z-score less than 1 during the experimental window for the cue responses (left panel) and port entry responses (right panel).

(B) Histogram showing the photoresponse latencies of recorded units up to the cutoff used for detection.

(C) Type 3 units are inhibited by blue light illumination in the LH (n=14/198 units, n=12 animals).

(D) Perievent raster histograms of a Type 3 unit that responds to the cue, nosepoke and port entry of the sucrose retrieval task.

(E) Population Z-score plots showing the average response of all Type 3 units.

(F) Of all Type 3 units, 50% responded exclusively to the port entry (n=7/14), while 7% responded to both the port entry and the reward-predictive cue (n=1/14).

(G) Graphical representation of Z-scores during the experimental windows for cue, no cue, and port entry, for Type 1, Type 2, Type 3, and no photoresponse units.

Error bars indicate ±SEM.

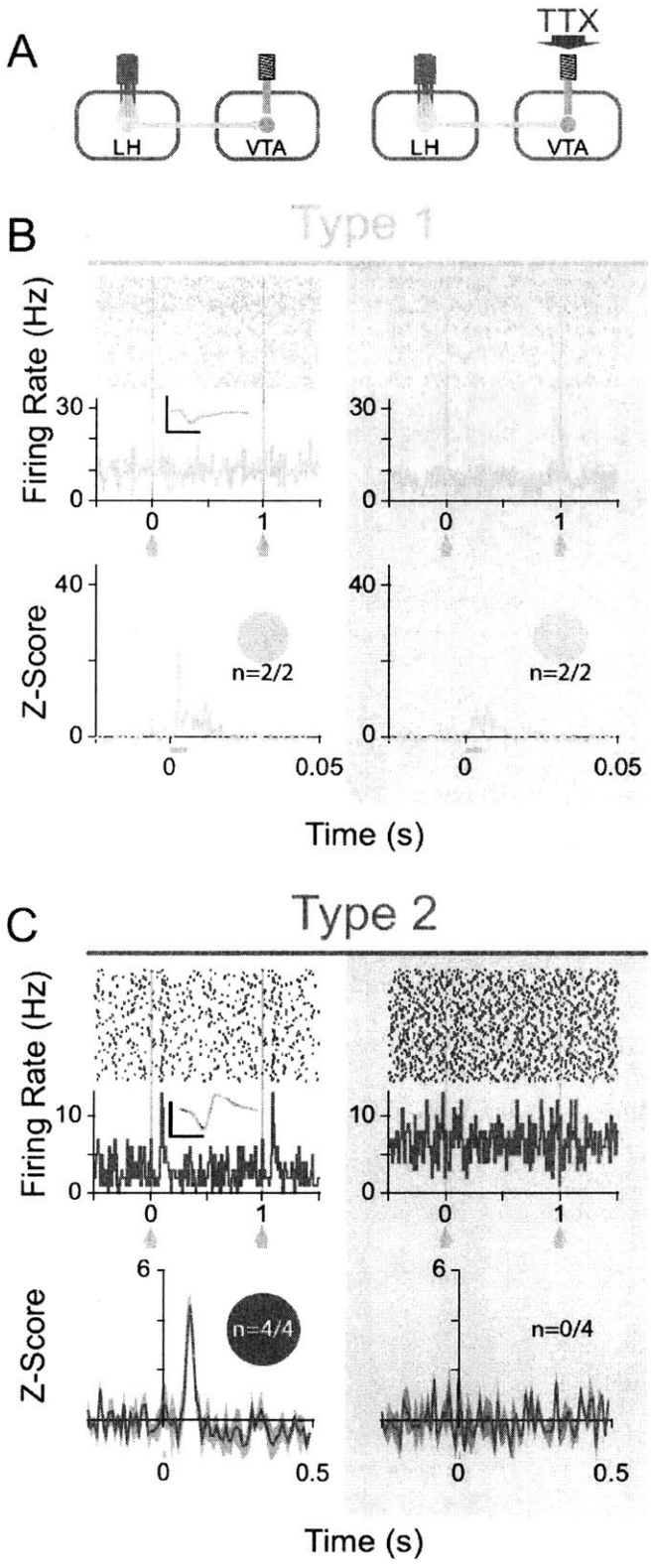
A
TTX
LH
VTA
LH
VTA
B
Type 1
Firing Rate (Hz)
30
0
0
1
30
0
0
1
Z-Score
40
0
n=2/2
0
0.05
40
0
n=2/2
0
0.05
Time (s)
C
Type 2
Firing Rate (Hz)
10
0
0
1
10
0
0
1
Z-Score
6
n=4/4
0
0.5
6
n=0/4
0
0.5
Time (s)

Figure S3. Related to Figure 2

(A) As a complementary approach to expressing halorhodopsin in the VTA to mediate inhibition, a cannula was implanted above the VTA, and tetrodotoxin (TTX) was infused to inhibit the VTA.

(B and C) (B) Type 1 (n=2/40 units, n=4 animals) photoresponse properties were unaffected (100%) by the inhibition of the VTA, (C) whereas Type 2 (n=4/40 units, n=4 animals) photoresponse properties were abolished (100%) by TTX inhibition of the VTA. Inset circles represent the number of units that were photoresponsive during each epoch.

Error bars indicate ±SEM.

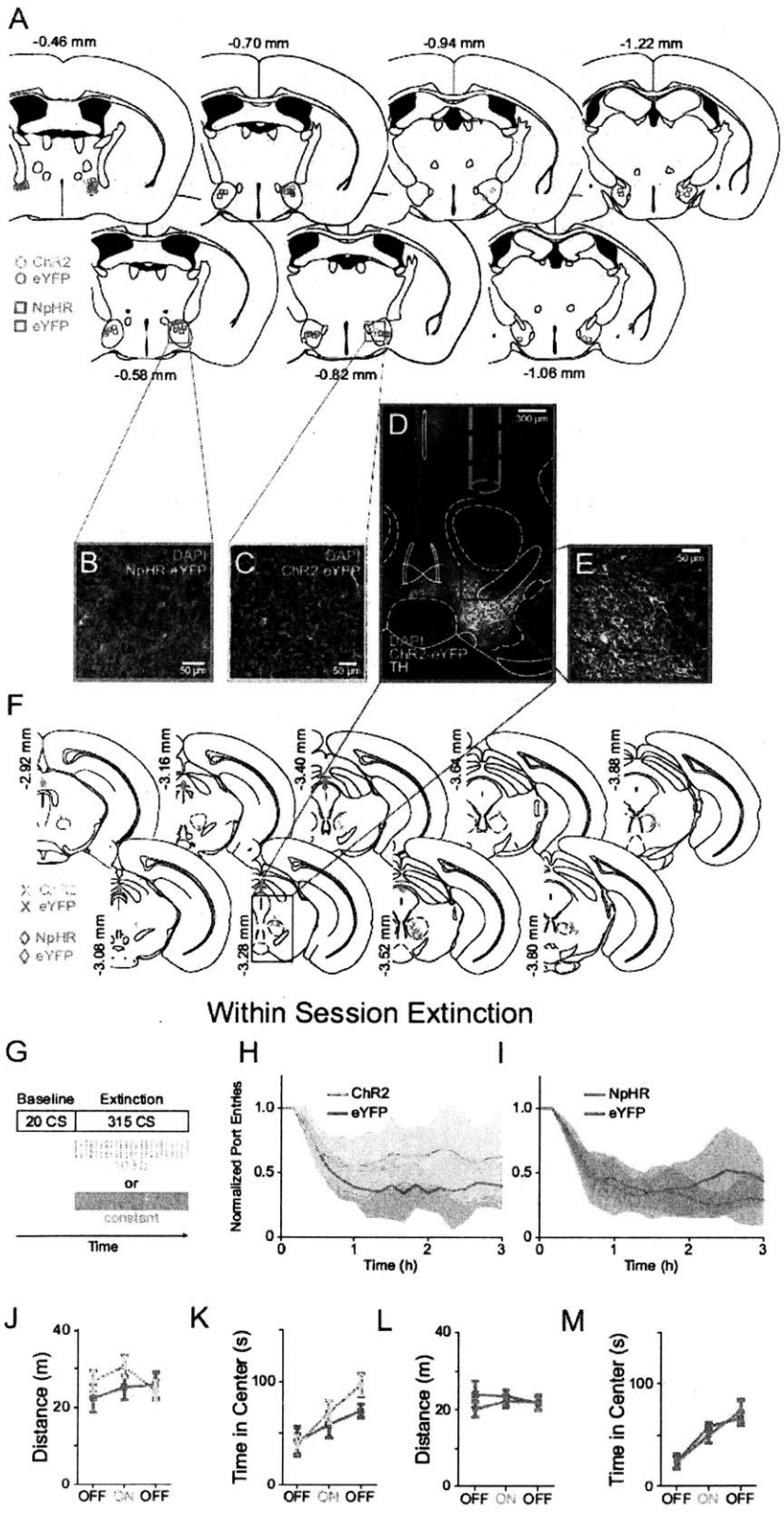
A
-0.46 mm
-0.70 mm
-0.94 mm
-1.22 mm
ChR2
eYFP
NpHR
eYFP
-0.58 mm
-0.82 mm
-1.06 mm
B
DAPI
NpHR eYFP
C
DAPI
ChR2 eYFP
D
DAPI
ChR2 eYFP
TH
E
F
-2.92 mm
-3.16 mm
-3.40 mm
-3.64 mm
-3.88 mm
-3.08 mm
-3.28 mm
-3.52 mm
-3.80 mm
ChR2
eYFP
NpHR
eYFP
Within Session Extinction
G
Baseline
Extinction
20 CS
315 CS
or
constant
Time
H
ChR2
eYFP
Normalized Port Entries
Time (h)
I
NpHR
eYFP
Time (h)
J
Distance (m)
OFF ON OFF
K
Time in Center (s)
OFF ON OFF
L
Distance (m)
OFF ON OFF
M
Time in Center (s)
OFF ON OFF

Figure S4. Related to Figure 5

(A) Injection sites in the LH for AAV_5-CaMKIIα-ChR2-eYFP (green), AAV_5-CaMKIIα-eNpHR3.0-eYFP (orange) and AAV_5-CaMKIIα-eYFP control (grey) in mice used for behavioral tasks in Figure 5.

(B and C) (B) High-magnification confocal image showing NpHR-expressing neurons and (C) ChR2-expressing neurons in the LH.

(D) Confocal image showing the placement of an optic fiber located above ChR2-expressing terminals within the VTA.

(E) High magnification image of ChR2-expressing fibers in the VTA surrounding TH+ cells.

(F) Location of optic fiber tips implanted above the VTA used to illuminate LH terminals.

(G) Following completion of the sucrose-seeking task, mice were tested for extinction resistance. After a baseline of 20 cues which were coupled with sucrose deliveries, 315 cues were given where no sucrose deliveries were made over a three hour period.

(H) Optical activation of LH terminals in the VTA during extinction showed a trend towards increasing extinction resistance in ChR2-expressing mice (n=7) compared with eYFP controls (n=7).

(I) Optical inhibition during extinction showed a trend towards decreasing extinction resistance in NpHR-expressing mice (n=10) compared with eYFP controls (n=8).

(J and K) ChR2-mediated excitation of LH terminals in the VTA had no effect on (J) locomotion or (K) anxiety compared with eYFP controls.

(L and M) Similarly, NpHR-mediated inhibition had no effect on (L) locomotion or (M) anxiety compared with eYFP controls.

Error bars indicate ±SEM.

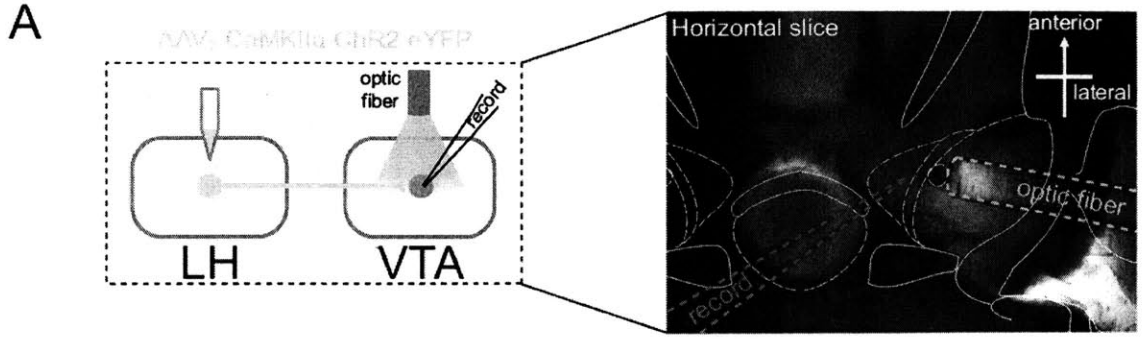

Dopamine Neurons

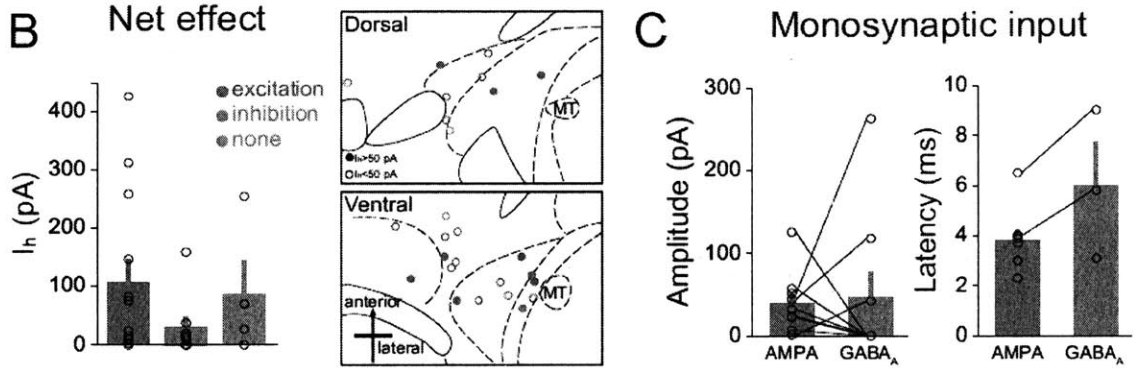

GABA Neurons

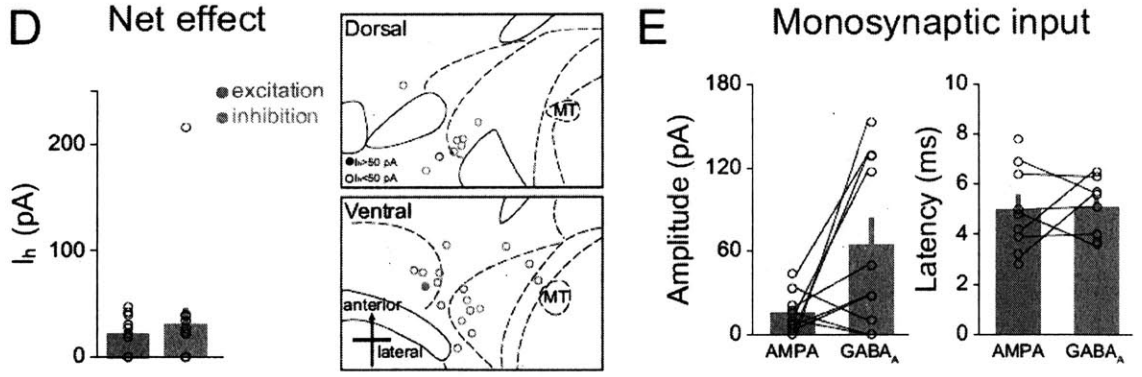

Figure S5. Related to Figure 6

(A) ChR2 was expressed in the LH by injection of AAV_5-CaMKIIα-ChR2-eYFP, and at least 6 weeks later brain slices were prepared containing the VTA. Example DIC image of a horizontal brain slice showing the location of the optic fiber resting on the slice (blue dashed line) and the recording electrode within the VTA (red dashed line).

(B) The net effect of optical stimulation of LH terminals on VTA dopamine neurons was assessed in current-clamp mode with a 5 ms 473 nm light pulse. Additionally, the hyperpolarization-activated cation current (I_h) was measured in voltage-clamp with a 1 s hyperpolarizing step from a holding potential of -50 mV to -120 mV. Bar chart displaying the mean amplitude of the I_h in TH+ neurons which responded with predominantly excitation (red), inhibition (blue) or showed no response (grey) to LH input. Horizontal brain maps showing the location of all recorded TH+ neurons with filled circles indicating an I_h amplitude of >50 pA and open circles indicating an amplitude of <50 pA.

(C) The composition of monosynaptic input was evaluated in voltage-clamp in the presence of TTX/4AP, with optically-evoked AMPAR-mediated currents (red) recorded at a holding potential of -70 mV and $GABA_AR$-mediated currents (blue) recorded at a holding potential of 0 mV. Bar charts showing the relative amplitude and latency of AMPAR-mediated and $GABA_AR$-mediated currents.

(D) Bar chart and horizontal maps displaying the I_h amplitude of VTA GABA neurons responding with either excitation or inhibition to optical stimulation of LH terminals.

(E) Bar charts showing the amplitude and latency of optically-evoked AMPAR-mediated and $GABA_AR$-mediated monosynaptic input onto VTA GABA neurons.

Error bars indicate ±SEM.

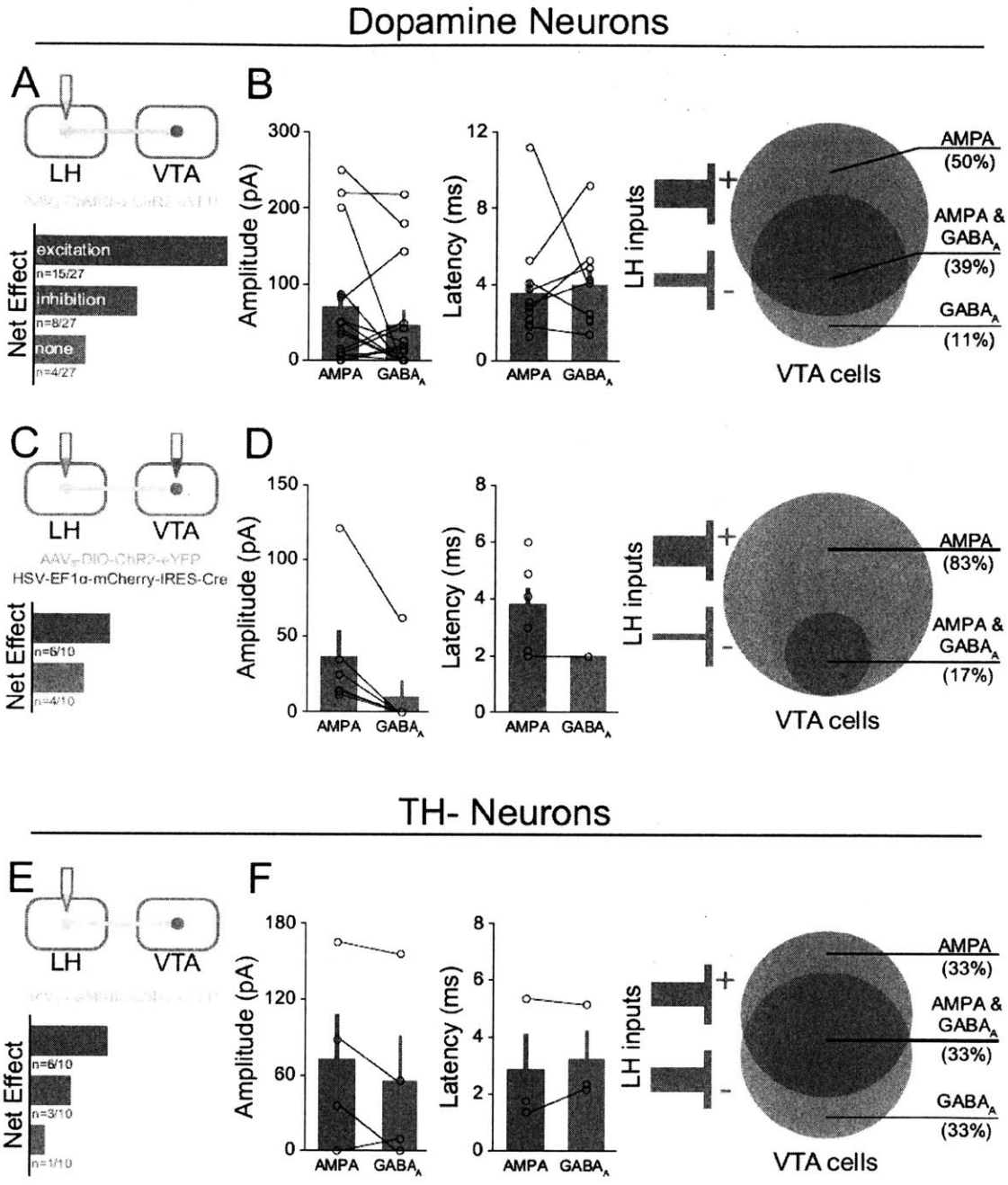
Dopamine Neurons
A
LH
VTA
Net Effect
excitation
n=15/27
inhibition
n=8/27
none
n=4/27
B
Amplitude (pA)
300
200
100
0
AMPA
GABA$_A$
Latency (ms)
12
8
4
0
AMPA
GABA$_A$
LH inputs
+
-
AMPA
(50%)
AMPA &
GABA$_A$
(39%)
GABA$_A$
(11%)
VTA cells
C
LH
VTA
AAV$_5$-DIO-ChR2-eYFP
HSV-EF1α-mCherry-IRES-Cre
Net Effect
n=6/10
n=4/10
D
Amplitude (pA)
150
100
50
0
AMPA
GABA$_A$
Latency (ms)
8
6
4
2
0
AMPA
GABA$_A$
LH inputs
+
-
AMPA
(83%)
AMPA &
GABA$_A$
(17%)
VTA cells
TH- Neurons
E
LH
VTA
Net Effect
n=6/10
n=3/10
n=1/10
F
Amplitude (pA)
180
120
60
0
AMPA
GABA$_A$
Latency (ms)
8
6
4
2
0
AMPA
GABA$_A$
LH inputs
+
-
AMPA
(33%)
AMPA &
GABA$_A$
(33%)
GABA$_A$
(33%)
VTA cells

Figure S6. Related to Figure 6

(A and C) ChR2-expression of LH terminals in the VTA was achieved either (A) by injection of AAV_5-CaMKIIα-ChR2-eYFP into the LH, or (C) by injection of AAV_5-DIO-ChR2-eYFP into the LH and HSV-EF1α-mCherry-IRES-Cre into the VTA. Optical stimulation of LH terminals in brain slices from these animals resulted in net excitation (red), net inhibition (blue) or no response (grey) in identified VTA dopamine neurons.

(B and D) Composition of the optically-evoked current recorded in voltage-clamp (in the absence of TTX/4AP) with bar charts showing the amplitude and latency of AMPAR-mediated and $GABA_AR$-mediated currents and Venn diagrams indicating the proportion of neurons receiving each type of input.

(E and F) (E) The net effect of optical stimulation on TH-immunonegative VTA neurons recorded in wild-type mice which had received an injection of AAV_5-CaMKIIα-ChR2-eYFP into the LH and (F) the amplitude, latency, and composition of optically-evoked currents recorded in voltage-clamp.

Error bars indicate ±SEM.

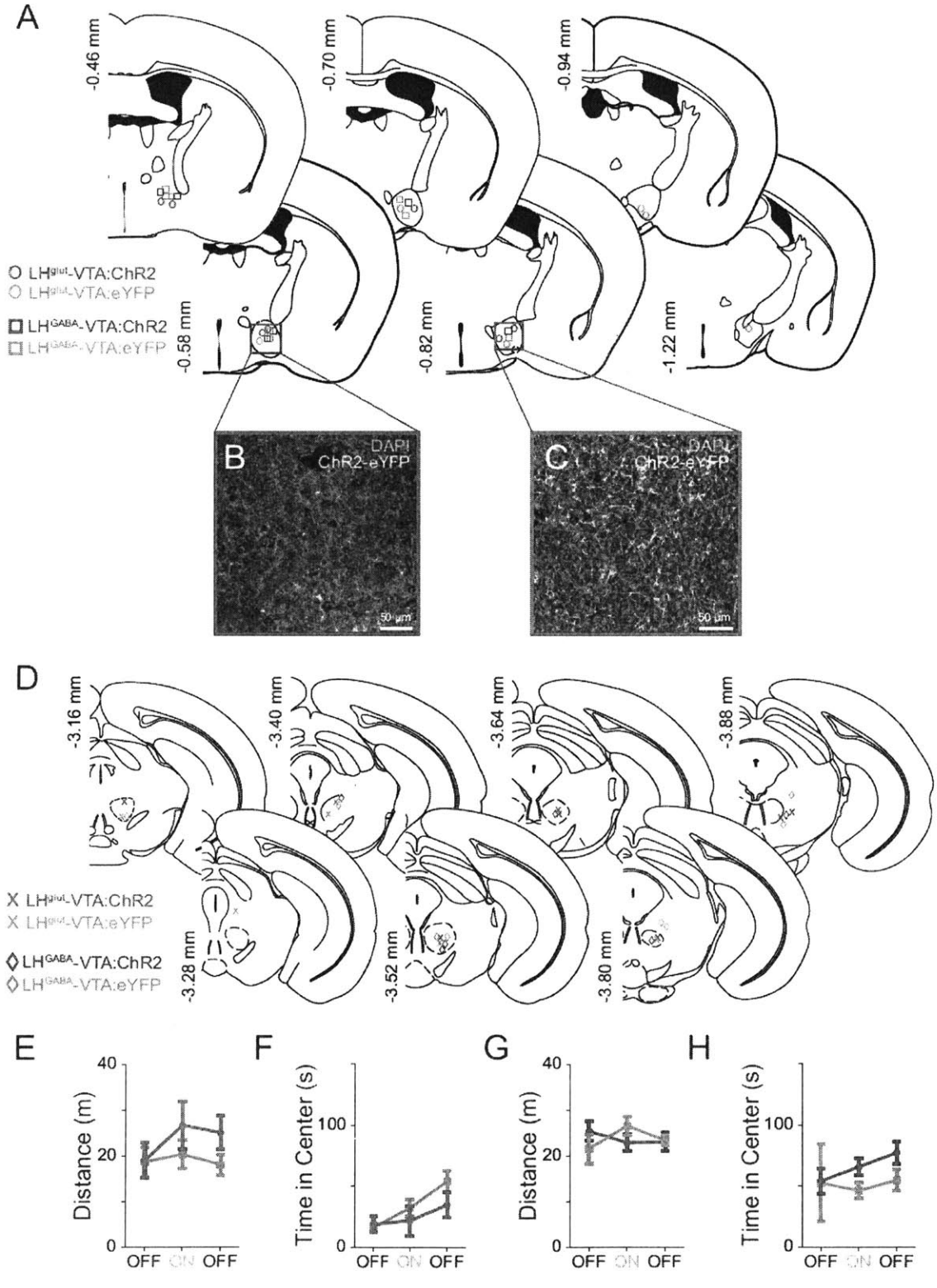
A
-0.46 mm
-0.70 mm
-0.94 mm
-0.58 mm
-0.82 mm
-1.22 mm
LHglut-VTA:ChR2
LHglut-VTA:eYFP
LHGABA-VTA:ChR2
LHGABA-VTA:eYFP
B
DAPI
ChR2-eYFP
50 µm
C
DAPI
ChR2-eYFP
50 µm
D
-3.16 mm
-3.40 mm
-3.64 mm
-3.88 mm
-3.28 mm
-3.52 mm
-3.80 mm
LHglut-VTA:ChR2
LHglut-VTA:eYFP
LHGABA-VTA:ChR2
LHGABA-VTA:eYFP
E
Distance (m)
40
20
0
OFF ON OFF
F
Time in Center (s)
100
0
OFF ON OFF
G
Distance (m)
40
20
0
OFF ON OFF
H
Time in Center (s)
100
0
OFF ON OFF

Figure S7. Related to Figure 7

(A) Injection sites for AAV_5-DIO-ChR2-eYFP in LH^{glut}-VTA:ChR2 (red) and LH^{GABA}-VTA:ChR2 (blue) mice and AAV_5-DIO-eYFP in eYFP control (grey) mice used for behavioral tasks in Figure 7.

(B and C) ChR2-expressing neurons in the LH of a (B) LH^{GABA}-VTA:ChR2 mouse and a (C) LH^{glut}-VTA:ChR2 mouse.

(D) Location of optic fiber tips implanted above the VTA used to illuminate terminals from the LH.

(E and F) Optical stimulation had no effect on (E) locomotion or (F) anxiety in LH^{glut}-VTA:ChR2 mice compared to LH^{glut}-VTA:eYFP controls.

(G and H) Optical stimulation also had no effect on (G) locomotion or (H) anxiety in LH^{GABA}-VTA:ChR2 mice compared to LH^{GABA}-VTA:eYFP controls.

Error bars indicate ±SEM.

Chapter 3

Lateral Hypothalamic Inputs to the VTA Bidirectionally Modulate Dopamine Release and Behavioral Activation

The excitatory and inhibitory inputs from the lateral hypothalamus to the ventral tegmental area play opposing roles in modulating motivational or consummatory behaviors through a disinhibition mechanism in the VTA to control dopamine release

Adapted from Nieh et al., Neuron (in press)

3.0 Contributions and Acknowledgements

Conception: Edward H. Nieh and Kay M. Tye

Surgical Injections and Implantations: Edward H. Nieh

Behavioral Experiments – Real Time Place Preference/Aversion: Edward H. Nieh, Romy Wichmann

Behavioral Experiments – Intracranial Self-Stimulation: Edward H. Nieh, Romy Wichmann, Kara N. Presbrey

Behavioral Experiments – Social Interaction: Edward H. Nieh, Romy Wichmann

Behavioral Experiments – Four-Chamber Novel Object: Edward H. Nieh, Romy Wichmann

Behavioral Scoring: Kara N. Presbrey, Ehsan M. Izadmehr

c-Fos Cell Counting: Romy Wichmann, Christopher A. Leppla, Kara N. Presbrey, Ehsan M. Izadmehr

Fast-Scan Cyclic Voltammetry: Caitlin M. Vander Weele

Fiber Photometry: Edward H. Nieh

Ex Vivo Patch-Clamp Experiments: Gillian A. Matthews

Histology: Edward H. Nieh, Gillian A. Matthews, Kara N. Presbrey, Ehsan M. Izadmehr, Caitlin M. Vander Weele

Confocal Microscopy: Edward H. Nieh, Gillian A. Matthews, Caitlin M. Vander Weele

3.1 Summary

Projections from the lateral hypothalamus (LH) to the ventral tegmental area (VTA), containing both GABAergic and glutamatergic components, encode conditioned responses and control compulsive reward-seeking behavior. GABAergic neurons in the LH have been shown to mediate appetitive and feeding-related behaviors. Here, we show that the GABAergic component of the LH-VTA pathway supports positive reinforcement and place preference, while the glutamatergic component mediates place avoidance. In addition, our results indicate that photoactivation of these projections modulates other behaviors, such as social interaction and perseverant investigation of a novel object. We provide evidence that photostimulation of the GABAergic LH-VTA component, but not the glutamatergic component, increases dopamine (DA) release in the nucleus accumbens (NAc) via inhibition of local VTA GABAergic neurons. Our study clarifies how GABAergic LH inputs to the VTA can contribute to generalized behavioral activation across multiple contexts, consistent with a role in increasing motivational salience.

3.2 Background

Dopamine (DA) release from ventral tegmental area (VTA) DA neurons promotes goal-directed behavior (Gallistel et al., 1985; Grace et al., 2007; Phillips et al., 2003), enhances the salience of environmental stimuli (Berridge and Robinson, 1998; Everitt et al., 1999; Wyvell and Berridge, 2000), increases behavioral vigor (Niv et al., 2006; Salamone et al., 2005, 1994), and mediates the reinforcing properties of rewards (Chiara and Imperato, 1988; Roberts and Koob, 1982; Wise, 2006). Importantly, excitotoxic lesions of the lateral hypothalamus (LH) evoke similar pathologies to those observed after DA-depletion – including aphagia (Grossman et al., 1978; Stricker et al., 1978) – which suggests that LH input to the VTA is a critical circuit element in modulating motivation, perhaps via its action on VTA DA neurons. Indeed, the LH provides one of the most robust inputs to the VTA (Phillipson, 1979; Watabe-Uchida et al., 2012).

The LH has historically been implicated in both reward processing (Hoebel and Teitelbaum, 1962; Olds and Milner, 1954) and feeding behaviors (Anand and Brobeck, 1951; Burton et al., 1976; Powley and Keesey, 1970). The cells that comprise the LH-VTA projection are diverse: glutamatergic, GABAergic, and/or peptidergic in nature. Several studies have shown modulatory effects of LH peptidergic populations on the VTA, including orexin/hypocretin (Borgland et al., 2006; Harris et al., 2005) and neurotensin (Kempadoo et al., 2013; Opland et al., 2013). While these studies clearly demonstrate that the peptidergic LH-VTA circuit modulates reward and motivation, recent studies have also highlighted the importance of GABA and glutamate in the LH. Jennings and colleagues identified a GABAergic population in the LH,

independent of the melanin-concentrating hormone (MCH) and orexin/hypocretin populations, that encodes reward-seeking or feeding (Jennings et al., 2015).

Additionally, we recently demonstrated that activation of the GABAergic LH projection to the VTA increases feeding, while the glutamatergic projection may play more of a regulatory role (Nieh et al., 2015). However, as previous studies have shown, feeding behavior can be driven by either the motivation to escape the negative affective state of hunger (Betley et al., 2015) or the motivation to obtain food as a primary reinforcer (Jennings et al., 2015). Our first goal was to determine whether the motivation to engage in feeding behavior evoked by GABAergic LH-VTA stimulation was due to the aversive drive state associated with hunger (negative valence) or the rewarding properties associated with food (positive valence).

Furthermore, previous studies have shown that nonspecific hypothalamic activation via electrical stimulation can elicit feeding, drinking, gnawing, motor effects, as well as sexual behaviors (Singh et al., 1996; Valenstein et al., 1968). As a result, our second goal was to investigate whether LH-VTA stimulation was specific to controlling feeding or generalizable across multiple motivated behaviors.

Finally, LH projections to the VTA likely influence motivation by modulating the activity of DA neurons. It has been suggested that activation of the glutamatergic component of the LH-VTA projection provides excitatory drive onto VTA DA neurons (Kempadoo et al., 2013; You et al., 2001). Kempadoo and colleagues showed that NMDA blockade in the VTA attenuates the ability of neurotensin-expressing LH-VTA projections to drive reward-seeking (Kempadoo et al., 2013). However, it is unknown how LH input to the VTA modulates DA release in downstream targets because the VTA is also a heterogeneous structure and contains

dopaminergic, GABAergic, and glutamatergic cell types (Dobi et al., 2010; Nair-Roberts et al., 2008). Therefore, our third goal was to elucidate the downstream effects of GABAergic and glutamatergic LH-VTA inputs on DA neurotransmission.

3.3 Results

3.3.1 Activation of the GABAergic or Glutamatergic LH-VTA Projection Promotes Approach or Avoidance, Respectively

In order to study the effect of GABAergic LH-VTA activation on behavior, we injected AAV_5-DIO-ChR2-eYFP or AAV_5-DIO-eYFP into the LH of vesicular GABA transporter (VGAT)::Cre mice and placed an optic fiber over the VTA to illuminate LH GABAergic axon terminals (Figure 1A and S1). To test whether stimulating the GABAergic component of the LH-VTA projection (LH^{GABA}-VTA) would support place preference or avoidance, we placed mice into a 3-chamber apparatus where one side of the chamber was paired with optical stimulation (473 nm, 10 Hz, 20 mW, 5 ms pulses; Figure 1B). Surprisingly, we found that LH^{GABA}-VTA:ChR2 mice spent significantly more time in the chamber paired with stimulation than the chamber without stimulation when compared with their eYFP counterparts (Figure 1B and 1C). In addition, to test whether LH^{GABA}-VTA activation could support intracranial self-stimulation (ICSS), we placed mice into an operant chamber with an active and inactive nosepoke operandum. An active nosepoke response was paired with a compound light/sound cue and optogenetic stimulation (473 nm, 10 Hz, 20 mW, 5 ms pulses, 1 s duration) and an inactive nosepoke response was paired only with a cue. LH^{GABA}-VTA:ChR2 mice made significantly more responses in the active nosepoke compared with the inactive nosepoke – an effect not observed in the eYFP controls (Figure 1D). These data show that mice prefer LH^{GABA}-VTA stimulation and are willing to perform an instrumental response in order to receive that stimulation.

In order to determine how activation of the glutamatergic component of the LH-VTA projection (LH^{glut}-VTA) influences motivation, we used the same optogenetic approach and behavioral assays described above in vesicular glutamate transporter 2 (VGLUT2)::Cre mice (Figure 1E and S1). In contrast to the robust preference supported by LH^{GABA}-VTA stimulation, activation of the glutamatergic projection was avoided by mice in the real-time place preference/avoidance assay (RTPP/A; Figure 1F and 1G). Consistent with these results, LH^{glut}-VTA:ChR2 mice did not show a preference for the active nosepoke in the ICSS task (Figure 1H). Taken together, these data suggest that activation of the glutamatergic component of the LH-VTA projection supports avoidance.

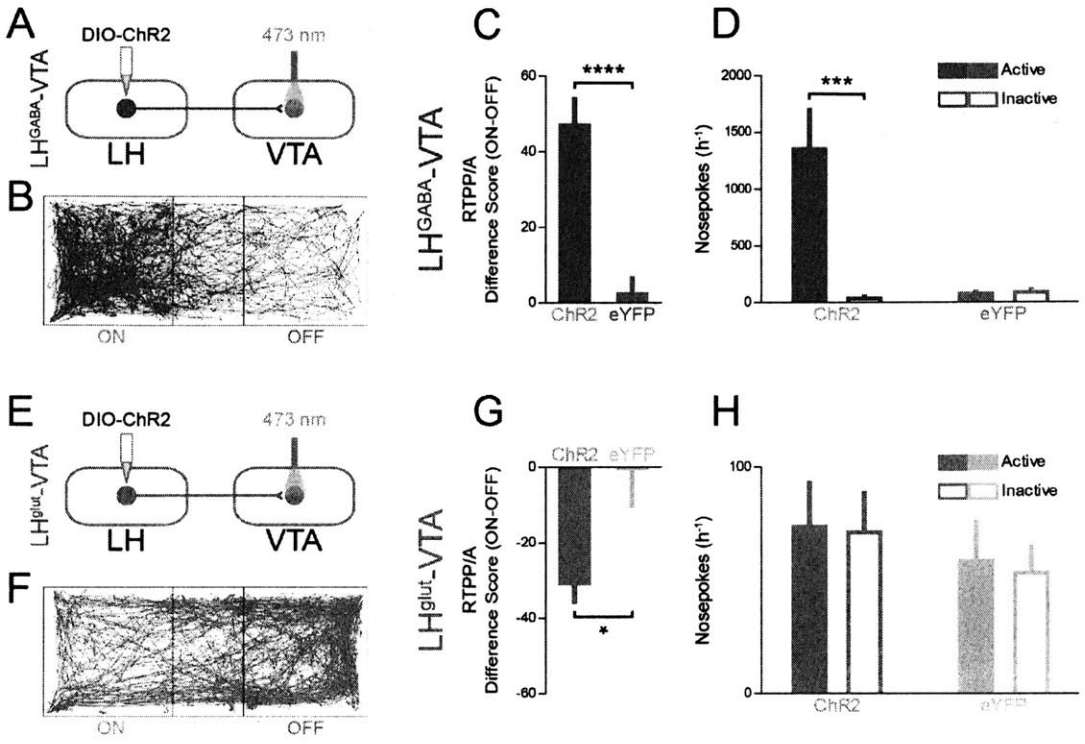
A
DIO-ChR2
473 nm
LH
VTA
LHGABA-VTA
B
ON
OFF
C
LHGABA-VTA
RTPP/A
Difference Score (ON-OFF)
****
ChR2
eYFP
D
***
Active
Inactive
Nosepokes (h-1)
ChR2
eYFP
E
DIO-ChR2
473 nm
LH
VTA
LHglut-VTA
F
ON
OFF
G
LHglut-VTA
RTPP/A
Difference Score (ON-OFF)
ChR2
eYFP
*
H
Active
Inactive
Nosepokes (h-1)
ChR2

Figure 1. Photostimulation of the GABAergic LH-VTA Projection Promotes Approach, While Activation of the Glutamatergic LH-VTA Projection Promotes Avoidance

(A) VGAT::Cre mice were injected with AAV_5-DIO-ChR2-eYFP or AAV_5-DIO-eYFP into the LH, and an optic fiber was implanted over the VTA.

(B) Representative track from the real-time place preference/avoidance (RTPP/A) assay of an LH^{GABA}-VTA:ChR2 mouse moving through an open chamber where one side was paired with blue light stimulation (473 nm, 10 Hz, 20 mW, 5 ms pulses).

(C) LH^{GABA}-VTA:ChR2 mice had a significantly greater difference score (percentage time spent in stimulation side minus percentage time spent in non-stimulation side) than LH^{GABA}-VTA:eYFP mice (n=8 ChR2, n=10 eYFP; two-tailed, unpaired Student's t-test, ****$p<0.0001$).

(D) LH^{GABA}-VTA:ChR2 mice made significantly more responses at the active nosepoke paired with blue light stimulation (473 nm, 10 Hz, 20 mW, 5 ms pulses, 1 s duration) than the inactive nosepoke as compared with eYFP controls (n=6 ChR2, n=8 eYFP; two-way ANOVA revealed a group x nosepoke interaction, $F_{1,12}=19.40$, $p=0.0009$; Bonferroni post-hoc analysis, ***$p<0.001$).

(E) VGLUT2::Cre mice were injected with AAV_5-DIO-ChR2-eYFP or AAV_5-DIO-eYFP into the LH, and an optic fiber was implanted over the VTA.

(F) Representative track from the RTPP/A assay of an LH^{glut}-VTA:ChR2 mouse.

(G) LH^{glut}-VTA:ChR2 mice had a significantly lower difference score than LH^{glut}-VTA:eYFP mice in the RTPP/A assay (n=7 ChR2, n=9 eYFP; two-tailed, unpaired Student's t-test, *p=0.0175).

(H) Optical stimulation did not have any significant effects on intracranial self-stimulation in LH^{glut}-VTA:ChR2 compared with eYFP controls (n=7 ChR2, n=6 eYFP; two-way ANOVA: group x nosepoke interaction, $F_{1,11}$=0.05, p=0.8307).

Error bars indicate ±SEM. See also Figures S1 and S2.

3.3.2 GABAergic and Glutamatergic Components of the LH-VTA Pathway Distinctly Modulate Motivated Behaviors

Next, we sought to determine whether stimulation of the LH^{GABA}-VTA projection could drive other behaviors in addition to feeding and approach. To assess the effect of LH^{GABA}-VTA stimulation on social interaction, VGAT::Cre mice with the same surgical injections and implants as described above were placed in a cage with a novel juvenile male or adult female intruder (Figure 2A). Time spent engaging in social interaction (e.g. grooming, investigating the face or hind regions, or mounting of the intruder) was measured for three consecutive three-minute epochs, during which blue light (473 nm, 20 Hz, 20 mW, 5 ms pulses) was used to activate LH^{GABA}-VTA projections throughout the second epoch. LH^{GABA}-VTA:ChR2 mice spent significantly more time interacting with both juvenile (Figure 2B) and female intruders (Figure 2C) during the stimulation epoch as compared with eYFP controls. In contrast, while we did not detect any significant differences in interaction with juvenile intruders between LH^{glut}-VTA:ChR2 mice and their controls, possibly due to a strong epoch effect (Figure 2D), we did find that LH^{glut}-VTA:ChR2 mice spent significantly less time interacting with female intruders during the stimulation epoch as compared with their controls (Figure 2E).

These data, together with our previous work (Nieh et al., 2015), suggest that the LH-VTA projection plays a role in multiple motivated behaviors, including feeding, approach/avoidance, and social interaction, with the GABAergic component promoting behavioral responding and the glutamatergic component suppressing it. Thus, we hypothesized that instead of playing a specific role in modulating each of these behaviors individually, the LH-VTA pathways might serve to change a larger behavioral state in the animal, such as a change in overall motivational level, that

can manifest as the investigation of any salient target, regardless of what that target object may be (e.g., food, social stimulus).

To test this, we placed experimental mice into an open field with four chambers, each containing a novel object (Figure 2F). Mice were allowed to explore the open field for one hour and were stimulated using blue light (473 nm, 20 Hz, 20 mW, 5 ms pulses) for three-minute epochs at three-minute intervals. Our goal was to determine if mice would spend more or less time with the most salient object, in this case the most proximal object, upon LH^{GABA}-VTA or LH^{glut}-VTA stimulation. We quantified the time spent investigating the objects and found that LH^{GABA}-VTA:ChR2 mice spent significantly more time investigating the objects during optical stimulation compared with eYFP controls (Figure 2G), while LH^{glut}-VTA:ChR2 mice spent significantly less time investigating objects during optical stimulation compared with their eYFP controls (Figure 2H). Additionally, we quantified the number of zone crossings, defined as transitions between zones, where each zone was the quadrant wherein each novel object was placed. LH^{GABA}-VTA:ChR2 mice made significantly fewer zone crossings during optical stimulation than eYFP controls (Figure 2I), while LH^{glut}-VTA:ChR2 made significantly more zone crossings during optical stimulation than their eYFP controls (Figure 2J). Together, these results suggest that activating the GABAergic LH-VTA projection promotes investigation of the most proximal salient object, while activating the glutamatergic projection reduces investigation of this object and increases exploration of the other chambers.

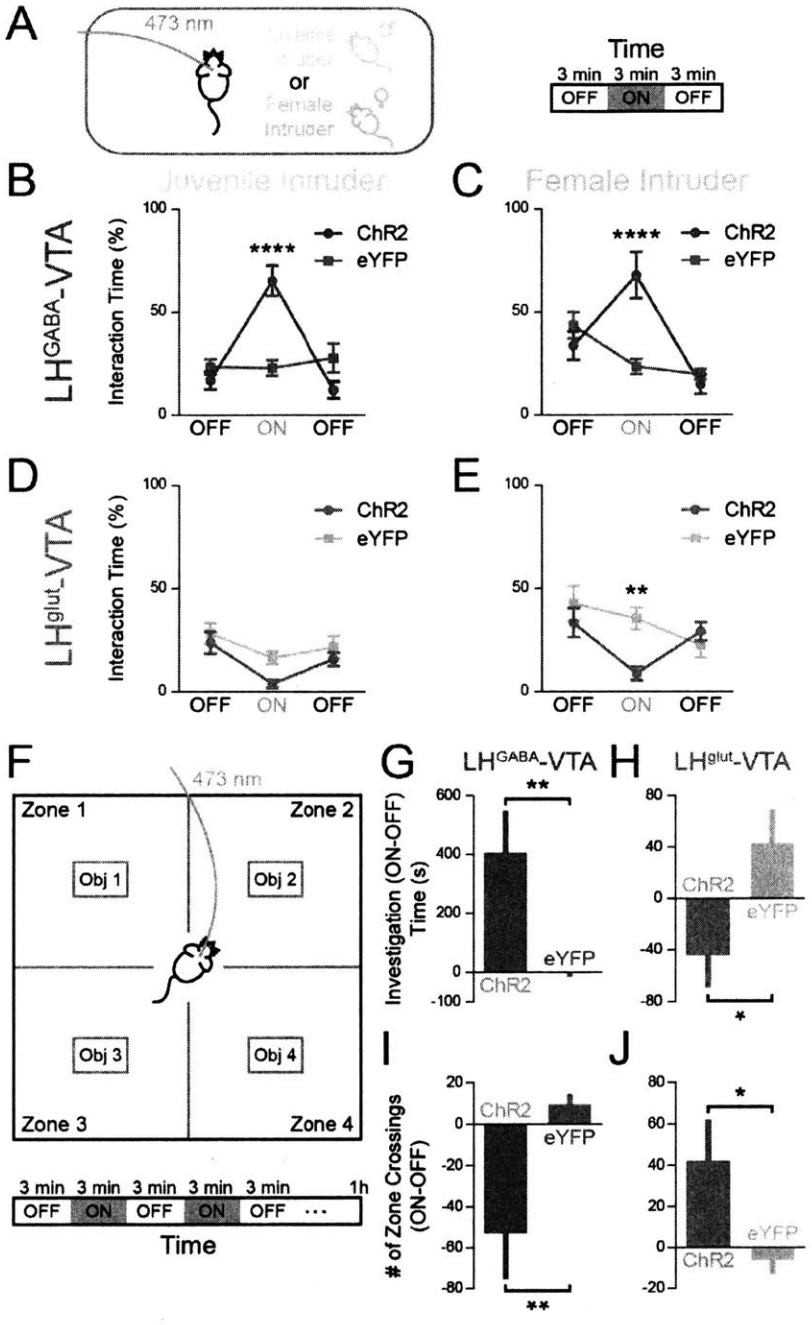
A
473 nm
or
Female Intruder
Time
3 min 3 min 3 min
OFF ON OFF
B
Juvenile Intruder
C
Female Intruder
LHGABA-VTA
Interaction Time (%)
ChR2
eYFP
****
OFF ON OFF
D
LHglut-VTA
E
**
F
473 nm
Zone 1
Zone 2
Obj 1
Obj 2
Obj 3
Obj 4
Zone 3
Zone 4
3 min 3 min 3 min 3 min 3 min 1h
OFF ON OFF ON OFF ...
Time
G
LHGABA-VTA
Investigation (ON-OFF) Time (s)
H
LHglut-VTA
I
# of Zone Crossings (ON-OFF)
J
*

Figure 2. Photostimulation of the GABAergic LH-VTA Projection Promotes Social Interaction and Object Investigation, while Photostimulation of the Glutamatergic LH-VTA Projection Suppresses These Behaviors

(A) To assess social interaction, mice were placed into a cage with a novel juvenile male or an adult female intruder. Time spent interacting was quantified for three consecutive three-minute epochs, with the second epoch paired with blue light stimulation (473 nm, 20 Hz, 20 mW, 5 ms pulses).

(B and C) (B) LH^{GABA}-VTA:ChR2 mice showed increased time spent interacting with juvenile male intruders compared with LH^{GABA}-VTA:eYFP controls during the ON epoch (n=10 ChR2, n=11 eYFP; two-way ANOVA revealed a group x epoch interaction, $F_{2,38}=23.62$, $p<0.0001$; Bonferroni post-hoc analysis, ****$p < 0.0001$), (C) as well as with female intruders (n=11 ChR2, n=10 eYFP; two-way ANOVA revealed a group x epoch interaction, $F_{2,38}=10.05$, $p=0.0003$; Bonferroni post-hoc analysis, ****$p<0.0001$).

(D and E) (D) LH^{glut}-VTA:ChR2 mice did not show a significant difference in time spent interacting with juvenile male intruders compared with LH^{glut}-VTA:eYFP mice, likely due to a strong epoch effect (n=8 ChR2, n=12 eYFP; two-way ANOVA revealed a significant epoch effect, $F_{2,36}=10.05$, $p=0.0003$), (E) but did show a significant decrease in interaction during the ON epoch with female intruders (n=7 ChR2, n=6 eYFP; two-way ANOVA revealed a group x epoch interaction, $F_{2,22}=7.45$, $p=0.0034$; Bonferroni post-hoc analysis, **$p<0.01$).

(F) In order to examine the effects of GABAergic and glutamatergic LH-VTA stimulation on motivational salience, mice were placed into an open field chamber with four zones, each containing a novel object. Mice were allowed to freely explore the chamber for one hour while receiving blue light stimulation (473 nm, 20 Hz, 20 mW, 5 ms pulses) for three-minute epochs at three-minute intervals.

(G and H) (G) LH^{GABA}-VTA:ChR2 mice had a significantly greater difference score in time spent investigating the novel objects (ON-OFF) than their eYFP counterparts (n=7 ChR2, n=8 eYFP; two-tailed, unpaired Student's t-test, **p=0.0070), while (H) LH^{glut}-VTA:ChR2 mice had a significantly lower difference score than their respective eYFP counterparts (n=8 ChR2, n=7 eYFP; two-tailed, unpaired Student's t-test, *p=0.0250).

(I and J) (I) LH^{GABA}-VTA:ChR2 mice had a significantly lower difference score for the number of zone crossings (ON-OFF) than their eYFP counterparts (n=7 ChR2, n=8 eYFP; two-tailed, unpaired Student's t-test, **p=0.0080), while (J) LH^{glut}-VTA:ChR2 mice had a significantly higher difference score (n=8 ChR2, n=7 eYFP; two-tailed, unpaired Student's t-test, *p=0.0372) than their respective eYFP counterparts.

Error bars indicate ±SEM. See also Figures S1 and S2.

3.3.3 Inhibition of the GABAergic LH-VTA Pathway Attenuates Behavioral Responding in Motivated Animals

We next considered whether inhibiting the GABAergic or glutamatergic LH-VTA projection would be sufficient to produce changes in behavioral responding. In VGAT::Cre and VGLUT2::Cre mice, we bilaterally injected AAV_5-DIO-NpHR-eYFP or AAV_5-DIO-eYFP into the LH and implanted an optic fiber over the VTA (Figure S3). In the RTPP/A, ICSS, and juvenile/female social interaction assays, we did not detect any significant effects of inhibition of either projection on behavior (Figure S2C-H).

Previously, we demonstrated that activating the LH^{GABA}-VTA projection increased feeding in sated mice (Nieh et al., 2015). To explore the necessity of this projection in feeding, we placed food-restricted mice into an empty chamber with two cups, one of which contained a moist food pellet (Figure 3A). In addition to a significant group x epoch effect (Figure 3B), LH^{GABA}-VTA:NpHR mice showed a significantly greater decrease in time spent feeding during optical inhibition from the baseline epoch compared with eYFP controls (Figure 3C). However, LH^{glut}-VTA:NpHR mice did not show any change in time spent feeding upon optical inhibition compared with their eYFP controls (Figure 3D and 3E). In the four-chamber novel object test (Figure 3F), unrestricted LH^{GABA}-VTA:NpHR mice spent significantly less time investigating the objects (Figure 3G) and made significantly more zone crossings (Figure 3I) during optical inhibition when compared with eYFP controls. No significant differences were found upon LH^{glut}-VTA inhibition (Figure 3H and 3J).

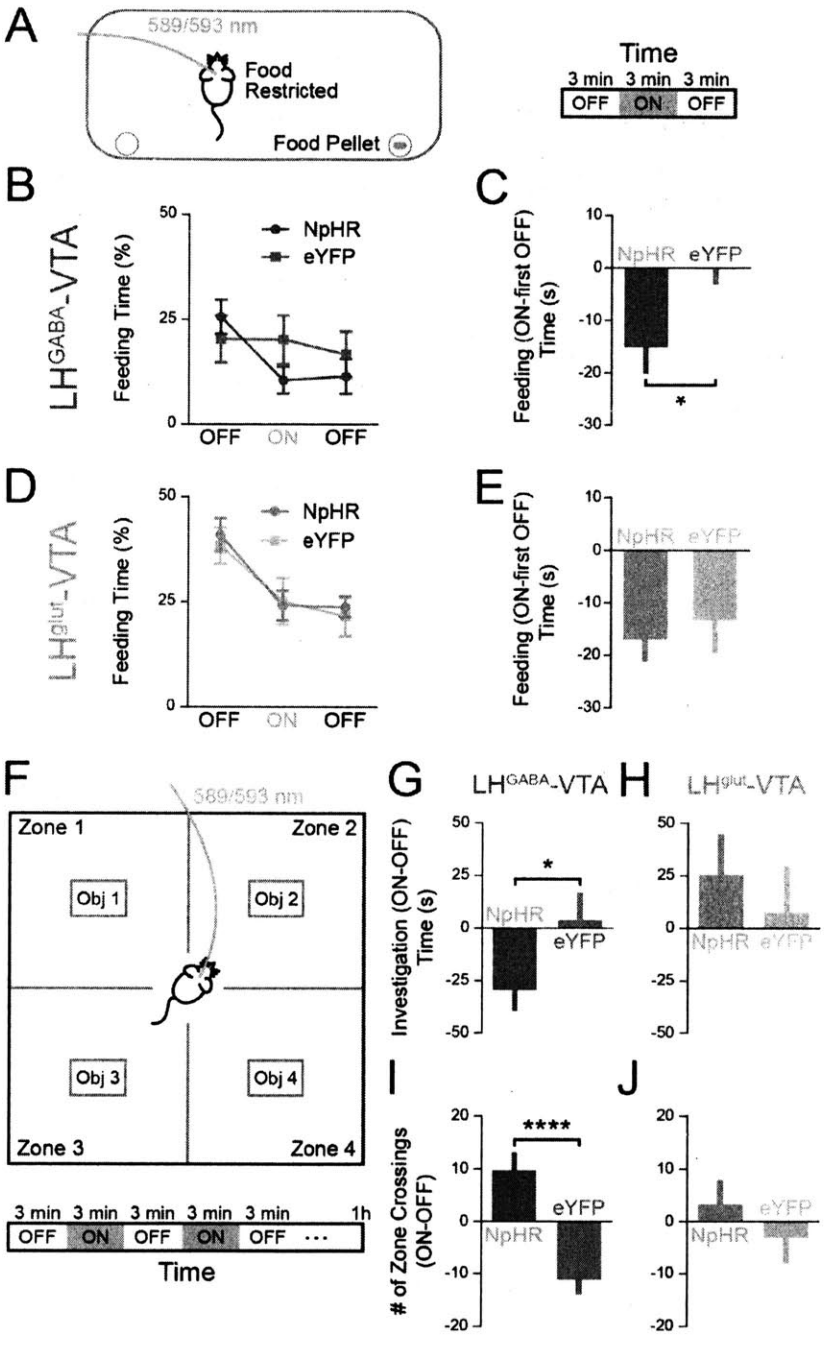
A
589/593 nm
Food Restricted
Food Pellet
Time
3 min 3 min 3 min
OFF ON OFF
B
LH GABA-VTA
Feeding Time (%)
NpHR
eYFP
OFF ON OFF
C
Feeding (ON-first OFF) Time (s)
NpHR eYFP
*
D
LH glut-VTA
Feeding Time (%)
NpHR
eYFP
OFF ON OFF
E
Feeding (ON-first OFF) Time (s)
NpHR eYFP
F
589/593 nm
Zone 1
Zone 2
Obj 1
Obj 2
Obj 3
Obj 4
Zone 3
Zone 4
3 min 3 min 3 min 3 min 3 min 1h
OFF ON OFF ON OFF ...
Time
G
LH GABA-VTA
Investigation (ON-OFF) Time (s)
*
NpHR
eYFP
H
LH glut-VTA
NpHR eYFP
I
# of Zone Crossings (ON-OFF)
****
eYFP
NpHR
J
eYFP
NpHR

Figure 3. Inhibition of the GABAergic LH-VTA Projection of Animals in a Motivated State Suppresses Behavioral Responding

(A) Food-restricted mice were placed into an empty chamber with two cups, one of which held a moist food pellet, while the other was empty. Time spent feeding was quantified for three consecutive three-minute epochs, with the second epoch paired with yellow light stimulation (589/593 nm, constant, 5 mW).

(B) There was a significant interaction of light stimulation on time spent feeding in LHGABA-VTA:NpHR mice relative to eYFP controls (n=8 NpHR, n=9 eYFP; two-way ANOVA revealed a group x epoch interaction, F2,30=4.46, p=0.0202).

(C) In addition, LH^{GABA}-VTA:NpHR mice had a significantly lower difference score in time spent feeding (ON-first OFF) when compared with eYFP controls (n=8 NpHR, n=9 eYFP; two-tailed, unpaired Student's t-test, *p=0.0210).

(D and E) (D) Meanwhile, no effect was found in LH^{glut}-VTA:NpHR mice and their controls on the amount of time spent feeding (n=10 NpHR, n=7 eYFP; two-way ANOVA: group x epoch interaction, $F_{2,30}$=0.17, p=0.8484), or (E) in difference score (n=10 NpHR, n=7 eYFP; two-tailed, unpaired Student's t-test, p=0.5963).

(F, G, and H) (F) In the four-chamber novel object test, (G) LH^{GABA}-VTA:NpHR mice had a significantly lower difference score in investigation time (ON-OFF) than eYFP controls (n=7 NpHR, n=8 eYFP; two-tailed, unpaired Student's t-test, *p=0.0305), while (H) LH^{glut}-VTA:NpHR mice showed no differences from their eYFP controls (n=10 NpHR, n=7 eYFP; two-tailed, unpaired Student's t-test, p=0.5358).

(I and J) (I) LH^{GABA}-VTA:NpHR mice also had a significantly greater difference score in the number of zone crossings (ON-OFF) than eYFP controls (n=8 NpHR, n=8 eYFP; two-tailed, unpaired Student's t-test, ****$p<0.0001$), while (J) LH^{glut}-VTA:NpHR mice showed no differences from their eYFP controls (n=10 NpHR, n=7 eYFP; two-tailed, unpaired Student's t-test, $p=0.3247$).

Error bars indicate ±SEM. See also Figures S2 and S3.

3.3.4 Modulation of Dopamine Release in the Nucleus Accumbens by LH-VTA Projections

We next examined the consequence of LH^{GABA}-VTA and LH^{glut}-VTA activation on the activity of dopaminergic and non-dopaminergic neurons in the VTA. We quantified the co-expression of c-Fos (an immediate early gene used to indicate recent neural activity) and tyrosine hydroxylase (TH; the rate-limiting enzyme in DA synthesis) in the VTA of mice that had received either GABAergic or glutamatergic LH-VTA stimulation (Figure 4A). This revealed that LH^{GABA}-VTA stimulation induced more c-Fos+ DA (TH+) neurons than LH^{glut}-VTA stimulation (Figure 4B), suggesting that stimulation of the LH^{GABA}-VTA pathway enhances the activity of VTA DA neurons.

We next explored how activation of the LH^{GABA}-VTA pathway influences downstream DA signaling in the nucleus accumbens (NAc) using *in vivo* fast-scan cyclic voltammetry (FSCV) (Figures 4 and S4). We found that LH^{GABA}-VTA activation robustly increased extracellular DA concentration ([DA]) in the NAc (Figure 4C-F). In many subjects, evoked DA release was composed primarily of individual phasic DA release events, or 'transients' (Figures 4D and S4B), which are indicative of phasic firing of VTA DA neurons (Dreyer et al., 2016; Owesson-White et al., 2012). To further confirm recorded signals as DA, mice were administered the D_2 receptor antagonist, raclopride, which is known to increase [DA] and DA transients in the NAc (Andersson et al., 1995; Aragona et al., 2008). In the presence of D_2 receptor antagonism, LH^{GABA}-VTA stimulation significantly increased DA neurotransmission in the NAc (Figure 4G-I and S4C).

In contrast, LH^{glut}-VTA activation (Figure 4J) caused a decrease in current at the oxidation potential for DA, indicative of a pause in DA neurotransmission in the NAc, leading to

a significant reduction in [DA] at baseline (Figures 4K-M and S4D) and after D_2 receptor blockade (Figures 4N-P and S4E). Consistent with the idea that LH^{glut}-VTA activation results in suppression of activity in NAc-projecting VTA DA neurons, stimulation offset often evoked a phasic DA transient (Figure 4K and S4D) – likely resulting from rebound activity arising from prolonged hyperpolarization of VTA DA cell bodies. Together, these data indicate that GABAergic and glutamatergic LH-VTA projections bidirectionally modulate DA release, with the GABAergic projection increasing DA release and the glutamatergic projection decreasing DA release in the NAc.

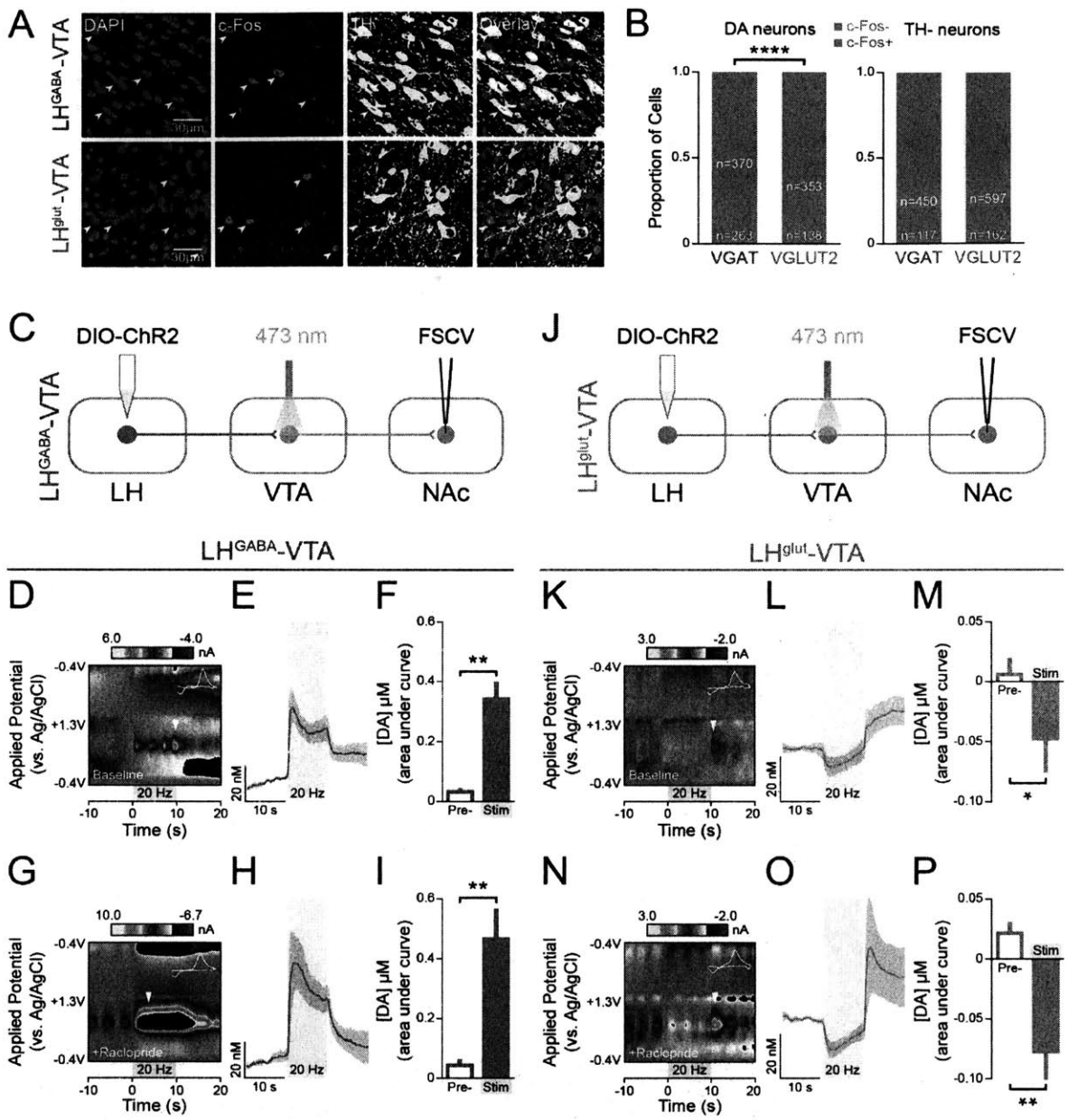
A
DAPI
c-Fos
TH
Overlay
LHGABA-VTA
LHglut-VTA
B
DA neurons
TH- neurons
c-Fos-
c-Fos+
****
Proportion of Cells
n=370
n=353
n=450
n=597
VGAT
VGLUT2
C
DIO-ChR2
473 nm
FSCV
LHGABA-VTA
LH
VTA
NAc
J
LHglut-VTA
LHGABA-VTA
LHglut-VTA
D
E
F
K
L
M
Applied Potential (vs. Ag/AgCl)
Baseline
20 Hz
Time (s)
[DA] µM (area under curve)
Pre-
Stim
G
H
I
N
O
P
+Raclopride

Figure 4. Optogenetic Activation of the GABAergic LH-VTA Projection Increases, while Activation of the Glutamatergic LH-VTA Projection Suppresses, Dopamine Release in the NAc

(A) Representative confocal images from the VTA of LH^{GABA}-VTA:ChR2 (top) and LH^{glut}-VTA:ChR2 (bottom) mice showing c-Fos+ (red) and TH+ (yellow) neurons in the VTA after photostimulation (473 nm, 20 Hz, 20 mW, 5 ms pulses, 10 min duration).

(B) Proportion of DA (TH+) neurons (left) and TH- neurons (right) that either co-express or do not co-express c-Fos after LH^{GABA}-VTA or LH^{glut}-VTA photostimulation. Mice receiving LH^{GABA}-VTA stimulation showed a significantly greater proportion of cells co-expressing TH and c-Fos compared with mice receiving LH^{glut}-VTA stimulation (Chi-square=21.77, ****$p<0.0001$).

(C) VGAT::Cre mice were injected with AAV_5-DIO-ChR2-eYFP into the LH, and an optic fiber was implanted over the VTA. Anesthetized fast-scan cyclic voltammetry (FSCV) recordings were obtained from the nucleus accumbens (NAc).

(D and E) Optical activation of the LH^{GABA}-VTA projection evoked DA release in the NAc. (D) Representative false color plot showing an increase in current at the oxidation potential for DA (~0.65 V) upon LH^{GABA}-VTA photostimulation (473 nm, 20 Hz, 20 mW, 5 ms pulses, 10 s duration), (E) which is also evident in the averaged population data after conversion into DA concentration.

(F) Quantification of extracellular DA concentration ([DA]) as area under the curve showed that LH^{GABA}-VTA stimulation caused a significant increase in DA release in the NAc (compared with pre-stimulation; n=6 mice; two-tailed, paired Student's t-test, **p=0.0013).

(G and H) Under D_2 receptor blockade (intraperitoneal (IP) raclopride), LH^{GABA}-VTA stimulation also increased NAc DA neurotransmission (G) as seen in the representative color plot (H) and averaged population data.

(I) Quantification of [DA] as area under the curve revealed a significant increase in DA release under D_2 receptor blockade (n=6 mice; two-tailed, paired Student's t-test, **p=0.0037).

(J) VGLUT2::Cre mice were prepared for FSCV as described above for VGAT::Cre mice.

(K and L) LH^{glut}-VTA stimulation caused a pause in NAc DA release under resting, baseline conditions. (K) Representative false color plot showing a decrease in current at the oxidation potential for DA in response to LH^{glut}-VTA stimulation (473 nm, 20 Hz, 20 mW, 5 ms pulses, 10 s duration). Stimulation offset was accompanied by a "rebound" DA transient, likely caused by rebound firing following hyperpolarization of VTA DA neurons during stimulation, which was also observed in the (L) averaged population data after conversion to [DA].

(M) Quantification of [DA] as area under the curve showed that LH^{glut}-VTA stimulation caused a significant decrease in [DA] in the NAc under resting conditions (n=5 mice; two-tailed, paired Student's t-test, *p=0.0325).

(N and O) Under the influence of raclopride, LH^{glut}-VTA activation robustly inhibited NAc DA release observed in the (N) representative color plot and (O) population average.

(P) Quantification of [DA] showed that LH^{glut}-VTA activation caused a significant and robust decrease in [DA] under D_2 receptor blockade (n=6 mice; two-tailed, paired Student's t-test, **p=0.0089).

Color plot insets: cyclic voltammograms (CVs) at time-points indicated by the inverted white triangles. Error bars indicate ±SEM. See also Figure S4.

3.3.5 Effects of GABAergic LH-VTA Stimulation on Dopamine Neurotransmission Occur Via Disinhibition in the VTA

Our previous work demonstrated that GABAergic neurons in the VTA receive both monosynaptic GABAergic and glutamatergic input from the LH (Nieh et al., 2015), and previous studies have shown that VTA GABA neurons inhibit VTA DA neurons (Tan et al., 2012; van Zessen et al., 2012). Together with our results from FSCV, we hypothesized that activation of the GABAergic projection from the LH elicits DA release in the NAc by suppressing the inhibition of VTA DA neurons by local VTA GABA neurons.

In order to test this hypothesis, we simultaneously photostimulated the GABAergic LH-VTA projection while recording the neural activity of VTA GABA neurons. To achieve this, we used a combination of the red-shifted depolarizing opsin, ChrimsonR (Klapoetke et al., 2014), and the genetically-encodable calcium indicator, GCaMP6m (Chen et al., 2013b). We injected VGAT::Cre mice with AAV_8-hSyn-FLEX-ChrimsonR-tdTomato into the LH and AAV_5-CAG-FLEX-GCaMP6m into the VTA and implanted two optic fibers over the VTA (Figure 5A-C). This enabled us to shine yellow (593 nm) light into the VTA through one optic fiber to activate GABAergic axon terminals arising from the LH expressing ChrimsonR, while shining low levels of blue light (473 nm, 30-80 μW, constant) through the second optic fiber to excite GCaMP6m expressed in VTA GABA neurons and measure emitted green (525 nm) fluorescence using fiber photometry (Gunaydin et al., 2014). In control mice, we injected AAV_5-DIO-eYFP into the VTA instead of AAV_5-CAG-FLEX-GCaMP6m to observe changes in fluorescence that could be due to movement-related or other artifacts. In awake mice, freely moving in their home cage, we activated the LH^{GABA}-VTA projection with either 20 Hz (593 nm, 5-10mW, 5 ms pulses, 1 s

duration) or constant yellow light (593 nm, 5-10 mW, 1 s duration) and observed a significant decrease in emitted fluorescence when compared with pre-stimulation fluorescence and fluorescence from control mice (Figure 5D and 5E). This significant decrease in fluorescence reflects a decrease in VTA GABA neural activity and suggests that LH^{GABA}-VTA stimulation significantly reduces activity in VTA GABA neurons.

Finally, we performed whole-cell patch-clamp recordings from VTA TH+ (dopamine) and TH- (putative GABA) neurons in VGAT::Cre and VGLUT2::Cre mice (Figure 6A). This revealed that the amplitudes of inhibitory postsynaptic currents (IPSCs) elicited by LH^{GABA}-VTA stimulation were significantly greater in putative GABA neurons compared with DA neurons in the VTA (Figure 6B). Similarly, the amplitudes of excitatory postsynaptic currents (EPSCs) elicited by LH^{glut}-VTA stimulation were also significantly greater in putative GABA neurons compared with DA neurons in the VTA (Figure 6C). These data suggest that although the LH sends excitatory and inhibitory projections to both DA and GABA neurons in the VTA (Nieh et al., 2015), the relative strengths of these inputs is greater onto putative GABA neurons. Taken together, our data show that activating an inhibitory projection from the LH to the VTA supports appetitive behaviors though inhibition of VTA GABA neurons, which causes disinhibition of DA neurons to increase DA release in the NAc (Figure 6D).

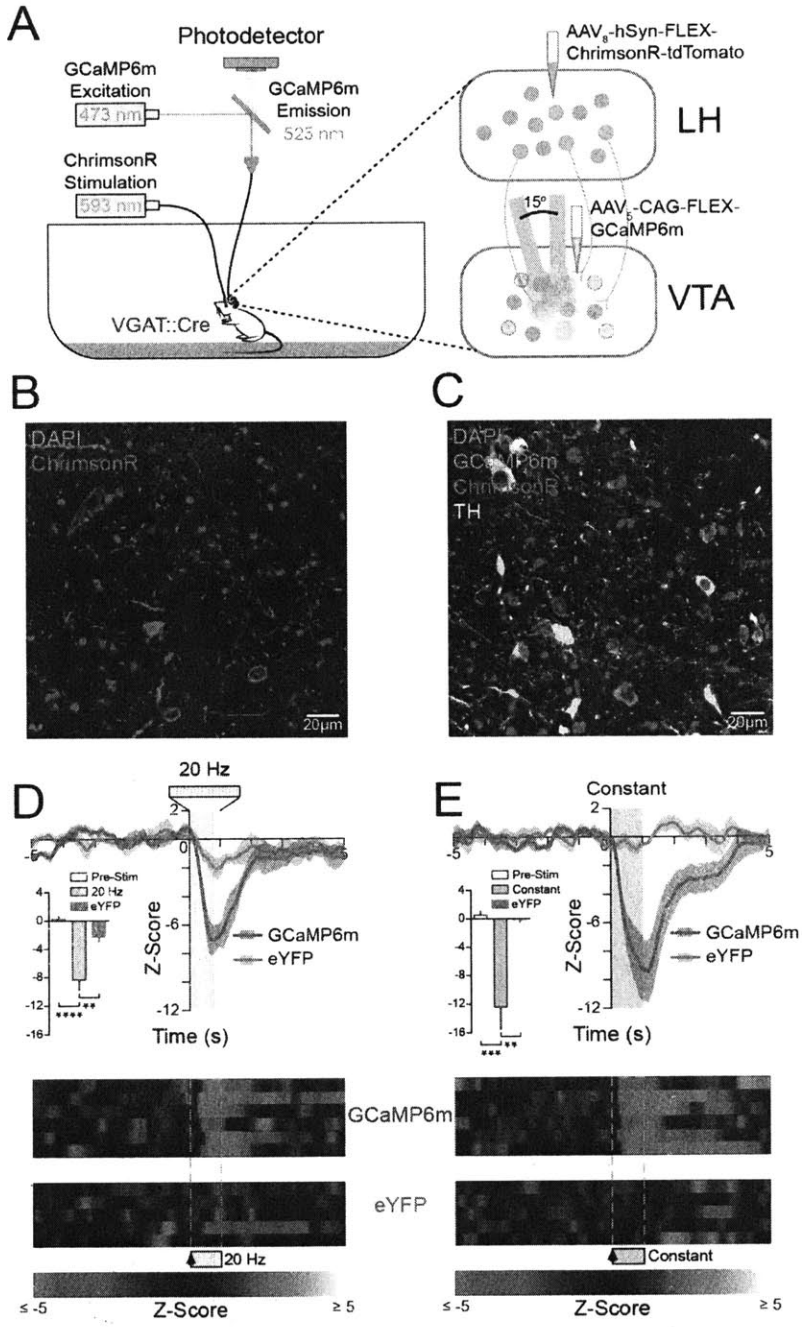
A
Photodetector
GCaMP6m Excitation
473 nm
GCaMP6m Emission
525 nm
ChrimsonR Stimulation
593 nm
VGAT::Cre
AAV9-hSyn-FLEX-ChrimsonR-tdTomato
LH
15°
AAV5-CAG-FLEX-GCaMP6m
VTA
B
DAPI
ChrimsonR
20μm
C
DAPI
GCaMP6m
ChrimsonR
TH
20μm
D
20 Hz
Pre-Stim
20 Hz
eYFP
Z-Score
GCaMP6m
eYFP
Time (s)
E
Constant
Pre-Stim
Constant
eYFP
Z-Score
GCaMP6m
eYFP
Time (s)
GCaMP6m
eYFP
20 Hz
Constant
≤ -5
Z-Score
≥ 5

Figure 5. GABAergic LH Inputs Inhibit GABA Neurons in the VTA

(A) In order to activate GABAergic LH-VTA projections and record from GABA neurons in the VTA simultaneously, VGAT::Cre mice were injected with AAV_8-hSyn-FLEX-ChrimsonR-tdTomato into the LH and AAV_5-CAG-FLEX-GCaMP6m into the VTA with two optic fibers implanted over the VTA.

(B) Confocal image showing ChrimsonR+ cells bodies in the LH (red).

(C) Confocal image showing GCaMP6m+ cell bodies in the VTA (green), ChrimsonR+ fibers (red), and TH+ neurons (white).

(D) 20 Hz LH^{GABA}-VTA photostimulation (593 nm, 5-10 mW, 5 ms pulses, 1 s duration) caused a decrease in GCaMP6m fluorescence in VTA GABA neurons, as seen in both population averages for Z-Scores as well as individual heat maps, indicating a decrease in neural activity of VTA GABA neurons. Inset bar graph: the quantification of the area under the curve for stimulation (0-2 s), compared with pre-stimulation (-2-0 s) and eYFP controls (0-2 s) showed that 20 Hz stimulation (593 nm, 5-10 mW, 1 s duration) caused a significant decrease in VTA GABA neural activity (n=6 GCaMP6m, n=5 eYFP; one-way ANOVA, $F_{2,14}=24.39$, ****$p<0.0001$, Bonferroni post-hoc analysis, **$p<0.01$, ****$p<0.0001$).

(E) Photostimulation of the LH^{GABA}-VTA projection with constant light (593 nm, 5-10 mW, 1 s duration) also caused a significant decrease in GABA neural activity. Inset bar graph (n=6 GCaMP6m, n=5 eYFP; one-way ANOVA, $F_{2,14}=15.75$, ***p=0.0003, Bonferroni post-hoc analysis, **p<0.01, ***p<0.001).

Error bars indicate ±SEM.

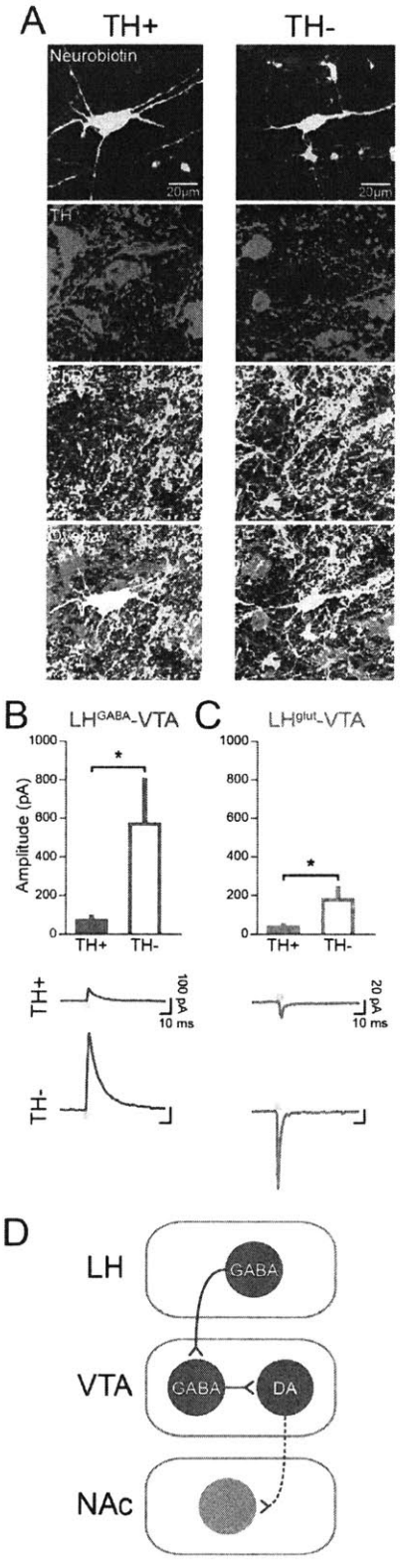
A
TH+
TH-
Neurobiotin
20μm
TH
B
LH^GABA-VTA
C
LH^glut-VTA
Amplitude (pA)
1000
800
600
400
200
0
*
TH+
TH-
100 pA
10 ms
20 pA
10 ms
D
LH
GABA
VTA
GABA
DA
NAc

Figure 6. GABAergic and Glutamatergic LH Projections are Stronger onto Putative GABA Neurons than Dopamine Neurons in the VTA

(A) Whole-cell patch-clamp recordings were made from VTA neurons in brain slices prepared from VGAT::Cre and VGLUT2::Cre mice expressing ChR2 in a Cre-dependent manner in the LH. Neurons were filled with neurobiotin during recording and subsequently processed with immunohistochemistry for TH (red).

(B) ChR2-expressing terminals were activated with a 5 ms blue light pulse to elicit inhibitory post-synaptic currents (IPSCs) in VGAT::Cre mice. IPSC amplitude was significantly greater in TH- VTA cells than TH+ cells (n=9 TH+, n=7 TH-; two-tailed, unpaired Student's t-test, *p=0.0270).

(C) Similarly, in VGLUT2::Cre mice, the amplitude of optically-evoked excitatory post-synaptic currents (EPSCs) was significantly greater in TH- VTA cells than TH+ cells (n=5 TH+, n=5 TH-; two-tailed, unpaired Student's t-test, *p=0.0464).

(D) Model representing the GABAergic projection from the LH onto GABA cells in the VTA. Activation of the GABAergic LH-VTA projection results in disinhibition of VTA DA neurons and therefore increases DA release in the NAc.

Error bars indicate ±SEM. See also Figure S5.

3.4 Discussion

3.4.1 The Role of Inhibitory Input onto GABAergic Interneurons in the VTA

The LH projection to the VTA has been well studied for its involvement in reward processing and feeding behaviors (Bielajew and Shizgal, 1986; Hoebel and Teitelbaum, 1962; Kempadoo et al., 2013; Nieh et al., 2015; Stuber and Wise, 2016). The glutamatergic component of the LH-VTA projection has been proposed to be responsible for supporting positive reinforcement. Specifically, it has been suggested that glutamatergic fibers from the LH travelling to the VTA might contribute to LH and VTA evoked self-stimulation (You et al., 2001). Additionally, NMDA receptor antagonism in the VTA has been shown to block optogenetically-induced ICSS of LH-VTA projections, implicating the involvement of glutamate release from the LH to the VTA (Kempadoo et al., 2013).

However, our findings contradict this notion and instead demonstrate that the GABAergic component of the LH-VTA pathway mediates the reward-related properties observed in this circuit. This is evidenced by our finding that mice will self-stimulate for GABAergic LH-VTA stimulation, but not glutamatergic LH-VTA stimulation (Figure 1D and 1H). Furthermore, photostimulation of LH^{GABA}-VTA is preferred, while photostimulation of LH^{glut}-VTA is avoided (Figure 1B-C and 1F-G).

As a result, our findings counter the interpretation proposed by Kempadoo and colleagues (2013) and may be reconciled by evidence that infusion of NMDA receptor antagonists in the VTA is known to prevent spontaneous burst-firing in DA neurons (Chergui et al., 1993; Grace et al., 2007; Johnson et al., 1992). Therefore, an alternative interpretation is that their manipulation

not only blocked glutamate action from the LH, but also prevented burst-firing of DA neurons. The model for glutamatergic activation of VTA playing the major role in generating reward-related behaviors was attractive because of the known influence on positive reinforcement by VTA DA neuron stimulation. However, our experiments present evidence for the inhibitory projection to the VTA as the principal mediator of appetitive behaviors. This apparent paradox -- in which an inhibitory input to the VTA causes DA release in the NAc to cause behavioral activation -- was resolved upon our finding that GABAergic LH inputs are stronger onto putative GABA neurons in the VTA than DA neurons (Figure 6) and that stimulating this projection inhibits these VTA GABA neurons (Figure 5), thereby allowing for disinhibition of DA neurons projecting to the NAc.

Our study follows experiments from other groups showing that animals are willing to self-administer GABAergic agonists into the VTA (David et al., 1997; Ikemoto et al., 1997, 1998). At the time, the reason why animals would do this was not well understood, but it was known that $GABA_A$ receptors were expressed on both VTA DA neurons (Sugita et al., 1992) and VTA GABA neurons (Rick and Lacey, 1994). Johnson and North first hypothesized that mu-opioid receptor agonists, such as morphine, act in the VTA via disinhibition through GABA neurons (Johnson and North, 1992), while Bocklisch and colleagues showed that cocaine can also disinhibit VTA DA neurons through potentiation of inhibitory NAc projections to VTA GABA neurons (Bocklisch et al., 2013). Our results are generally consistent with other recent studies indicating the role for LH GABA neurons (Jennings et al., 2015) and their projection to the VTA (Barbano et al., 2016) in supporting positive reinforcement and appetitive behaviors, though nuances in behavior may be attributed to our targeting a more anterior portion of the LH.

Our work is the first to show direct relationships between activating LH GABA projections to the VTA, the suppression of GABA neuron activity in the VTA, and downstream DA release in the NAc.

3.4.2 Noteworthy Nuances

Because the medial/lateral location of dopamine neurons within the VTA has been shown to indicate a difference in projection target, with dopamine neurons in medial VTA projecting to the NAc medial shell and mPFC and dopamine neurons in lateral VTA projecting to the NAc lateral shell (Lammel et al., 2008, 2011, 2012) , we generated maps with the location of each TH+ or TH- cell we recorded from in Figure 6 with the area of the symbol proportional to the recorded EPSC or IPSC (Figure S5). However, there did not appear to be any differences in the medial/lateral locations of the recorded TH+ with respect to amplitude, and therefore, it does not appear that the GABAergic or glutamatergic LH-VTA projection has preferential input to either population of DA neurons within the VTA.

As a result of the gnawing behavior that occurs in an empty chamber, we conducted the real-time place preference/avoidance and intracranial self-stimulation experiments at 10 Hz instead of 20 Hz to minimize the amount of gnawing that might confound the results (read more on gnawing in Nieh et al., 2015). There was much less gnawing in the resident-intruder and novel object assays, likely due to the presence of very salient stimuli, so 20 Hz stimulation was used to maximize the effect. Voltammetry experiments show that LH^{GABA}-VTA or LH^{glut}-VTA

stimulation at either 10 Hz or 20 Hz evoke the same pattern of dopamine release and suppression, respectively (Figure 4 and S4).

3.4.3 The LH-VTA Circuit as an Environment-Dependent Modulator of Motivational Salience

While both the LH and VTA have long been identified as areas involved in feeding and reward, we show evidence that activation of individual components of the LH-VTA projection can also modulate social behaviors. Valenstein and colleagues proposed the notion of "substitutability" based on their observations that animals will eat, drink, or gnaw upon LH stimulation dependent on the availability of food, water, or a wooden block, respectively (Valenstein et al., 1968). Other studies using electrical stimulation have also reported that LH activation can evoke locomotor effects, gnawing, ejaculation, and aggression (Albert et al., 1979; Singh et al., 1996), and more recently, Navarro and colleagues showed that stimulating specifically the GABAergic neurons in the LH can induce consummatory behaviors towards saccharin, water, or wood (Navarro et al., 2015). Our results showing that stimulation of GABAergic LH inputs to the VTA causes DA release in the NAc also brings into conversation a large field involved in the study of DA as a substrate for behavioral activation, initiation vigor, arousal, and motivational salience (Berridge and Robinson, 1998; Horvitz, 2000; Ko and Wanat, 2016; Salamone and Correa, 2012). Several studies have shown that subsecond fluctuations in ventral striatal DA are enhanced prior to the performance of an instrumental action (Collins et al., 2016; Hamid et al., 2016; Howe et al., 2013), which is consistent with the idea that DA signaling supports motivated approach behavior (Ciano et al., 2001; Saunders and Robinson, 2012).

Our present results support these ideas as a whole, in that neither LH stimulation nor DA release in the NAc is specific to individual behaviors, such as feeding, but may instead cause an increase in many different behaviors by supporting a change in the motivational state of the animal. In our study, we showed that GABAergic LH-VTA stimulation causes DA release in the NAc, commensurate with a motivational state change in the animal, and caused the animal to obtain, approach, and/or investigate salient stimuli. The context of the environment and the nature of the stimulus determined which action the animal would take. In the social interaction task, wherein the salient stimulus was the intruder mouse, GABAergic LH-VTA stimulation promoted interaction with the intruder, and in the four-chamber novel object task, wherein the salient stimulus was the most proximal object, GABAergic LH-VTA stimulation induced increased investigation of the object (Figure 2).

Importantly, glutamatergic LH-VTA stimulation suppressed interaction with intruders, reduced investigation of objects, caused avoidance in the RTPP/A assay, and decreased DA release in the NAc. As a result, the glutamatergic LH-VTA component could also be modulating motivation levels in order to promote avoidance. However, because our experiments in this current study only focused on rewarding or neutral target stimuli, future experiments should explore how glutamatergic LH-VTA stimulation/inhibition affects behavior in the presence of aversive target stimuli. While glutamatergic LH-VTA inhibition did not appear to have any significant effects in the experiments of the current study, we speculate that in an assay where animals must avoid an aversive stimulus, glutamatergic LH-VTA stimulation may suppress the animal's motivation to avoid that stimulus.

3.4.4 LH-VTA as Part of a Distributed Neural Circuit

Importantly, optogenetic activation may not recapitulate the physiological role of a given projection. While photostimulation of the GABAergic input from LH to VTA produced robust changes, the photoinhibition induced relatively modest changes in behavior. This may be due to a floor effect, or more likely, reflects that the LH input to the VTA is only one of multiple contributing factors that influence VTA activity and subsequent behavioral changes.

Another important note is that terminal stimulation does not rule out the possibility of antidromic activation. Thus it is possible that activation of LH-VTA terminals can cause antidromic activation of the cells bodies in the LH, which could recruit other downstream structures, including the bed nucleus of the stria terminalis, dorsal raphe, amygdala, and lateral habenula (Berk and Finkelstein, 1982; Saper et al., 1979). In addition, while we have recorded DA levels in the NAc as a result of activating the GABAergic or glutamatergic components of the LH-VTA projection, it is unknown whether these projections also have an effect on DA levels in dorsal striatum and/or prefrontal cortex. Considering DA release in the dorsal striatum is also critical for feeding (Szczypka et al., 1999b, 2001) and compulsive behaviors (Ito et al., 2002; Vanderschuren et al., 2005; Willuhn et al., 2012), future experiments studying the differences in DA release in dorsal/ventral striatum from LH-VTA stimulation would provide another level of insight into this circuit.

Additionally, the GABAergic LH-VTA projection synapses onto both GABA and DA neurons in the VTA, even if the primary input is onto VTA GABA neurons (Figure 5 and 6). It is also possible that within the GABAergic LH-VTA projection, there may be further subdivisions that uniquely contribute to distinct motivated behaviors (e.g. feeding, thirst, sex), but by

stimulating the entire projection, we are activating these motivated behaviors together. In addition, disinhibiting DA neurons by activating GABAergic LH-VTA inputs is physiologically different from directly activating DA neurons. A single GABA interneuron in the VTA could have widespread effects onto many DA neurons simultaneously. By activating the GABAergic LH-VTA input, we may also be causing peptidergic co-release within the VTA or via axon collaterals, since a subset of GABA-expressing LH neurons also express peptides such as neurotensin (Leinninger et al., 2009; Opland et al., 2013).

3.5 Conclusion

Homeostasis can be maintained with three elements (Cannon, 1929). The first detects the current state of the system (detector), the second compares the current state to the set point (evaluator), and the third adjusts the state of the system towards the set point (adjuster), where the set point is defined as the optimal state of any given system.

We previously showed that stimulating the LH-VTA projection can cause mice to seek a sugar reward even in the face of a negative consequence (Nieh et al., 2015). In this study, we showed that the GABAergic component of this projection is positively reinforcing and increases behavioral activation generalizable across multiple motivated behaviors. One explanation is that activating this projection may be simulating the rewarding value that is then attributed to the most salient proximal stimulus. Another possible explanation is that the LH may play the role of the evaluator within a homeostatic circuit, integrating inputs from the periphery and upstream cortical areas (Berthoud and Münzberg, 2011; Diorio et al., 1993) to compute differences

between the current state and the target set points, and the VTA may play the role of the adjuster, enhancing or suppressing dopamine release to generate downstream motor action. Taken together, our manipulations of the LH-VTA projection may either circumvent the detection and evaluation elements in a homeostatic model or increase motivation by an anatomically distinct reward-related system. Therefore, in contrast to other neural populations that cause feeding due to hunger when stimulated, such as the agouti-related peptide (AGRP) cells of the arcuate nucleus (Betley et al., 2015), LH^{GABA}-VTA stimulation appears to evoke feeding by increasing the motivation for food rewards.

Thus we conjecture that the GABAergic LH-VTA component is more likely to be involved in disorders such as compulsive eating, where the primary cause of overeating is not hunger. Importantly, because inhibiting this projection suppresses feeding when animals are in a highly motivated state, the GABAergic LH-VTA pathway could serve as an important target for drug action in the treatment of these disorders. Furthermore, our data show that this projection not only modulates feeding, but also other appetitive behaviors. As a result, a hyperactive population of LH-VTA GABA neurons could induce overeating or compulsive eating and thus elevate food intake to maladaptive levels, but could also potentially lead to compulsive behaviors towards other stimuli as well. This idea that a malfunction in one neural population may result in compulsive behaviors towards multiple stimuli may be a root cause in a subset of addictive disorders in human patients, given the observed comorbidity of binge eating disorder with compulsive buying (Faber et al., 1995) or pathological gambling with substance abuse (Black and Moyer, 1998; Cunningham-Williams et al., 1998).

In conclusion, our study elucidates how the GABAergic and glutamatergic LH-VTA components can work together to produce approach and avoidance behaviors by modulating motivational state through midbrain DA release and identifies a possible target for therapeutic intervention in compulsive eating and other addictive disorders.

3.6 Methods and Materials

3.6.1 Animals and Stereotaxic Surgery

Mice were housed in a reverse 12-hour light-dark cycle room with *ad libitum* food and water provided. All procedures involving the handling of animals were in accordance with guidelines from the NIH and approved by the MIT Institutional Animal Care and Use Committee. Surgery was performed on mice under aseptic conditions and body temperature was maintained with a heating pad. Mice were anesthetized with isoflurane (5% for induction, 1-2% for maintenance) and placed in a digital small animal stereotax (David Kopf Instruments, Tujunga, CA, USA). All measurements were made relative to bregma for virus/implant surgeries. Viral injection was performed using a beveled 33 gauge microinjection needle with a 10 μL microsyringe (Nanofil; WPI, Sarasota, FL, USA) delivering virus at a rate of 0.1 μL/min with a microsyringe pump (UMP3; WPI, Sarasota, FL, USA) and controller (Micro4; WPI, Sarasota, FL, USA). After the injection was completed, two minutes were allowed to pass before withdrawing the needle 50-100 μm and leaving it for an additional 10 minutes before the needle was then slowly withdrawn completely. After surgery, mice recovered from anesthesia under a heat lamp.

For ChR2 and corresponding control mice used in behavioral, fast-scan cyclic voltammetry (FSCV), and *ex vivo* electrophysiology experiments, 0.3-0.5 μL of an anterogradely travelling adeno-associated virus serotype 5 (AAV_5), encoding channelrhodopsin-2 (ChR2)-eYFP, under a double-floxed inverted open-reading frame construct (DIO) (AAV_5-EF1α-DIO-ChR2(H134R)-eYFP) or a null version of the virus only carrying eYFP (AAV_5-EF1α-DIO-eYFP) was injected into the LH (anteroposterior (AP): -0.4 to -0.8 mm; mediolateral (ML): 1.0 mm;

dorsoventral (DV): -4.9 to -5.35 mm) in VGAT::IRES-Cre (VGAT::Cre; RRID: IMSR_JAX:016962) or VGLUT2::IRES-Cre (VGLUT2::Cre; RRID: IMSR_JAX:016963) mice. In addition, a manually-constructed optic fiber (300 μm core, 0.37 NA) (Thorlabs, Newton, NJ, USA) held in a 2.5 mm ferrule (Precision Fiber Products, Milpitas, CA, USA) was implanted directly above the VTA (AP: -3.1 to -3.6 mm; ML: 0.60 to 0.70 mm; DV: -3.5 to -4.1 mm). For NpHR and corresponding control mice, 0.3-0.5 μL of AAV_5, encoding enhanced halorhodopsin 3.0 (NpHR)-eYFP, under a DIO construct (AAV_5-EF1α-DIO-NpHR-eYFP) or AAV_5-EF1α-DIO-eYFP was injected bilaterally into the LH (AP: -0.4 to -0.8 mm; ML: ±1.0 mm; DV: -4.9 to -5.35 mm), and an optic fiber (400 μm core, 0.48 NA) was implanted medially above the VTA in both hemispheres (AP: -3.1 to -3.6 mm; ML: 0.0 to 0.5 mm; DV: -2.5 mm to -3.2 mm). A layer of adhesive cement (C&B Metabond; Parkell, Edgewood, NY, USA) followed by cranioplastic cement (Ortho-Jet; Lang, Wheeling, IL, USA) was used to secure the optic fiber to the skull.

For mice used in photometry experiments, 0.3-0.5 μL of an anterogradely travelling adeno-associated virus serotype 8 (AAV_8) encoding ChrimsonR-tdTomato under a flip-excision (FLEX) switch (AAV_8-hSyn-FLEX-ChrimsonR-tdTomato) was injected into the LH (AP: -0.4 to -0.8 mm; ML: 1.0 mm; DV: -4.9 to -5.35 mm). In addition, an AAV_5 carrying the genetically-encoded calcium indicator (GCaMP6m; AAV_5-CAG-FLEX-GCaMP6m) was injected into the VTA (AP: -3.1 to -3.6 mm; ML: 0.60 to 0.70 mm; DV: -4.3 to -4.75 mm). One fiber (300 μm core, 0.37 NA or 400 μm core, 0.48 NA) held in a 2.5 mm ferrule was implanted in the VTA (AP: -3.1 to -3.6 mm; ML: 0.60 to 0.70 mm; DV: -4.0 to -4.3 mm). A second fiber (300 μm core, 0.37 NA) held in a 1.25 mm ferrule was implanted in the contralateral hemisphere at a 15° angle to the right targeting the VTA (AP: -3.1 to -3.6 mm; ML: -1.02 to -0.70 mm; DV: -3.0 to -3.5 mm). Adhesive cement and cranioplastic cement were used to secure the optic fibers as above.

3.6.1.1 Viral Constructs

Recombinant AAV vectors were serotyped with AAV_5 or AAV_8 coat proteins, and those carrying ChR2, NpHR, or ChrimsonR were packaged by the University of North Carolina Vector Core (Chapel Hill, NC, USA). Viruses carrying GCaMP6m were packaged by the University of Pennsylvania Vector Core (Philadelphia, PA, USA).

3.6.2 Behavioral Experiments

Behavioral testing was performed during the active dark phase and at least four weeks following surgery to allow sufficient time for transgene expression. Optic fiber implants were connected to a patch cable with a ceramic sleeve (PFP, Milpitas, CA, USA), which was connected to a commutator (rotary joint; Doric, Québec, Canada) via an FC/PC adapter to allow unrestricted movement. A second patch cable, with a FC/PC connector at either end (Doric, Québec, Canada), was connected to the commutator and then connected to a 473 nm, 589 nm, or 593 nm diode-pumped solid state (DPSS) laser (OEM Laser Systems, Draper, UT, USA). A Master-8 pulse stimulator (A.M.P.I., Jerusalem, Israel) was used to control the output of the 473 nm laser. The 593 nm laser was pulsed using a shutter (SR475; Stanford Research Systems, Sunnyvale, CA, USA) and shutter driver (SR474; Stanford Research Systems, Sunnyvale, CA, USA).

3.6.2.1 Real-time Place Preference/Avoidance (RTPP/A)

Mice were placed in a (57.15 cm x 22.5 cm x 30.5 cm) open chamber consisting of left and right chambers (each 24.5 cm x 22.5 cm) and a center compartment (8 cm x 22.5 cm). Mice were allowed to freely move between compartments for 30 minutes, during which entry into one of the two sides was paired with photostimulation (ChR2: 473 nm, 10 Hz, 20 mW, 5 ms pulses; NpHR: 589/593 nm, constant, 5 mW). The side paired with stimulation was counterbalanced between mice. A video camera positioned above the chamber recorded each trial, and mouse locations/velocity were tracked and analyzed using Ethovision XT software (Noldus, Wageningen, Netherlands). Difference scores were calculated by subtracting the percentage of time spent in the non-stimulated side from the percentage of time spent in the stimulated side.

3.6.2.2 Intracranial Self-Stimulation (ICSS)

Mice were removed from *ad libitum* food one day prior to testing to facilitate behavioral responding. Mice were placed into a sound-attenuated operant chamber (Med Associates, Inc., St. Albans, VT, USA) containing two illuminated nosepoke ports ("active" and "inactive") and speakers to play tones and white noise. A response into either nosepoke port was accompanied by illumination of a cue-light (positioned above the nosepoke port) and a distinct 1 s tone (1 or 1.5 kHz, counterbalanced). A nosepoke response into the "active" port resulted in delivery of photostimulation (ChR2: 473 nm, 10 Hz, 20 mW, 5 ms pulses, 1 s duration; NpHR: 589/593 nm, constant, 5 mW, 1 s duration), while no stimulation was delivered for a nosepoke response in the "inactive" port (counterbalanced between mice). Mice were allowed to explore for one hour.

Nosepoke ports were baited with a small amount of crushed sucrose pellets to encourage investigation, and white noise was played throughout the session.

3.6.2.3 Social Interaction (Resident-Intruder) Assay

Mice were placed into a clean cage and given 5 minutes to explore the environment. A juvenile male (3-4 weeks of age, VGAT::Cre or VGLUT2::Cre) or adult female (C57/BL6) mouse was placed into the cage, and a nine minute recording session with three consecutive three-minute epochs was initiated. In the second epoch, mice were photostimulated (ChR2: 473 nm, 20 Hz, 20 mW, 5 ms pulses; NpHR: 589/593 nm, constant, 5 mW). The behavior of the experimental mouse was manually scored by blinded experimenters for social behavior, e.g. grooming of the intruder, sniffing of the face or hind regions, and mounting, using ODLog behavioral analysis software (Macropod Software). Mice that never spent more than 5% of time in any epoch interacting with the intruder mouse were excluded.

3.6.2.4 Four-Chamber Novel Object Task

Mice were placed into an open chamber (50 cm x 53 cm), which was divided into four regions. A distinct novel object was placed into the center of each of the regions. Mice were allowed to explore the chamber for one hour and were stimulated (ChR2: 473 nm, 20 Hz, 20 mW, 5 ms pulses; NpHR: 589/593 nm, constant, 5 mW) for three-minute epochs at three-minute intervals. A video camera positioned above the chamber recorded each session and mouse

locations/velocity were tracked and analyzed using Ethovision XT software (Noldus, Wageningen, Netherlands). Zone crossings were identified by Ethovision XT as events where mice crossed from one zone to another. Investigation of objects was manually scored by blinded experimenters using ODLog behavioral analysis software (Macropod Software). Difference scores for investigation time were calculated by subtracting the total amount of time spent investigating objects during OFF epochs from the total amount of time spent investigating objects during ON epochs. Difference scores for the number of zone crossings were calculated by subtracting the total number of zone crossings during OFF epochs from the total number of zone crossings during the ON epochs. One data point was rejected as an outlier using Chauvenet's criterion.

3.6.2.5 Feeding Task

Mice were allowed to explore a chamber with two empty plastic cups placed in opposite corners of the chamber for a period of 5 minutes (habituation). A moist food pellet was then placed into one of the cups (counterbalanced between mice), and a nine minute recording session with three consecutive three-minute epochs was initiated. In the second epoch, mice were photostimulated (NpHR: 589/593 nm, constant, 5 mW). The amount of time spent feeding was manually scored by blinded experimenters using ODLog behavioral analysis software (Macropod Software). Difference scores for feeding were calculated by subtracting the amount of time spent feeding during the first OFF epoch from the amount of time spent feeding during the ON epoch.

3.6.3 *In Vivo* Fast-Scan Cyclic Voltammetry (FSCV)

Anesthetized *in vivo* FSCV experiments were conducted similar to those previously described (Matthews et al., 2016). Following behavioral experimentation, mice were anesthetized with 30% urethane (1.5 g/kg, IP) diluted in sterile saline and placed in a stereotaxic frame located within a faraday cage. NAc measurements were obtained by using the VTA fiber implant coordinates as reference. Small craniotomies were made above the NAc (~AP: 1.0, ML: 1.0) and contralateral cortex through the existing implant/dental cement. A chlorinated silver (Ag/AgCl) reference electrode was implanted in the contralateral cortex and cemented in place (C&B Metabond; Parkell, Edgewood, NY, USA). A glass-encased carbon fiber electrode (~120-150 μm in length, epoxied seal) was lowered just dorsal of the NAc (DV: -2.9 from brain surface) and was allowed to equilibrate for 20 minutes at 60 Hz and 10 minutes at 10 Hz. Voltammetric recordings were collected using Tarheel CV at 10 Hz by applying a triangular waveform (-0.4 V to +1.3 V to -0.4 V, 400 V/s) to the carbon-fiber electrode versus the Ag/AgCl reference, as has been described previously (Vander Weele et al., 2014). Following cycling, electrodes were lowered into the NAc in 200 μm steps until changes in dopamine release were detected after optical activation of the LH inputs to the VTA using blue light (473 nm, 20Hz, 20 mW, 5 ms pulses, 10 s duration). Data were collected in 30-second files with the stimulation onset occurring ten seconds into the file. 20-25 recordings were collected at 60-second intervals and background subtracted at approximately the lowest current value prior to stimulation onset.

Following completion of baseline recordings, mice were administered the D2 receptor antagonist, raclopride (Sigma-Aldrich, St. Louis, MO, USA, 5.0 mg/kg diluted in sterile saline, IP), as a positive control and to enhance background dopamine levels. Raclopride recordings

commenced 10 minutes after injection. Carbon-fiber electrodes were pre-calibrated in known concentrations of dopamine (1000, 500, 250 nM) as previously described (Badrinarayan et al., 2012) and calibration data were used to convert *in vivo* signals to changes in dopamine concentration using chemometric, principal component regression, and residual analyses using a custom LabView program (Umich CV, Courtesy of Richard Keithley; Keithley et al., 2009). For quantitation of evoked DA, area under the curve was calculated during the 10 s stimulation period (0-10 s) compared with basal fluctuations during the 10 s period prior to stimulation onset (-10-0 s). Following recordings, mice were transcardially perfused, fixed, and processed (as described below) to confirm viral expression and placements of the optic fibers and recording electrode tracks.

3.6.4 Photometry

For the photometry system, 473 nm light from a DPSS laser (30-80 μW; OEM Laser Systems, Draper, UT, USA) was filtered through a neutral density filter (1.0 optical density, Thorlabs, Newton, NJ, USA) held in a filter wheel (FW1A, Thorlabs, Newton, NJ, USA), sent through a chopper (400±10 Hz; SR540 Chopper Controller, Stanford Research Systems, Sunnyvale, CA, USA) through a 473 nm filter (LD01-473, Semrock, Rochester, NY, USA), reflected off a dichroic mirror (FF495, Semrock, Rochester, NY, USA) and coupled through a fiber collimation package (F240FC-A, Thorlabs, Newton, NJ, USA) into a patch cable connected to the ferrule of the upright optic fiber implanted in the mouse via a ceramic sleeve (Precision Fiber Products, Milpitas, CA, USA). GCaMP6m fluorescence emanating through the implanted optic fiber was collected through a 525 nm filter (FF03-525, Semrock, Rochester, NY, USA) into

a photodetector (Model 2151, Newport Corporation, Irvine, CA, USA). The signal was passed through a lock-in amplifier (100 ms, 12 dB, 500 mV; SR810, Stanford Research Systems, Sunnyvale, CA, USA) and digitized and collected with a LabJack U6-PRO (250 Hz sampling frequency; LabJack, Lakewood, CO, USA). For stimulation of GABAergic LH terminals in the VTA, mice were placed in their home cage, and 20 Hz stimulation (593 nm, 5-10 mW, 5 ms pulses, 1 s duration) was given every 10 seconds for 30 trials into the angled optic fiber implanted in the mouse. This was then repeated using 30 trials of one second constant stimulation (593 nm, 5-10 mW). The raw signal was divided by a linear fit to normalize the baseline over the recording session. Z-scores were taken using the 5 seconds prior to stimulation as baseline.

3.6.5 *Ex Vivo* Electrophysiology

Brain slices were prepared from VGAT::Cre or VGLUT2::Cre mice which had received an injection of AAV_5-DIO-ChR2-eYFP or AAV_5-DIO-ChR2-mCherry into the LH at least 7 weeks prior. Mice were deeply anesthetized by IP injection of sodium pentobarbital (200 mg/kg) before transcardial perfusion with 20 mL ice-cold modified ACSF (composition in mM: NaCl 87, KCl 2.5, NaH2PO4*H20 1.3, MgCl2*6H2O 7, NaHCO3 25, sucrose 75, ascorbate 5, CaCl2*2H2O 0.5, in ddH20; osmolarity 323-328 mOsm, pH 7.20-7.35) saturated with carbogen gas (95% oxygen, 5% carbon dioxide). The brain was rapidly dissected out of the cranial cavity and 300 μm horizontal slices containing the VTA were prepared on a vibrating-blade microtome (Leica VT1000S, Leica Microsystems, Wetzlar, Germany). Brain slices were then given at least 1 hour to recover in a holding chamber containing ACSF (composition in mM: NaCl 126, KCl

2.5; NaH2PO4*H20 1.25, MgCl2*6H2O 1, NaHCO3 26, glucose 10, CaCl2*2H2O 2.4, in ddH20; osmolarity 299-301 mOsm; pH 7.30-7.40) saturated with carbogen gas at 32 °C.

For electrophysiology, slices were transferred to a recording chamber and continuously perfused at a rate of 2 mL/min with fully oxygenated ACSF at 30-32 °C. Electrodes for recording were pulled from thin-walled borosilicate glass capillary tubing on a P-97 puller (Sutter Instrument, Novato, CA, USA) and had resistances of 4-7 MΩ when filled with internal solution (composition in mM: potassium gluconate 125, NaCl 10, HEPES 20, MgATP 3, and 0.1% neurobiotin, in ddH20; osmolarity 287 mOsm; pH 7.30). Whole-cell patch-clamp recordings were performed using a Multiclamp 700B amplifier and Clampex 10.4 software (Molecular Devices, Sunnyvale, CA, USA). Signals were low-pass filtered at 1 kHz and digitized at 10 kHz using a Digidata 1550 (Molecular Devices, Sunnyvale, CA, USA). Cell capacitance, series resistance, and input resistance were frequently measured during recordings to monitor cell health. Neurons were visualized via a 40X water-immersion objective on an upright microscope (Scientifica, Uckfield, UK) equipped with IR-DIC optics and a QImaging Retiga EXi camera (QImaging, Surrey, BC, Canada). The region containing ChR2-expressing terminals in the VTA was identified by brief illumination through a 470 nm LED light source (pE-100; CoolLED, River Way, UK). A subset of VGAT::Cre mice received an injection of AAV_5-DIO-ChR2-mCherry into the LH and AAV_5-DIO-eYFP into the VTA in order to identify GABA neurons. In these brain slices, ChR2-expressing terminals were visualized by illumination through a 595 nm LED light source (pE-100; CoolLED, River Way, UK) and GABA neurons in the VTA by brief illumination through the 470 nm LED light source (pE-100; CoolLED, River Way, UK).

Neurons were recorded in voltage-clamp mode at a holding potential of -70 mV in VGLUT2::Cre mice to elicit glutamatergic excitatory postsynaptic currents and at 0 mV in VGAT::Cre mice to elicit GABAergic inhibitory postsynaptic currents. ChR2-expressing terminals were activated by a 5 ms pulse of 470 nm LED light, delivered through the objective, every 20 s. Analysis was subsequently performed in Clampfit 10.4 software (Molecular Devices, Sunnyvale, CA, USA). The average light-evoked current was calculated using at least 12 stable sweeps, from which peak current amplitude and onset latency were measured.

To determine the TH content of recorded neurons, brain slices were subsequently processed with immunohistochemistry. Recorded slices were fixed in 4% paraformaldehyde (PFA) overnight at 4 °C, then washed four times in phosphate-buffered saline (PBS) for 10 minutes each wash. Slices were then blocked in 1x PBS containing 0.3% Triton X-100 (PBS-T 0.3%) with 5% normal donkey serum (NDS) (Jackson ImmunoResearch Labs, West Grove, PA, USA) for 1 hour at room temperature followed by incubation in primary antibody solution: chicken anti-TH (1:1000; Millipore Cat# AB9702, RRID: AB_570923; Millipore, Billerica, MA, USA) in 1x PBS-T 0.3% with 3% NDS for 18-24 hours at 4 °C. Slices were subsequently washed four times in 1x PBS (for 10 minutes each) and then transferred to secondary antibody solution: Alexa Fluor 647-conjugated donkey anti-chicken (1:1000; Jackson ImmunoResearch Labs Cat# 703-605-155, RRID: AB_2340379; Jackson ImmunoResearch Labs, West Grove, PA, USA) and 405-conjugated streptavidin (1:1000; Biotium, Hayward, CA, USA) in 1x PBS-T 0.1% with 3% NDS for 2 hours at room temperature. After a further four washes in 1x PBS (for 10 minutes each), slices were mounted onto glass slides and cover-slipped using polyvinyl alcohol (PVA) mounting medium with DABCO (Sigma-Aldrich, St. Louis, MO, USA).

3.6.6 Histology

3.6.6.1 Perfusion and Storage

Subjects were deeply anesthetized with sodium pentobarbital (200 mg/kg; IP) and transcardially perfused with 20 mL of Ringer's solution followed by 20 mL of cold 4% PFA dissolved in 1x PBS. The brain was extracted and placed in 4% PFA solution and stored at 4 °C for at least 24 hours. Brains were then transferred to a 30% sucrose solution in 1x PBS for 24 hours at room temperature. Brains were sectioned into 40-60 μm slices on a sliding microtome (HM420; Thermo Fischer Scientific, Waltham, MA, USA). Sections were stored in 1x PBS at 4 °C until immunohistochemical processing.

3.6.6.2 Immunohistochemistry

Sections were blocked in 1x PBS-T 0.3% with 3% NDS (Jackson ImmunoResearch Labs, West Grove, PA, USA), for one hour at room temperature. LH sections were incubated in a DNA-specific fluorescent probe (DAPI: 4',6-Diamidino-2-Phenylindole; 1:50,000 in 1x PBS) for 30 minutes, washed four times for 10 minutes each in 1x PBS, mounted on glass microscope slides, and cover-slipped using PVA mounting medium with DABCO (Sigma-Aldrich, St. Louis, MO, USA). VTA sections were incubated in a solution containing chicken anti-TH (1:500; Millipore Cat# AB9702, RRID: AB_570923; Millipore, Billerica, MA, USA) and rabbit anti-c-Fos (1:500; Santa Cruz Biotechnology Cat# sc-52, RRID: AB_2106783; Santa Cruz Biotechnology, Dallas, TX, USA) in 1x PBS-T 0.1% (or 1x PBS-T 0.3%) with 3% NDS for 24 hours at room temperature or 24-48 hours at 4 °C. Sections were then washed four times (10

minutes each) with 1x PBS and immediately transferred to secondary antibody solution containing Alexa Fluor 647-conjugated donkey or goat anti-chicken (1:500; Jackson ImmunoResearch Labs Cat# 703-605-155, RRID: AB_2340379; Jackson ImmunoResearch Labs Cat# 103-605-155, RRID: AB_2337392; Jackson ImmunoResearch Labs, West Grove, PA, USA), Cy3-conjugated donkey anti-rabbit (1:500; Jackson ImmunoResearch Labs Cat# 711-165-152, RRID: AB_2307443; Jackson ImmunoResearch Labs, West Grove, PA, USA), and DAPI (1:50,000) in 1x PBS containing 3% NDS for two hours at room temperature. In some animals in which c-Fos was not analyzed, Cy3-conjugated donkey anti-chicken (1:500; Jackson ImmunoResearch Labs Cat# 703-165-155, RRID: AB_2340363; Jackson ImmunoResearch Labs, West Grove, PA, USA) was used. Sections were washed four times (10 minutes each) in 1x PBS, mounted on glass microscope slides, and cover-slipped with PVA-DABCO.

3.6.6.3 Confocal Microscopy

Fluorescent images were captured using a confocal scanning microscope (Olympus FV1000, Olympus, Center Valley, PA, USA) with FluoView software (Olympus, Center Valley, PA, USA) under a 10x/0.40 NA dry objective or a 40x/1.30 NA oil immersion objective. The locations of the virus injection sites were estimated by comparing the surgical injection coordinates and the presence of dense eYFP-expressing cell bodies. The locations of optic fiber tips and carbon-fiber recording electrodes were determined by the presence of a lesion in the slices.

3.6.6.4 Cell Counting

For c-Fos cell counting, following behavioral experiments, VGLUT2::Cre and VGAT::Cre mice were stimulated for ten minutes in a dark, sound-attenuating room (473 nm, 20 Hz, 20 mW, 5 ms pulses). Eighty minutes later, mice were anesthetized and transferred to the lab. Approximately 5-10 minutes later, mice were transcardially perfused and the brains processed and imaged as described above. Two blinded experimenters counted 400-500 DAPI+ cells randomly distributed throughout the VTA and then identified cells for their co-expression with TH and c-Fos, or lack thereof.

For cell counting to quantify the proportion of ChR2+ or NpHR+ cells throughout the LH, ~100-200 random DAPI+ cells were identified (ChR2: right hemisphere; NpHR: both hemispheres) in the LH, and then the number of those cells that were also co-expressing ChR2 or NpHR were counted to generate a relative proportion of LH neurons that were ChR2+ or NpHR+. Counting was done in 40x z-stacks (8 slices in 3 μm steps) taken in the LH at -0.6 AP just lateral/ventral to the fornix, and at -1.0 and -1.4 AP lateral to the fornix.

3.6.7 Statistics

Statistical analyses were performed using GraphPad Prism (GraphPad Software, Inc., La Jolla, CA, USA), OriginPro 8.6 (OriginLab, Northhampton, MA, USA), and MATLAB (Mathworks, Natick, MA, USA). Group comparisons were made using two-way ANOVA followed by Bonferroni post-hoc tests to control for multiple comparisons. Paired and unpaired

Student's t-tests, as well as one-way repeated measures ANOVA were used to make single-variable comparisons, and Chi-squared tests were used to compare populations.

3.7 Supplemental Figures

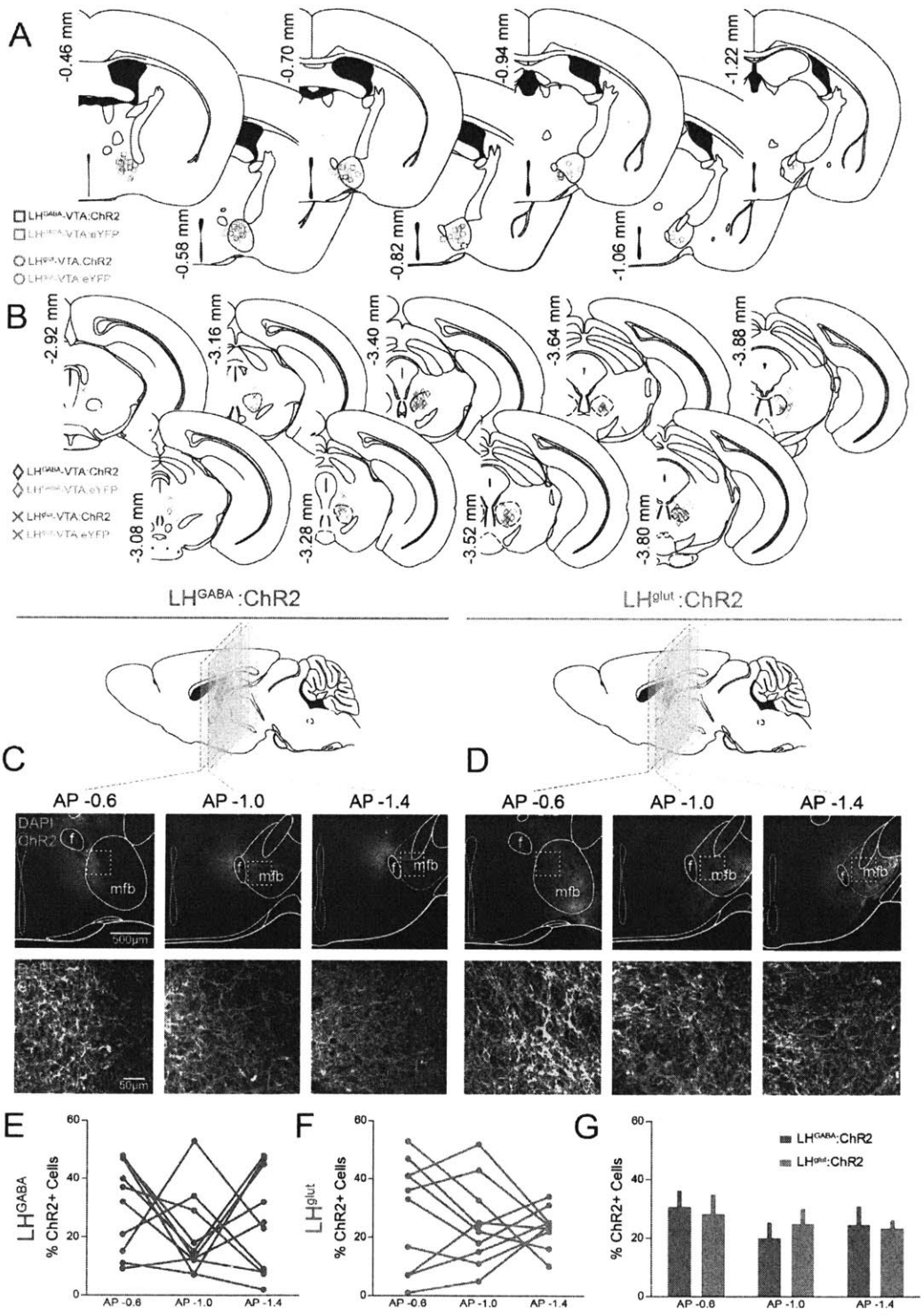

Figure S1. Related to Figures 1 and 2

(A) Estimated injection sites in the LH for AAV_5-DIO-ChR2-eYFP in VGAT::Cre (blue) and VGLUT2::Cre (red) mice, as well as for AAV_5-DIO-eYFP in eYFP controls (grey).

(B) Location of optic fiber tips implanted in VGAT::Cre (blue) and VGLUT2::Cre (red) ChR2+ mice, as well as in the eYFP controls (grey).

(C and D) (C) Low- (top) and high- (bottom) magnification confocal images from representative LH^{GABA}:ChR2 and (D) LH^{glut}:ChR2 mice showing the expression of ChR2 in the LH at three different AP coordinates. Dotted boxes indicate approximately where high-magnification 40x images were taken.

(E and F) (E) Quantification of the percentage of LH neurons that were ChR2+ at three different AP coordinates in LH^{GABA}:ChR2 (n=10) and (F) LH^{glut}:ChR2 (n=10) mice.

(G) No significant differences were found between expression at different AP coordinates in either LH^{GABA}:ChR2 or LH^{glut}:ChR2 mice (two-way ANOVA: group effect, $F_{2,36}=1.38$, $p=0.2651$; AP-coordinate effect, $F_{1,18}=0.01$, $p=0.9256$).

Error bars indicate ±SEM.

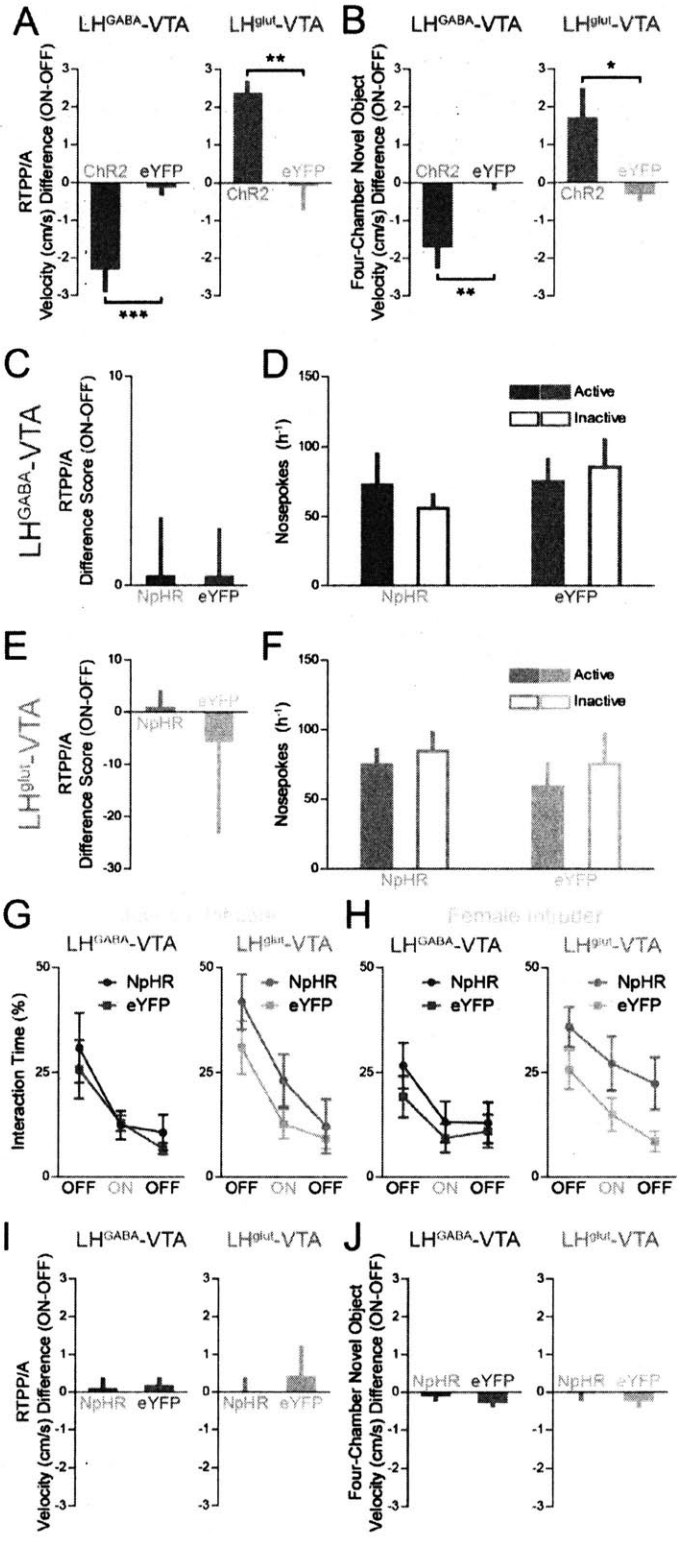
A
LH^GABA-VTA
LH^glut-VTA
RTPP/A
Velocity (cm/s) Difference (ON-OFF)
ChR2
eYFP
**
***
B
Four-Chamber Novel Object
*
C
LH^GABA-VTA
RTPP/A
Difference Score (ON-OFF)
NpHR
D
Nosepokes (h^-1)
Active
Inactive
E
LH^glut-VTA
F
G
Interaction Time (%)
NpHR
OFF ON OFF
H
I
J

Figure S2. Related to Figures 1, 2, and 3

(A and B) (A) LH^{GABA}-VTA:ChR2 mice had a significantly lower difference score in velocity (ON-OFF) than their eYFP counterparts, while LH^{glut}-VTA:ChR2 mice had a significantly higher difference score than their eYFP counterparts in the real-time place preference/avoidance (RTPP/A) assay (n=8 LH^{GABA}-VTA:ChR2, n=10 LH^{GABA}-VTA:eYFP; two-tailed, unpaired Student's t-test, ***p=0.0006; n=7 LH^{glut}-VTA:ChR2, n=9 LH^{glut}-VTA:eYFP; two-tailed, unpaired Student's t-test, **p=0.0064) and (B) the four-chamber novel object task (n=7 LH^{GABA}-VTA:ChR2, n=8 LH^{GABA}-VTA:eYFP; two-tailed, unpaired Student's t-test, **p=0.0049; n=9 LH^{glut}-VTA:ChR2, n=7 LH^{glut}-VTA:eYFP; two-tailed, unpaired Student's t-test, *p=0.0242).

(C and D) (C) No significant differences were found in LH^{GABA}-VTA:NpHR mice when compared with eYFP controls in the RTPP/A (n=9 NpHR, n=9 eYFP; two-tailed, unpaired Student's t-test, p=0.9956) or (D) intracranial self-stimulation (ICSS; n=9 NpHR, n=9 eYFP; two-way ANOVA: group x epoch interaction, $F_{1,16}$=1.89, p=0.1887) assays.

(E and F) (E) No significant differences were found in LH^{glut}-VTA:NpHR mice when compared with eYFP controls in the RTPP/A (n=10 NpHR, n=6 eYFP; two-tailed, unpaired Student's t-test, p=0.6206) or (F) ICSS (n=10 NpHR, n=7 eYFP; two-way ANOVA: group x epoch interaction, $F_{1,15}$=0.09, p=0.7744) assays.

(G and H) (G) No significant differences were found in social interaction with either juvenile (n=7 LH^{GABA}-VTA:NpHR, n=8 LH^{GABA}-VTA:eYFP; two-way ANOVA: group x epoch interaction, $F_{2,26}=0.25$, p=0.7840; n=10 LH^{glut}-VTA:NpHR, n=7 LH^{glut}-VTA:eYFP; two-way ANOVA: group x epoch interaction, $F_{2,30}=0.80$, p=0.4570) or (H) female intruders (n=9 LH^{GABA}-VTA:NpHR, n=8 LH^{GABA}-VTA:eYFP; two-way ANOVA: group x epoch interaction, $F_{2,30}=0.93$, p=0.4060; n=10 LH^{glut}-VTA:NpHR, n=7 LH^{glut}-VTA:eYFP; two-way ANOVA: group x epoch interaction, $F_{2,30}=0.09$, p=0.9154) in the social interaction assay for either LH^{GABA}-VTA:NpHR or LH^{glut}-VTA:NpHR mice compared with their respective eYFP controls.

(I and J) (I) There were no significant differences in velocity for either LH^{GABA}-VTA:NpHR or LH^{glut}-VTA:NPHR mice when compared with their eYFP controls in either the RTPP/A assay (n=9 LH^{GABA}-VTA:NpHR, n=9 LH^{GABA}-VTA:eYFP; two-tailed, unpaired Student's t-test, p=0.7362; n=10 LH^{glut}-VTA:NpHR, n=6 LH^{glut}-VTA:eYFP; two-tailed, unpaired Student's t-test, p=0.5514) or (J) the four-chamber novel object task (n=8 LH^{GABA}-VTA:NpHR, n=8 LH^{GABA}-VTA:eYFP; two-tailed, unpaired Student's t-test, p=0.1187; n=10 LH^{glut}-VTA:NpHR, n=7 LH^{glut}-VTA:eYFP; two-tailed, unpaired Student's t-test, p=0.5514).

Error bars indicate ±SEM.

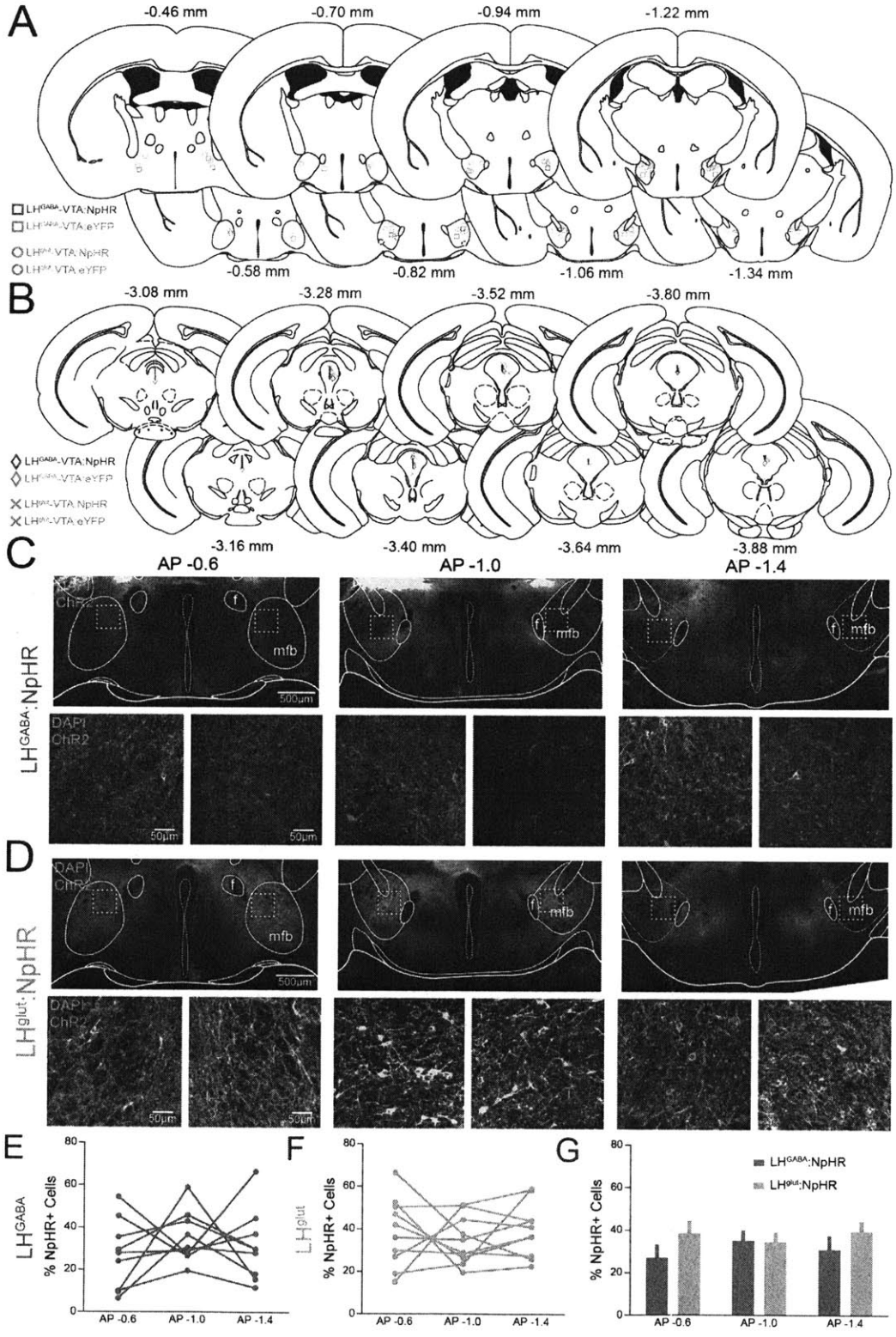
A
-0.46 mm
-0.70 mm
-0.94 mm
-1.22 mm
-0.58 mm
-0.82 mm
-1.06 mm
-1.34 mm
B
-3.08 mm
-3.28 mm
-3.52 mm
-3.80 mm
-3.16 mm
-3.40 mm
-3.64 mm
-3.88 mm
C
AP -0.6
AP -1.0
AP -1.4
LHGABA:NpHR
DAPI
ChR2
mfb
500μm
50μm
D
LHglut:NpHR
E
LHGABA
% NpHR+ Cells
F
LHglut
G
LHGABA:NpHR
LHglut:NpHR

Figure S3. Related to Figure 3

(A) Estimated injection sites in the LH for AAV_5-DIO-NpHR-eYFP in VGAT::Cre (purple) and VGLUT2::Cre (orange) mice, as well as for AAV_5-DIO-eYFP in eYFP controls (grey).

(B) Location of optic fiber tips implanted in VGAT::Cre (purple) and VGLUT2::Cre (orange) NpHR+ mice, as well as in the eYFP controls (grey).

(C and D) (C) Low- (top) and high- (bottom) magnification confocal images from representative LH^{GABA}:NpHR and (D) LH^{glut}:NpHR mice showing the expression of NpHR in the LH at three different AP coordinates. Dotted boxes indicate approximately where high-magnification 40x images were taken.

(E and F) (E) Quantification of the percentage of LH neurons that were NpHR+ at three different AP coordinates in LH^{GABA}:NpHR (n=9) and (F) LH^{glut}:NpHR mice (n=10).

(G) No significant differences were found between expression at different AP coordinates in either LH^{GABA}:NpHR or LH^{glut}:NpHR mice (two-way ANOVA: group effect, $F_{2,34}=0.18$, $p=0.8375$; AP-coordinate effect, $F_{1,17}=2.85$, $p=0.1094$).

Error bars indicate ±SEM.

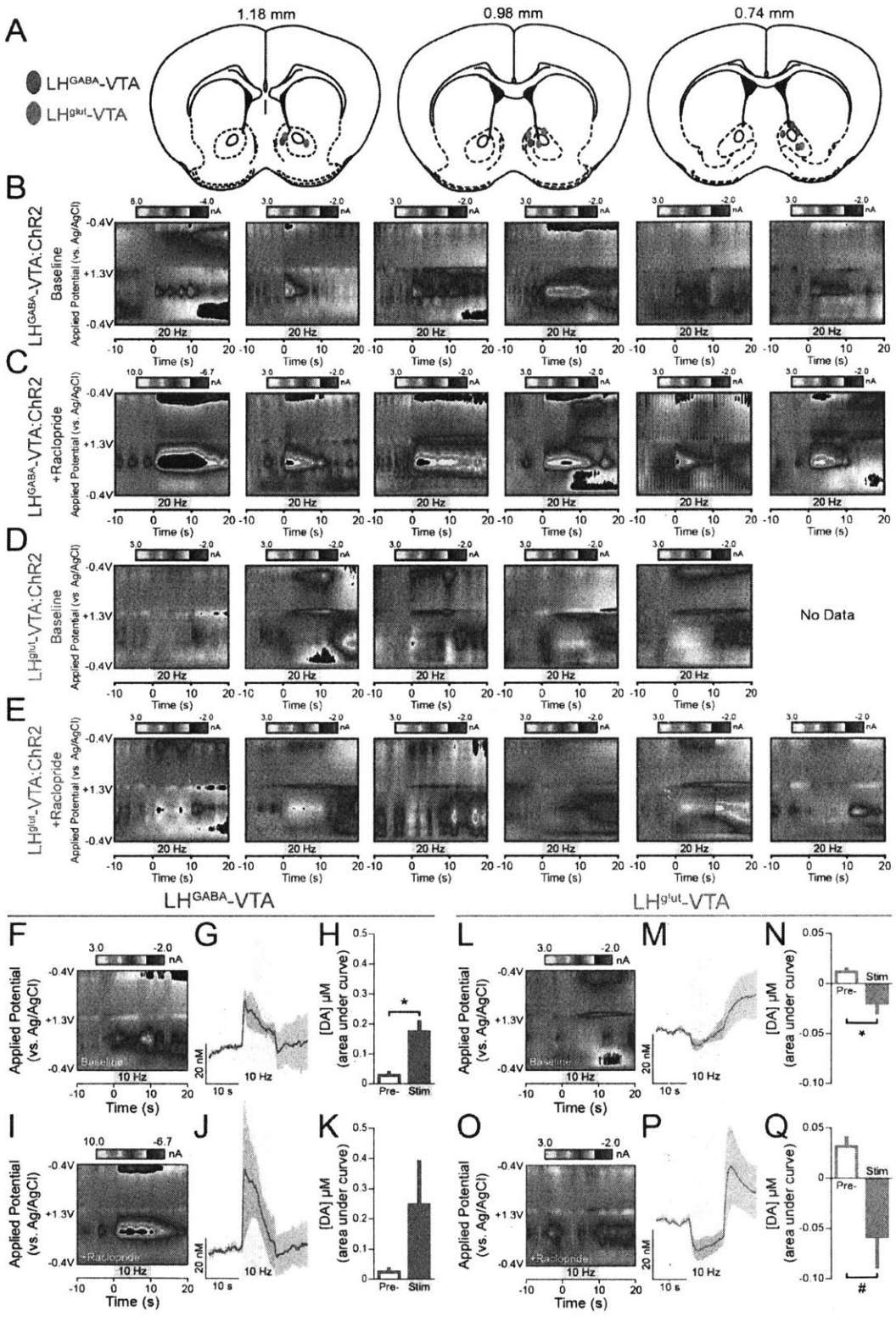
A
1.18 mm
0.98 mm
0.74 mm
LHGABA-VTA
LHglut-VTA
B
LHGABA-VTA:ChR2
Baseline
C
LHGABA-VTA:ChR2
+Raclopride
D
LHglut-VTA:ChR2
Baseline
No Data
E
LHglut-VTA:ChR2
+Raclopride
Applied Potential (vs. Ag/AgCl)
-0.4V
+1.3V
20 Hz
Time (s)
LHGABA-VTA
LHglut-VTA
F
G
H
I
J
K
L
M
N
O
P
Q
Applied Potential (vs. Ag/AgCl)
Baseline
+Raclopride
10 Hz
20 nM
10 s
[DA] µM (area under curve)
Pre-
Stim
*
#

Figure S4. Related to Figure 4

(A) Locations of FSCV electrode tips in the NAc of VGAT::Cre (blue; n=6 mice; n=6 baseline recording locations, n=6 raclopride recording locations) and VGLUT2::Cre (red; n=6 mice, n=5 baseline recording locations, n=6 raclopride recording locations) mice. Recording locations were reconstructed using electrode track and recording depth (distance from brain surface).

(B and C) (B) Representative false color plots from each subject under baseline recording conditions and (C) with raclopride in LH^{GABA}-VTA:ChR2 mice.

(D and E) (D) Representative false color plots for each recording site under baseline recording conditions and (E) with raclopride in LH^{glut}-VTA:ChR2 mice.

(F and G) 10 Hz LH^{GABA}-VTA photostimulation (473 nm, 20 mW, 5 ms pulses, 10 s duration) evoked DA release in the NAc under baseline, resting conditions. (F) Representative false color plot showing dopamine release in response to stimulation, which is also evident in the (G) averaged population data after conversion into DA concentration.

(H) Quantification of extracellular dopamine concentration ([DA]) as area under the curve shows that 10 Hz LH^{GABA}-VTA activation caused a significant increase in DA release in the NAc (compared with pre-stimulation) (n=4 mice; two-tailed, paired Student's t-test, *p=0.0145).

(I and J) Under D2 receptor blockade (raclopride, IP), 10 Hz LH^{GABA}-VTA activation increased NAc DA neurotransmission as seen in the (I) representative color plot and (J) averaged population data.

(K) Quantification of [DA] as area under the curve did not show a significant decrease in evoked release (n=4 mice; two-tailed, paired Student's t-test, p=0.1973).

(L and M) Similar to 20 Hz stimulation, 10 Hz LH^{glut}-VTA stimulation (473 nm, 20 mW, 5 ms pulses, 10 s duration) caused a pause in NAc DA release under resting, baseline conditions. (L) Representative false color plot shows a decrease in DA release in response to stimulation. 10 Hz stimulation offset was often accompanied by a small "rebound" DA increase, which is also observed in the (M) averaged population data after conversion to [DA].

(N) Quantification of [DA] as area under the curve shows that 10 Hz LH^{glut}-VTA activation caused a significant decrease in [DA] in the NAc under resting conditions (n=5 mice; two-tailed, paired Student's t-test, *p=0.0178).

(O and P) Under the influence of raclopride, 10 Hz LH^{glut}-VTA activation inhibited NAc DA release observed in the (O) representative color plot and (P) population average.

(Q) Quantification of [DA] shows that LH^{glut}-VTA activation caused a trending decrease in [DA] under D2 receptor blockade (n=6 mice; two-tailed, paired Student's t-test, #p=0.0624).

Error bars indicate ±SEM.

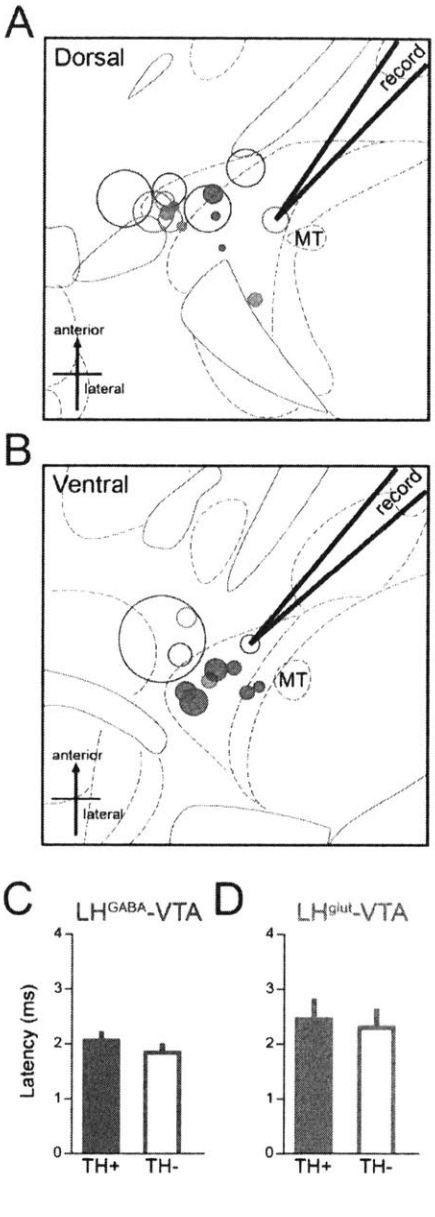
A
Dorsal
record
MT
anterior
lateral
B
Ventral
record
MT
anterior
lateral
C
LH^GABA-VTA
Latency (ms)
0
1
2
3
4
TH+
TH-
D
LH^glut-VTA
0
1
2
3
4
TH+
TH-

Figure S5. Related to Figure 6

(A and B) Horizontal brain maps of (A) dorsal and (B) ventral VTA slices showing the locations of all recorded TH+ (filled) and TH- (open) neurons with the areas of the circles indicating the relative amplitudes of the recorded inhibitory postsynaptic currents (IPSCs) in VGAT::Cre mice (blue) and excitatory postsynaptic currents (EPSCs) in VGLUT2::Cre mice (red).

(C and D) (C) No significant differences were found in the onset latencies of optically-evoked IPSCs in TH+ and TH- neurons (n=9 TH+, n=7 TH-; two-tailed, unpaired Student's t-test, p=0.2510) or (D) in the onset latencies of optically-evoked EPSCs in TH+ and TH- neurons (n=5 TH+, n=5 TH-; two-tailed, unpaired Student's t-test, p=0.7289).

Error bars indicate ±SEM.

Chapter 4

Conclusion: Discussion of the Work as a Whole, its Implications, and Future Directions of Research

Our work dissecting the greater mesolimbic dopamine system to understand how the individual components encode reward and feeding has allowed for a better understanding of the causes for overeating and obesity and offer neural targets for therapeutic intervention

4.1 The LH and the Greater Mesolimbic Dopamine Circuit

In the introduction, obesity was introduced as a rising global epidemic, and due to the health problems that arise from it, the children of today may be the first generation to live shorter lives than their parents (Harris et al., 2009; Olshansky et al., 2005). In addition, the problem with the overabundance of unhealthy foods has been exacerbated by the increase in the marketing of these foods, and the brain has fallen prey to these economic schemes to generate more consummatory behaviors.

Though obesity itself cannot be encoded in the brain, as obesity itself is not a behavioral phenotype, our studies have shown that behaviors which lead to obesity, such as eating, increased motivations to consume, and eating in the face of negative consequences are encoded in the circuits within the LH and VTA. In addition, other studies that have been published recently have helped to elucidate the circuit components that surround the LH and the greater mesolimbic dopamine system. In this first section of the conclusion, the focus will be on building a picture of the current understanding of this circuit and how it pertains to eating, reward, motivation, and obesity.

In a study published alongside our work, Jennings and colleagues showed that stimulating GABA neurons in the LH will increase feeding, while inhibiting them suppresses feeding (Jennings et al., 2015). They also show that a subset of these GABA neurons encode consumption, while others encode the operant behavior made to produce the food reward. Importantly, they also show that these GABA neurons in the LH are largely separate from orexin or MCH neurons. These results fall closely in line with our own work (Nieh et al., 2015). We show that LH neurons projecting to the VTA fire when animals approach the delivery port to

consume food in a manner similar to their neurons encoding consumption. Importantly, when we stimulate the GABAergic LH projection to the VTA, we can also evoke feeding, evidence that our LH neurons that project to the VTA are likely a subset of the GABA neurons in their study.

In Chapter 2, we also describe a second population of LH neurons – those that receive feedback from the VTA. These cells encoded the conditioned stimuli and/or the unconditioned stimuli. While we do not know if these cells are GABAergic or glutamatergic, Jennings and colleagues did record a group of GABAergic LH neurons that only responded to the nose-poke in a reward retrieval task. It is possible that the VTA-innervated LH neurons we recorded from that responded to the conditioned stimuli could be the same as this GABAergic population recorded by Jennings and colleagues. Importantly, they show that LH GABA neurons either encoded nose-poke or consumption and not both, and we show that VTA-projecting LH neurons are also separate from VTA-innervated LH neurons. None of the cells we recorded from exhibited two photoresponse latencies. This is interesting because it could add an additional layer of understanding to the connectivity in this circuit. Cells that project to the VTA don't receive innervation from the VTA, likely because they are involved in encoding two separate behavioral events.

Our work from Chapter 3 also showed that the GABAergic LH-VTA projection promotes motivational drive towards a stimulus, while the glutamatergic LH-VTA projection suppresses it. Initially, it was difficult to understand how activating an inhibitory projection to the VTA could be promoting rewarding behaviors. However, we show that this occurs through a disinhibitory mechanism in the VTA, where GABAergic LH neurons synapse onto GABAergic neurons in the VTA, which in turn are known to inhibit dopamine neurons in the VTA (Tan et al., 2012; van

Zessen et al., 2012). These results contradict previous data from another group and a previously-accepted attractive model in which an excitatory projection from the LH to the VTA was believed to play the major role in reward-related behaviors (Kempadoo et al., 2013; You et al., 2001). However, our results of a disinhibition mechanism in the VTA mediating dopamine release were not completely unexpected. Evidence already existed that drugs of abuse utilize disinhibition in the VTA to produce aspects of their addictive actions (Bocklisch et al., 2013; Johnson and North, 1992).

Another important finding from our work is that stimulation of the GABAergic LH-VTA projection can produce a variety of behaviors, including feeding, gnawing, and social interaction, and that this happens through an increase in motivation or fixation towards a stimulus. These results fit very well with Valenstein and colleagues' work in substitutability (Valenstein et al., 1968) and Navarro and colleagues's work showing that stimulating GABAergic LH neurons can also induce consummatory behaviors towards saccharin, water, or wood (Navarro et al., 2015). In fact, activation of another group of orexigenic neurons, the agouti-related peptide (AGRP) neurons, which stimulate feeding via hunger instead of motivation (Betley et al., 2015), has also been shown to generate behavior towards non-food objects, in this case grooming, in a context where food is not available (Dietrich et al., 2015). Dietrich and colleagues refer to this behavior as a "displacement" behavior, where the animals will perform an action such as grooming when they have no food to feed on. Essentially, our work shows that we can evoke many behaviors from GABAergic LH-VTA stimulation, which are also the neurons that encode conditioned responding. In different contexts, i.e. in the presence of another animal or a novel object, the animals have a distinct way that they have learned to respond in these environments. As a result, GABAergic LH-VTA stimulation can cause the animals to make the distinct conditioned

responses that they have associated with each environment/stimulus – different stimuli will evoke different responses.

A question often asked is whether we know the inputs to these LH neurons that project to the VTA. While we haven't done any work in this direction, others have, and two areas of special importance are the NAc (Kelley et al., 2005; Mogenson et al., 1983; O'Connor et al., 2015; Thompson and Swanson, 2010) and the bed nucleus of the stria terminalis (BNST) (Jennings et al., 2013; Kim et al., 2013). O'Connor and colleagues showed that medium spiny neurons in the nucleus accumbens shell that express the dopamine D1R receptor (D1R-MSN) project to LH GABA neurons, and that inhibition of this projection prolongs feeding, while activation stops feeding. This is incredibly important because it shows a potentially closed loop within this system. LH GABA neurons project to GABA cells in the VTA (Chapter 3) and stimulating these projections increases dopamine release in the nucleus accumbens. Dopamine released into the nucleus accumbens activates D1R-MSNs that then project to the LH GABA neurons (O'Connor et al., 2015). It would be incredibly interesting to see whether these two populations of GABA neurons (VTA-projecting and D1R-MSN-innervated) are the same or separate populations. If they are the same, what is the purpose of this closed loop – is it simply a positive reinforcement loop to affectively increase gain, or is the information that is sent from these neurons computationally different by the time it is received again?

A second study by Jennings and colleagues shows that the BNST also provides an important projection to the LH (Jennings et al., 2013). They show that inhibitory synaptic inputs from the BNST innervate and suppress the activity of glutamatergic neurons in the LH and that activating this projection induces feeding in well-fed mice, while inhibiting this projection

suppresses feeding. Meanwhile, activating the glutamatergic LH neurons themselves also suppresses feeding and is aversive for animals. We showed in Chapter 3 that stimulating LH glutamatergic projections to the VTA is aversive as well, which ties in the results from these two studies. Importantly, while the NAc preferentially synapses onto GABAergic cells in the LH, the BNST synapses onto glutamatergic cells in the LH, providing two distinct inputs onto two distinct populations within the LH. Our work has shown that the projections from these two populations to the VTA mediate opposite effects, but we still do not know how these two projections interact with each other, which is a rich direction to proceed for future work.

4.2 Fitting our Work into the Existing Framework

The reasons why an animal feeds have been historically separated into two distinct causes – homeostasis and pleasure, i.e. the satiation of hunger or the hedonic value of food. In Clark Hull's drive-reduction theory, the motivation for action is considered to be in response to an aversive perturbation in homeostasis (Hull, 1943). This idea was borrowed from earlier work from Walter Cannon, who was the first to define homeostasis as a concept in which steady states in the body are regulated and maintained (Cannon, 1929, 1932). Related to homeostasis is the set point, which is the optimal state of any given system, and it was Kennedy who first suggested that body weight might have a set point that animals use to adjust food intake in order to maintain stable fat stores (Kennedy, 1953). In fact, studies relating to the lateral hypothalamus and its role in feeding brought forth the contemporaneous idea that the primary effect of LH lesion was to lower the set point for body weight (Keesey et al., 1976).

In addition to the idea of feeding in response to a disturbance in homeostasis, animals also appear to eat for the pleasure of food. Dogs with intragastric injections of food continue to eat and become overweight (Janowitz and Grossman, 1949; Turner et al., 1975), disrupting the natural homeostatic balance in energy. In this case, feeding for pleasure actually perturbed homeostasis, instead of reducing the perturbation.

An important difference between feeding due to hunger and feeding due to the rewarding value of food is valence – hunger is an aversive state that carries negative valence, while the reward from food is pleasurable and carries a positive valence. In Chapter 3, we noted that while stimulation of AGRP neurons causes feeding and real-time place aversion (Betley et al., 2015), stimulation of the GABAergic LH-VTA projection causes feeding and real-time place preference. One interpretation is that while the AGRP neurons cause feeding for drive-reduction, the GABAergic LH-VTA projection causes feeding for pleasure. However, another possible interpretation is that stimulating the GABAergic LH-VTA projection causes behavioral activation and carries a neutral valence, and the place preference and intracranial self-stimulation observed may be a result of actions generated by stimulation that are not necessarily hedonic or pleasurable in nature. The animal may spend more time in the stimulated zone because the stimulation is causing the animal explore the area, which is a natural action in response to the presence of a novel environment. Exploration has neither a positive or negative valence. In this interpretation for GABAergic LH-VTA stimulation, the role of the projection is to simply call the animal to action after upstream areas of the brain have decided the reason for action and before downstream areas of the brain can decide whether the result was positive or negative.

Depending on the context of the environment, stimulation of the GABAergic LH-VTA projection can evoke different behaviors. It's important to note that the experiments in Chapter 2 where we observed and quantified gnawing were all performed in a context where food was present or in the same environment where the animals had previously performed feeding-related tasks. As a result, gnawing, i.e. attempting to eat, other stimuli may be a result of activation of the GABAergic LH-VTA projection in an environment where the animal had learned that feeding was the most appropriate conditioned response.

Another interpretation relies on an older idea, Konrad Lorenz's hydraulic model, which conceptualizes motivational drive as a slow accumulation of motivation in a reservoir that can burst open if internal pressure or external stimuli are great enough (Lorenz and Leyhausen, 1973). Importantly, different behaviors are modelled as multiple receptacles that the drive can then flow into, and if the flow is too great, unintended behaviors can be activated as the drive overflows into nearby receptacles. In this model, it's possible that GABAergic LH-VTA activation filled the receptacle for the appropriate response for an animal to investigate an object, but also overfilled into the receptacle for feeding, which then caused the misdirected gnawing behaviors. This model has been extended to the idea of displacement behaviors, in which animals will perform actions that seem out of place or unintended in situations of high motivational drive, such as evidence that birds engaging in fight/flight actions will suddenly engage in eating or grooming (Tinbergen and Van Iersel, 1947), or that stimulating AGRP neurons in the absence of food will also cause gnawing or grooming behaviors (Dietrich et al., 2015).

4.3 The Treatment of Obesity

As we have shown, neurons in the LH that send projections to the VTA encode the conditioned response, in that they respond when the animal consumes a sugar reward after the predictive cue. When we stimulate these neurons, we can promote the motivation for these animals to seek the sugar reward, even in the face of physical harm. Importantly, inhibiting these neurons suppresses this motivation. In addition, we show that the GABAergic component of this projection drives this behavior, and that this feeding is generated by changing the motivation of the animal to consume the most salient stimulus.

Evidence from our work and the work of many neuroscientists over the last half-century have shown that feeding and reward are related behaviors. As such, we could expect that a dysfunction in feeding behavior may also result in dysfunction in other reward-related behaviors. Evidence has shown that patients with binge-eating disorder are more susceptible to compulsive buying (Faber et al., 1995), and over half of children who are obese also suffer from attention deficit/hyperactivity disorder (AD/HD) (Agranat-Meged et al., 2005). This comorbidity with AD/HD is especially interesting. If we believe that stimulation of the GABAergic LH-VTA is generating an increased motivation to consume a stimulus, which evidence from Chapter 3 suggests, misdirected attention in AD/HD patients to food could be induced by maladaptive GABAergic LH-VTA neurons.

In addition, the relationship between food and reward in the same brain networks that may mediate obesity makes obesity an even more difficult disease to treat. Neurological drugs that exist today are already riddled with unintended side-effects (Evans and McLeod, 2003; Grosset and Grosset, 2004; Haddad and Dursun, 2008). These side effects largely stem from two

causes. First, we do not fully understand the system that is being perturbed, and second, we are not able to target the specific area in the brain even if we do know the exact cause. In other dopamine-related diseases, such as Parkinson's disease, the symptoms of dyskinesia, bradykinesia, or tremors are always present, and putting an end to those symptoms permanently is a valid method of treatment. In the case of obesity, we cannot shut down feeding in the same way. When feeding is shut down in dopamine-deficient animals, these animals stop eating altogether and die of starvation (Szczypka et al., 1999a). Thus, for the treatment of obesity, overeating has to be controlled, while eating due to natural hunger should be maintained. In Chapter 2, we showed that inhibiting the LH-VTA projection will suppress sugar-seeking in the face of a negative consequence, but leave feeding of normal chow due to hunger intact. We proposed that this makes the LH-VTA projection a valid point of entry for therapeutic intervention. However, in Chapter 3, we found that situation was not so simple. This projection causes feeding changes by modulating attention or motivation to stimuli. So even if we inhibited the LH-VTA projection to suppress unhealthy feeding behaviors, there could still be unintended consequences for motivation and attention.

In this case, the proper treatment may be temporal, meaning that the inhibition of the LH-VTA projection should only happen when the patient is about to partake in unhealthy eating. Importantly, LH neurons projecting to VTA that encode conditioned responding increase their firing prior to the actual consumption of the sugar reward. As a result, we could effectively build a closed-loop system that detects when these neurons begin to fire to indicate that the patient is about to eat and suppress that activity before the consumption occurs. If we truly believe that we have identified a circuit involved in obesity, then the logical next step is to see if interventions in this circuit are valid to treat obesity in mouse models.

4.4 Into the Future

While the work I have presented in this thesis has provided new insight into the greater mesolimbic dopamine system, there is still much to understand. In the neuroscience subfield of circuit mapping, we treat each projection as if it were a single computational unit, but the brain does not function this way. Even if we target a single projection with a single neurotransmitter in a mouse, such as the GABAergic LH-VTA projection, this projection still contains thousands of neurons that are computationally heterogeneous. To really understand how the brain works, we need to understand the relevance of each of these neurons. How do they each change over time as an animal learns a task, or as the animal becomes sated? Are there neurons that are more or less susceptible to satiety? What happens when the animals are in different motivational states? Do the same neurons encode feeding for high-fat foods and feeding for high-sugar foods, or are there separate populations? What happens when animals become obese and addicted to food? Do neurons that encode feeding become overactive, or are neurons that previously encoded other behaviors recruited to encode food consumption? Importantly, how do these individual neurons interact with each other? What are the population dynamics involved in the neural encoding of feeding?

Because the speed of technological advances in food production has far surpassed the speed of evolution in our brains, we have been unable to cope with the new food-abundant and food-enriched environment, and this has led to the advent of the obesity epidemic. However, perhaps as technological advances in neuroscience gain speed and our understanding of the brain becomes clearer, we will be able to intervene in the fight against obesity and turn the tides. It is

with this fervor and spirit that I continue my career in science, and this thesis represents only the first of my many contributions.

Chapter 5

References

"If I have seen further, it is by standing on the shoulders of giants."

-Sir Isaac Newton, 1676

5.1 References

Abizaid, A., Liu, Z.-W., Andrews, Z.B., Shanabrough, M., Borok, E., Elsworth, J.D., Roth, R.H., Sleeman, M.W., Picciotto, M.R., Tschöp, M.H., et al. (2006). Ghrelin modulates the activity and synaptic input organization of midbrain dopamine neurons while promoting appetite. J. Clin. Invest. *116*, 3229–3239.

Adamantidis, A.R., Zhang, F., Aravanis, A.M., Deisseroth, K., and Lecea, L. de (2007). Neural substrates of awakening probed with optogenetic control of hypocretin neurons. Nature *450*, 420–424.

Agranat-Meged, A.N., Deitcher, C., Goldzweig, G., Leibenson, L., Stein, M., and Galili-Weisstub, E. (2005). Childhood obesity and attention deficit/hyperactivity disorder: A newly described comorbidity in obese hospitalized children. Int. J. Eat. Disord. *37*, 357–359.

Ahima, R.S., Prabakaran, D., Mantzoros, C., Qu, D., Lowell, B., Maratos-Flier, E., and Flier, J.S. (1996). Role of leptin in the neuroendocrine response to fasting. Publ. Online 18 July 1996 Doi101038382250a0 *382*, 250–252.

Ahima, R.S., Saper, C.B., Flier, J.S., and Elmquist, J.K. (2000). Leptin Regulation of Neuroendocrine Systems. Front. Neuroendocrinol. *21*, 263–307.

Albert, D.J., Nanji, N., Brayley, K.N., and Madryga, F.J. (1979). Hyperreactivity as well as mouse killing is induced by electrical stimulation of the lateral hypothalamus in the rat. Behav. Neural Biol. *27*, 59–71.

Alwan, A. (2011). Global status report on noncommunicable diseases 2010. World Health Organ. 176 pp.

Anand, B.K., and Brobeck, J.R. (1951a). Hypothalamic Control of Food Intake in Rats and Cats. Yale J. Biol. Med. *24*, 123–140.

Anand, B.K., and Brobeck, J.R. (1951b). Localization of a "feeding center" in the hypothalamus of the rat. Proc. Soc. Exp. Biol. Med. Soc. Exp. Biol. Med. N. Y. N *77*, 323–324.

Andersson, J.L., Nomikos, G.G., Marcus, M., Hertel, P., Mathe, J.M., and Svensson, T.H. (1995). Ritanserin potentiates the stimulatory effects of raclopride on neuronal activity and dopamine release selectively in the mesolimbic dopaminergic system. Naunyn. Schmiedebergs Arch. Pharmacol. *352*, 374–385.

Aponte, Y., Atasoy, D., and Sternson, S.M. (2011). AGRP neurons are sufficient to orchestrate feeding behavior rapidly and without training. Nat. Neurosci. *14*, 351–355.

Aragona, B.J., Cleaveland, N.A., Stuber, G.D., Day, J.J., Carelli, R.M., and Wightman, R.M. (2008). Preferential Enhancement of Dopamine Transmission within the Nucleus Accumbens Shell by Cocaine Is Attributable to a Direct Increase in Phasic Dopamine Release Events. J. Neurosci. *28*, 8821–8831.

Aston-Jones, G., Smith, R.J., Sartor, G.C., Moorman, D.E., Massi, L., Tahsili-Fahadan, P., and Richardson, K.A. (2010). Lateral hypothalamic orexin/hypocretin neurons: A role in reward-seeking and addiction. Brain Res. *1314*, 74–90.

Atallah, H.E., Lopez-Paniagua, D., Rudy, J.W., and O'Reilly, R.C. (2007). Separate neural substrates for skill learning and performance in the ventral and dorsal striatum. Nat. Neurosci. *10*, 126–131.

Atasoy, D., Betley, J.N., Su, H.H., and Sternson, S.M. (2012). Deconstruction of a neural circuit for hunger. Nature *488*, 172–177.

Austin, S.B., Melly, S.J., Sanchez, B.N., Patel, A., Buka, S., and Gortmaker, S.L. (2005). Clustering of Fast-Food Restaurants Around Schools: A Novel Application of Spatial Statistics to the Study of Food Environments. Am. J. Public Health *95*, 1575–1581.

Avena, N.M. (2007). Examining the addictive-like properties of binge eating using an animal model of sugar dependence. Exp. Clin. Psychopharmacol. Exp. Clin. Psychopharmacol. *15*, 481.

Avena, N.M., Rada, P., and Hoebel, B.G. (2008). Evidence for sugar addiction: Behavioral and neurochemical effects of intermittent, excessive sugar intake. Neurosci. Biobehav. Rev. *32*, 20–39.

Badrinarayan, A., Wescott, S.A., Vander Weele, C.M., Saunders, B.T., Couturier, B.E., Maren, S., and Aragona, B.J. (2012). Aversive Stimuli Differentially Modulate Real-Time Dopamine Transmission Dynamics within the Nucleus Accumbens Core and Shell. J. Neurosci. *32*, 15779–15790.

Barone, F.C., Wayner, M.J., Scharoun, S.L., Guevara-Aguilar, R., and Aguilar-Baturoni, H.U. (1981). Afferent connections to the lateral hypothalamus: a horseradish peroxidase study in the rat. Brain Res. Bull. *7*, 75–88.

Barson, J.R., Morganstern, I., Leibowitz, S.F., Barson, J.R., Morganstern, I., and Leibowitz, S.F. (2013). Complementary Roles of Orexin and Melanin-Concentrating Hormone in Feeding Behavior. Int. J. Endocrinol. Int. J. Endocrinol. *2013, 2013*, e983964

Basbaum, A.I., and Fields, H.L. (1979). The origin of descending pathways in the dorsolateral funiculus of the spinal cord of the cat and rat: Further studies on the anatomy of pain modulation. J. Comp. Neurol. *187*, 513–531.

Beckstead, R.M., Domesick, V.B., and Nauta, W.J. (1979). Efferent connections of the substantia nigra and ventral tegmental area in the rat. Brain Res. *175*, 191–217.

Belin, D., Mar, A.C., Dalley, J.W., Robbins, T.W., and Everitt, B.J. (2008). High impulsivity predicts the switch to compulsive cocaine-taking. Science *320*, 1352–1355.

Ben-Bassat, J., Peretz, E., and Sulman, F.G. (1959). Analgesimetry and ranking of analgesic drugs by the receptacle method. Arch. Int. Pharmacodyn. Thérapie *122*, 434–447.

Benton, D. (2010). The plausibility of sugar addiction and its role in obesity and eating disorders. Clin. Nutr. *29*, 288–303.

Berk, M.L., and Finkelstein, J.A. (1982). Efferent connections of the lateral hypothalamic area of the rat: An autoradiographic investigation. Brain Res. Bull. *8*, 511–526.

Berridge, K.C. (2006). The debate over dopamine's role in reward: the case for incentive salience. Psychopharmacology (Berl.) *191*, 391–431.

Berridge, K.C., and Robinson, T.E. (1998). What is the role of dopamine in reward: hedonic impact, reward learning, or incentive salience? Brain Res. Rev. *28*, 309–369.

Berridge, K.C., and Robinson, T.E. (2003). Parsing reward. Trends Neurosci. *26*, 507–513.

Berridge, K.C., Venier, I.L., and Robinson, T.E. (1989). Taste reactivity analysis of 6-hydroxydopamine-induced aphagia: implications for arousal and anhedonia hypotheses of dopamine function. Behav. Neurosci. *103*, 36–45.

Berthoud, H.-R., and Münzberg, H. (2011). The lateral hypothalamus as integrator of metabolic and environmental needs: from electrical self-stimulation to opto-genetics. Physiol. Behav. *104*, 29–39.

Betley, J.N., Cao, Z.F.H., Ritola, K.D., and Sternson, S.M. (2013). Parallel, redundant circuit organization for homeostatic control of feeding behavior. Cell *155*, 1337–1350.

Betley, J.N., Xu, S., Cao, Z.F.H., Gong, R., Magnus, C.J., Yu, Y., and Sternson, S.M. (2015). Neurons for hunger and thirst transmit a negative-valence teaching signal. Nature *521*, 180–185.

Bielajew, C., and Shizgal, P. (1986). Evidence implicating descending fibers in self-stimulation of the medial forebrain bundle. J. Neurosci. Off. J. Soc. Neurosci. *6*, 919–929.

Bittencourt, J.C., Presse, F., Arias, C., Peto, C., Vaughan, J., Nahon, J.-L., Vale, W., and Sawchenko, P.E. (1992). The melanin-concentrating hormone system of the rat brain: An immuno- and hybridization histochemical characterization. J. Comp. Neurol. *319*, 218–245.

Black, D.W., and Moyer, T. (1998). Clinical features and psychiatric comorbidity of subjects with pathological gambling behavior. Psychiatr. Serv. Wash. DC *49*, 1434–1439.

Bocklisch, C., Pascoli, V., Wong, J.C.Y., House, D.R.C., Yvon, C., Roo, M. de, Tan, K.R., and Lüscher, C. (2013). Cocaine Disinhibits Dopamine Neurons by Potentiation of GABA Transmission in the Ventral Tegmental Area. Science *341*, 1521–1525.

Borgland, S.L., Taha, S.A., Sarti, F., Fields, H.L., and Bonci, A. (2006). Orexin A in the VTA Is Critical for the Induction of Synaptic Plasticity and Behavioral Sensitization to Cocaine. Neuron *49*, 589–601.

Boutrel, B., Cannella, N., and de Lecea, L. (2010). The role of hypocretin in driving arousal and goal-oriented behaviors. Brain Res. *1314*, 103–111.

Brobeck, J.R. (1946). Mechanism of the Development of Obesity in Animals with Hypothalamic Lesions. Physiol. Rev. *26*, 541–559.

Burton, M.J., Rolls, E.T., and Mora, F. (1976). Effects of hunger on the responses of neurons in the lateral hypothalamus to the sight and taste of food. Exp. Neurol. *51*, 668–677.

Cador, M., Kelley, A.E., Le Moal, M., and Stinus, L. (1986). Ventral tegmental area infusion of substance P, neurotensin and enkephalin: Differential effects on feeding behavior. Neuroscience *18*, 659–669.

Cannon, W.B. (1929). Organization for Physiological Homeostasis. Physiol. Rev. *9*, 399–431.

Cannon, W.B. (1932). The wisdom of the body (New York, NY, US: W W Norton & Co).

Carr, G.D., and White, N.M. (1983). Conditioned place preference from intra-accumbens but not intra-caudate amphetamine injections. Life Sci. *33*, 2551–2557.

Carr, G.D., and White, N.M. (1986). Anatomical disassociation of amphetamine's rewarding and aversive effects: an intracranial microinjection study. Psychopharmacology (Berl.) *89*, 340–346.

Carraway, R., and Leeman, S.E. (1973). The Isolation of a New Hypotensive Peptide, Neurotensin, from Bovine Hypothalami. J. Biol. Chem. *248*, 6854–6861.

Carter, M.E., Adamantidis, A., Ohtsu, H., Deisseroth, K., and de Lecea, L. (2009). Sleep homeostasis modulates hypocretin-mediated sleep-to-wake transitions. J. Neurosci. Off. J. Soc. Neurosci. *29*, 10939–10949.

Carter, M.E., Soden, M.E., Zweifel, L.S., and Palmiter, R.D. (2013). Genetic identification of a neural circuit that suppresses appetite. Nature *503*, 111–114.

Cason, A.M., Smith, R.J., Tahsili-Fahadan, P., Moorman, D.E., Sartor, G.C., and Aston-Jones, G. (2010). Role of orexin/hypocretin in reward-seeking and addiction: implications for obesity. Physiol. Behav. *100*, 419–428.

Chen, B.T., Yau, H.-J., Hatch, C., Kusumoto-Yoshida, I., Cho, S.L., Hopf, F.W., and Bonci, A. (2013a). Rescuing cocaine-induced prefrontal cortex hypoactivity prevents compulsive cocaine seeking. Nature *496*, 359–362.

Chen, T.-W., Wardill, T.J., Sun, Y., Pulver, S.R., Renninger, S.L., Baohan, A., Schreiter, E.R., Kerr, R.A., Orger, M.B., Jayaraman, V., et al. (2013b). Ultra-sensitive fluorescent proteins for imaging neuronal activity. Nature *499*, 295–300.

Chergui, K., Charléty, P.J., Akaoka, H., Saunier, C.F., Brunet, J.-L., Buda, M., Svensson, T.H., and Chouvet, G. (1993). Tonic Activation of NMDA Receptors Causes Spontaneous Burst Discharge of Rat Midbrain Dopamine Neurons In Vivo. Eur. J. Neurosci. *5*, 137–144.

Chiara, G.D., and Imperato, A. (1988). Drugs abused by humans preferentially increase synaptic dopamine concentrations in the mesolimbic system of freely moving rats. Proc. Natl. Acad. Sci. *85*, 5274–5278.

Chiodo, L.A., Antelman, S.M., Caggiula, A.R., and Lineberry, C.G. (1980). Sensory stimuli alter the discharge rate of dopamine (DA) neurons: evidence for two functional types of DA cells in the substantia nigra. Brain Res. *189*, 544–549.

Ciano, P.D., Cardinal, R.N., Cowell, R.A., Little, S.J., and Everitt, B.J. (2001). Differential Involvement of NMDA, AMPA/Kainate, and Dopamine Receptors in the Nucleus Accumbens Core in the Acquisition and Performance of Pavlovian Approach Behavior. J. Neurosci. *21*, 9471–9477.

Cohen, J.Y., Haesler, S., Vong, L., Lowell, B.B., and Uchida, N. (2012). Neuron-type-specific signals for reward and punishment in the ventral tegmental area. Nature *482*, 85–88.

Coizet, V., Dommett, E.J., Redgrave, P., and Overton, P.G. (2006). Nociceptive responses of midbrain dopaminergic neurones are modulated by the superior colliculus in the rat. Neuroscience *139*, 1479–1493.

Collins, A.L., Greenfield, V.Y., Bye, J.K., Linker, K.E., Wang, A.S., and Wassum, K.M. (2016). Dynamic mesolimbic dopamine signaling during action sequence learning and expectation violation. Sci. Rep. *6*, 20231.

Cornwall, J., Cooper, J.D., and Phillipson, O.T. (1990). Afferent and efferent connections of the laterodorsal tegmental nucleus in the rat. Brain Res. Bull. *25*, 271–284.

Corsica, J.A., and Pelchat, M.L. (2010). Food addiction: true or false? Curr. Opin. Gastroenterol. *26*, 165.

Cota, D., Tschöp, M.H., Horvath, T.L., and Levine, A.S. (2006). Cannabinoids, opioids and eating behavior: The molecular face of hedonism? Brain Res. Rev. *51*, 85–107.

Cunningham-Williams, R.M., Cottler, L.B., Compton, W.M., and Spitznagel, E.L. (1998). Taking chances: problem gamblers and mental health disorders--results from the St. Louis Epidemiologic Catchment Area Study. Am. J. Public Health *88*, 1093–1096.

Dafny, N., Dong, W.Q., Prieto-Gomez, C., Reyes-Vazquez, C., Stanford, J., and Qiao, J.T. (1996). Lateral hypothalamus: Site involved in pain modulation. Neuroscience *70*, 449–460.

Date, Y., Ueta, Y., Yamashita, H., Yamaguchi, H., Matsukura, S., Kangawa, K., Sakurai, T., Yanagisawa, M., and Nakazato, M. (1999). Orexins, orexigenic hypothalamic peptides, interact with autonomic, neuroendocrine and neuroregulatory systems. Proc. Natl. Acad. Sci. *96*, 748–753.

David, V., Durkin, T.P., and Cazala, P. (1997). Self-administration of the GABAA antagonist bicuculline into the ventral tegmental area in mice: dependence on D2 dopaminergic mechanisms. Psychopharmacology (Berl.) *130*, 85–90.

Day, J.J., Roitman, M.F., Wightman, R.M., and Carelli, R.M. (2007). Associative learning mediates dynamic shifts in dopamine signaling in the nucleus accumbens. Nat. Neurosci. *10*, 1020–1028.

Delgado, J.M.R., and Anand, B.K. (1953). Increase of food intake induced by electrical stimulation of the lateral hypothalamus. Am. J. Physiol. *172*, 162–168.

Deroche-Gamonet, V., Belin, D., and Piazza, P.V. (2004). Evidence for addiction-like behavior in the rat. Science *305*, 1014–1017.

Dickinson, A., Smith, J., and Mirenowicz, J. (2000). Dissociation of Pavlovian and instrumental incentive learning under dopamine antagonists. Behav. Neurosci. *114*, 468–483.

Dietrich, M.O., Zimmer, M.R., Bober, J., and Horvath, T.L. (2015). Hypothalamic Agrp Neurons Drive Stereotypic Behaviors beyond Feeding. Cell *160*, 1222–1232.

DiLeone, R.J., Georgescu, D., and Nestler, E.J. (2003). Lateral hypothalamic neuropeptides in reward and drug addiction. Life Sci. *73*, 759–768.

Diorio, D., Viau, V., and Meaney, M.J. (1993). The role of the medial prefrontal cortex (cingulate gyrus) in the regulation of hypothalamic-pituitary-adrenal responses to stress. J. Neurosci. *13*, 3839–3847.

Dobi, A., Margolis, E.B., Wang, H.-L., Harvey, B.K., and Morales, M. (2010). Glutamatergic and Nonglutamatergic Neurons of the Ventral Tegmental Area Establish Local Synaptic Contacts with Dopaminergic and Nondopaminergic Neurons. J. Neurosci. *30*, 218–229.

Drewnowski, A. (1997). Taste preferences and food intake. Annu. Rev. Nutr. *17*, 237–253.

Dreyer, J.K., Vander Weele, C.M., Lovic, V., and Aragona, B.J. (2016). Functionally Distinct Dopamine Signals in Nucleus Accumbens Core and Shell in the Freely Moving Rat. J. Neurosci. *36*, 98–112.

Edwards, C.M., Abusnana, S., Sunter, D., Murphy, K.G., Ghatei, M.A., and Bloom, S.R. (1999). The effect of the orexins on food intake: comparison with neuropeptide Y, melanin-concentrating hormone and galanin. J. Endocrinol. *160*, R7–R12.

Evans, W.E., and McLeod, H.L. (2003). Pharmacogenomics — Drug Disposition, Drug Targets, and Side Effects. N. Engl. J. Med. *348*, 538–549.

Everitt, B.J., and Robbins, T.W. (2005). Neural systems of reinforcement for drug addiction: from actions to habits to compulsion. Nat. Neurosci. *8*, 1481–1489.

Everitt, B.J., Parkinson, J.A., Olmstead, M.C., Arroyo, M., Robledo, P., and Robbins, T.W. (1999). Associative processes in addiction and reward. The role of amygdala-ventral striatal subsystems. Ann. N. Y. Acad. Sci. *877*, 412–438.

Faber, R.J., Christenson, G.A., Zwaan, M. de, and Mitchell, J. (1995). Two Forms of Compulsive Consumption: Comorbidity of Compulsive Buying and Binge Eating. J. Consum. Res. *22*, 296–304.

Federal Trade Commission (2008). Marketing food to children and adolescents: A review of industry expenditures, activities, and self-regulations (Federal Trade Commission - Washington, DC).

Fields, H.L., Hjelmstad, G.O., Margolis, E.B., and Nicola, S.M. (2007). Ventral tegmental area neurons in learned appetitive behavior and positive reinforcement. Annu Rev Neurosci *30*, 289–316.

Flagel, S.B., Clark, J.J., Robinson, T.E., Mayo, L., Czuj, A., Willuhn, I., Akers, C.A., Clinton, S.M., Phillips, P.E.M., and Akil, H. (2011). A selective role for dopamine in stimulus-reward learning. Nature *469*, 53–57.

Forster, G.L., Falcon, A.J., Miller, A.D., Heruc, G.A., and Blaha, C.D. (2002). Effects of laterodorsal tegmentum excitotoxic lesions on behavioral and dopamine responses evoked by morphine and d-amphetamine. Neuroscience *114*, 817–823.

Friedman, J.M., and Halaas, J.L. (1998). Leptin and the regulation of body weight in mammals. Nature *395*, 763–770.

Gallistel, C.R., Gomita, Y., Yadin, E., and Campbell, K.A. (1985). Forebrain origins and terminations of the medial forebrain bundle metabolically activated by rewarding stimulation or by reward-blocking doses of pimozide. J. Neurosci. *5*, 1246–1261.

Gautvik, K.M., de Lecea, L., Gautvik, V.T., Danielson, P.E., Tranque, P., Dopazo, A., Bloom, F.E., and Sutcliffe, J.G. (1996). Overview of the most prevalent hypothalamus-specific mRNAs, as identified by directional tag PCR subtraction. Proc. Natl. Acad. Sci. U. S. A. *93*, 8733–8738.

Georgescu, D., Zachariou, V., Barrot, M., Mieda, M., Willie, J.T., Eisch, A.J., Yanagisawa, M., Nestler, E.J., and DiLeone, R.J. (2003). Involvement of the lateral hypothalamic peptide orexin in morphine dependence and withdrawal. J. Neurosci. Off. J. Soc. Neurosci. *23*, 3106–3111.

Girault J, and Greengard P (2004). THe neurobiology of dopamine signaling. Arch. Neurol. *61*, 641–644.

Glimcher, P.W., Margolin, D.H., Giovino, A.A., and Hoebel, B.G. (1984). Neurotensin: A new "reward peptide." Brain Res. *291*, 119–124.

Glimcher, P.W., Giovino, A.A., and Hoebel, B.G. (1987). Neurotensin self-injection in the ventral tegmental area. Brain Res. *403*, 147–150.

Gomori, A., Ishihara, A., Ito, M., Mashiko, S., Matsushita, H., Yumoto, M., Ito, M., Tanaka, T., Tokita, S., Moriya, M., et al. (2003). Chronic intracerebroventricular infusion of MCH causes obesity in mice. Melanin-concentrating hormone. Am. J. Physiol. Endocrinol. Metab. *284*, E583–E588.

Grace, A.A., Floresco, S.B., Goto, Y., and Lodge, D.J. (2007). Regulation of firing of dopaminergic neurons and control of goal-directed behaviors. Trends Neurosci. *30*, 220–227.

Green, L., and Rachlin, H. (1991). Economic substitutability of electrical brain stimulation, food, and water. J. Exp. Anal. Behav. *55*, 133–143.

Grill, H.J., and Norgren, R. (1978). The taste reactivity test. I. Mimetic responses to gustatory stimuli in neurologically normal rats. Brain Res. *143*, 263–279.

Grosset, K.A., and Grosset, D.G. (2004). Prescribed drugs and neurological complications. J. Neurol. Neurosurg. Psychiatry *75*, iii2–iii8.

Grossman, S.P., Dacey, D., Halaris, A.E., Collier, T., and Routtenberg, A. (1978). Aphagia and adipsia after preferential destruction of nerve cell bodies in hypothalamus. Science *202*, 537–539.

Grotto, M., and Sulman, F.G. (1967). Modified receptacle method for animal analgesimetry. Arch. Int. Pharmacodyn. Thérapie *165*, 152–159.

Guarraci, F.A., and Kapp, B.S. (1999). An electrophysiological characterization of ventral tegmental area dopaminergic neurons during differential pavlovian fear conditioning in the awake rabbit. Behav. Brain Res. *99*, 169–179.

Gunaydin, L.A., Grosenick, L., Finkelstein, J.C., Kauvar, I.V., Fenno, L.E., Adhikari, A., Lammel, S., Mirzabekov, J.J., Airan, R.D., Zalocusky, K.A., et al. (2014). Natural neural projection dynamics underlying social behavior. Cell *157*, 1535–1551.

Gutierrez, R., Lobo, M.K., Zhang, F., and de Lecea, L. (2011). Neural integration of reward, arousal, and feeding: Recruitment of VTA, lateral hypothalamus, and ventral striatal neurons. IUBMB Life *63*, 824–830.

Haddad, P.M., and Dursun, S.M. (2008). Neurological complications of psychiatric drugs: clinical features and management. Hum. Psychopharmacol. Clin. Exp. *23*, S15–S26.

Hamid, A.A., Pettibone, J.R., Mabrouk, O.S., Hetrick, V.L., Schmidt, R., Vander Weele, C.M., Kennedy, R.T., Aragona, B.J., and Berke, J.D. (2016). Mesolimbic dopamine signals the value of work. Nat. Neurosci. *19*, 117–126.

Hamilton, M.E., and Bozarth, M.A. (1988). Feeding elicited by dynorphin (1–13) microinjections into the ventral tegmental area in rats. Life Sci. *43*, 941–946.

Harris, G.C., and Aston-Jones, G. (2006). Arousal and reward: a dichotomy in orexin function. Trends Neurosci. *29*, 571–577.

Harris, G.C., Wimmer, M., and Aston-Jones, G. (2005). A role for lateral hypothalamic orexin neurons in reward seeking. Nature *437*, 556–559.

Harris, J.L., Brownell, K.D., and Bargh, J.A. (2009). The Food Marketing Defense Model: Integrating Psychological Research to Protect Youth and Inform Public Policy. Soc. Issues Policy Rev. *3*, 211–271.

Hawkins, M.F. (1986). Central nervous system neurotensin and feeding. Physiol. Behav. *36*, 1–8.

Hoebel, B.G., and Teitelbaum, P. (1962). Hypothalamic control of feeding and self-stimulation. Science *135*, 375–377.

Hommel, J.D., Trinko, R., Sears, R.M., Georgescu, D., Liu, Z.-W., Gao, X.-B., Thurmon, J.J., Marinelli, M., and DiLeone, R.J. (2006). Leptin receptor signaling in midbrain dopamine neurons regulates feeding. Neuron *51*, 801–810.

Horvitz, J.C. (2000). Mesolimbocortical and nigrostriatal dopamine responses to salient non-reward events. Neuroscience *96*, 651–656.

Howe, M.W., Tierney, P.L., Sandberg, S.G., Phillips, P.E.M., and Graybiel, A.M. (2013). Prolonged dopamine signalling in striatum signals proximity and value of distant rewards. Nature *500*, 575–579.

Hull, C.L. (1943). Principles of behavior: an introduction to behavior theory (Oxford, England: Appleton-Century).

Hutchings, J.B. (1977). The Importance of Visual Appearance of Foods to the Food Processor and the Consumer1. J. Food Qual. *1*, 267–278.

Hyman, S.E., Malenka, R.C., and Nestler, E.J. (2006). Neural mechanisms of addiction: the role of reward-related learning and memory. Annu. Rev. Neurosci. *29*, 565–598.

Ikemoto, S. (2007). Dopamine reward circuitry: two projection systems from the ventral midbrain to the nucleus accumbens-olfactory tubercle complex. Brain Res. Rev. *56*, 27–78.

Ikemoto, S., Murphy, J.M., and McBride, W.J. (1997). Self-infusion of GABA(A) antagonists directly into the ventral tegmental area and adjacent regions. Behav. Neurosci. *111*, 369–380.

Ikemoto, S., Murphy, J.M., and McBride, W.J. (1998). Regional differences within the rat ventral tegmental area for muscimol self-infusions. Pharmacol. Biochem. Behav. *61*, 87–92.

Ito, R., Dalley, J.W., Robbins, T.W., and Everitt, B.J. (2002). Dopamine release in the dorsal striatum during cocaine-seeking behavior under the control of a drug-associated cue. J. Neurosci. Off. J. Soc. Neurosci. *22*, 6247–6253.

Janowitz, H.D., and Grossman, M.I. (1949). Some factors affecting the food intake of normal dogs and dogs with esophagostomy and gastric fistula. Am. J. Physiol. *159*, 143–148.

Jaros, D., Rohm, H., and Strobl, M. (2000). Appearance Properties—A Significant Contribution to Sensory Food Quality? LWT - Food Sci. Technol. *33*, 320–326.

Jennings, J.H., Rizzi, G., Stamatakis, A.M., Ung, R.L., and Stuber, G.D. (2013). The inhibitory circuit architecture of the lateral hypothalamus orchestrates feeding. Science *341*, 1517–1521.

Jennings, J.H., Ung, R.L., Resendez, S.L., Stamatakis, A.M., Taylor, J.G., Huang, J., Veleta, K., Kantak, P.A., Aita, M., Shilling-Scrivo, K., et al. (2015). Visualizing hypothalamic network dynamics for appetitive and consummatory behaviors. Cell *160*, 516–527.

Jhou, T.C., Geisler, S., Marinelli, M., DeGarmo, B.A., and Zahm, D.S. (2009). The mesopontine rostromedial tegmental nucleus: a structure targeted by the lateral habenula that projects to the ventral tegmental area of Tsai and substantia nigra compacta. J. Comp. Neurol. *513*, 566–596.

Johnson, S.W., and North, R.A. (1992). Opioids Excite Dopamine Neurons by Hyperpolarization of Local Interneurons. J. Neurosci. *12*, 483–488.

Johnson, S.W., Seutin, V., and North, R.A. (1992). Burst firing in dopamine neurons induced by N-methyl-D-aspartate: role of electrogenic sodium pump. Science *258*, 665–667.

Kahn, D., Abrams, G.M., Zimmerman, E.A., Carraway, R., and Leeman, S.E. (1980). Neurotensin Neurons in the Rat Hypothalamus: An Immunocytochemical Study. Endocrinology *107*, 47–54.

Kalivas, P.W. (2005). The Neural Basis of Addiction: A Pathology of Motivation and Choice. Am. J. Psychiatry *162*, 1403–1413.

Kaufling, J., Veinante, P., Pawlowski, S.A., Freund-Mercier, M.-J., and Barrot, M. (2009). Afferents to the GABAergic tail of the ventral tegmental area in the rat. J. Comp. Neurol. *513*, 597–621.

Kawano, M., Kawasaki, A., Sakata-Haga, H., Fukui, Y., Kawano, H., Nogami, H., and Hisano, S. (2006). Particular subpopulations of midbrain and hypothalamic dopamine neurons express vesicular glutamate transporter 2 in the rat brain. J. Comp. Neurol. *498*, 581–592.

Kawauchi, H., Kawazoe, I., Tsubokawa, M., Kishida, M., and Baker, B.I. (1983). Characterization of melanin-concentrating hormone in chum salmon pituitaries. Nature *305*, 321–323.

Keesey, R.E., Boyle, P.C., Kemnitz, J.W., and Mitchel, J.S. (1976). Role of the Lateral Hypothalamus in Determining the Body Weight Set Point. Hunger Basic Mech. Clin. Implic. Novin W Wyrwicka G Bray Eds.

Keithley, R.B., Mark Wightman, R., and Heien, M.L. (2009). Multivariate concentration determination using principal component regression with residual analysis. TrAC Trends Anal. Chem. *28*, 1127–1136.

Kelley, A.E., and Berridge, K.C. (2002). The Neuroscience of Natural Rewards: Relevance to Addictive Drugs. J. Neurosci. *22*, 3306–3311.

Kelley, A.E., Baldo, B.A., and Pratt, W.E. (2005). A proposed hypothalamic-thalamic-striatal axis for the integration of energy balance, arousal, and food reward. J. Comp. Neurol. *493*, 72–85.

Kempadoo, K.A., Tourino, C., Cho, S.L., Magnani, F., Leinninger, G.-M., Stuber, G.D., Zhang, F., Myers, M.G., Deisseroth, K., Lecea, L. de, et al. (2013). Hypothalamic Neurotensin Projections Promote Reward by Enhancing Glutamate Transmission in the VTA. J. Neurosci. *33*, 7618–7626.

Kennedy, G.C. (1953). The Role of Depot Fat in the Hypothalamic Control of Food Intake in the Rat. Proc. R. Soc. Lond. B Biol. Sci. *140*, 578–592.

Kessler, D.A. (2010). The End of Overeating: Taking Control of the Insatiable American Appetite (Emmaus, Pa. : New York: Rodale Books).

Kim, S.-Y., Adhikari, A., Lee, S.Y., Marshel, J.H., Kim, C.K., Mallory, C.S., Lo, M., Pak, S., Mattis, J., Lim, B.K., et al. (2013). Diverging neural pathways assemble a behavioural state from separable features in anxiety. Nature *496*, 219–223.

Kirkham, T.C., and Williams, C.M. (2001). Synergistic efects of opioid and cannabinoid antagonists on food intake. Psychopharmacology (Berl.) *153*, 267–270.

Kiyatkin, E.A., and Gratton, A. (1994). Electrochemical monitoring of extracellular dopamine in nucleus accumbens of rats lever-pressing for food. Brain Res. *652*, 225–234.

Klapoetke, N.C., Murata, Y., Kim, S.S., Pulver, S.R., Birdsey-Benson, A., Cho, Y.K., Morimoto, T.K., Chuong, A.S., Carpenter, E.J., Tian, Z., et al. (2014). Independent optical excitation of distinct neural populations. Nat. Methods *11*, 338–346.

Klein, N. (2009). No Logo: 10th Anniversary Edition with a New Introduction by the Author (New York: Picador).

Ko, D., and Wanat, M.J. (2016). Phasic Dopamine Transmission Reflects Initiation Vigor and Exerted Effort in an Action- and Region-Specific Manner. J. Neurosci. *36*, 2202–2211.

Kojima, M., Hosoda, H., Date, Y., Nakazato, M., Matsuo, H., and Kangawa, K. (1999). Ghrelin is a growth-hormone-releasing acylated peptide from stomach. Nature *402*, 656–660.

Kokkotou, E., Jeon, J.Y., Wang, X., Marino, F.E., Carlson, M., Trombly, D.J., and Maratos-Flier, E. (2005). Mice with MCH ablation resist diet-induced obesity through strain-specific mechanisms. Am. J. Physiol. Regul. Integr. Comp. Physiol. *289*, R117–R124.

Krashes, M.J., Koda, S., Ye, C., Rogan, S.C., Adams, A.C., Cusher, D.S., Maratos-Flier, E., Roth, B.L., and Lowell, B.B. (2011). Rapid, reversible activation of AgRP neurons drives feeding behavior in mice. J. Clin. Invest. *121*, 1424–1428.

Krashes, M.J., Shah, B.P., Madara, J.C., Olson, D.P., Strochlic, D.E., Garfield, A.S., Vong, L., Pei, H., Watabe-Uchida, M., Uchida, N., et al. (2014). An excitatory paraventricular nucleus to AgRP neuron circuit that drives hunger. Nature *507*, 238–242.

Krügel, U., Schraft, T., Kittner, H., Kiess, W., and Illes, P. (2003). Basal and feeding-evoked dopamine release in the rat nucleus accumbens is depressed by leptin. Eur. J. Pharmacol. *482*, 185–187.

Lacey, M.G., Mercuri, N.B., and North, R.A. (1989). Two cell types in rat substantia nigra zona compacta distinguished by membrane properties and the actions of dopamine and opioids. J. Neurosci. *9*, 1233–1241.

Lammel, S., Hetzel, A., Häckel, O., Jones, I., Liss, B., and Roeper, J. (2008). Unique Properties of Mesoprefrontal Neurons within a Dual Mesocorticolimbic Dopamine System. Neuron *57*, 760–773.

Lammel, S., Ion, D.I., Roeper, J., and Malenka, R.C. (2011). Projection-Specific Modulation of Dopamine Neuron Synapses by Aversive and Rewarding Stimuli. Neuron *70*, 855–862.

Lammel, S., Lim, B.K., Ran, C., Huang, K.W., Betley, M.J., Tye, K.M., Deisseroth, K., and Malenka, R.C. (2012). Input-specific control of reward and aversion in the ventral tegmental area. Nature.

Land, B.B., Narayanan, N.S., Liu, R.-J., Gianessi, C.A., Brayton, C.E., Grimaldi, D.M., Sarhan, M., Guarnieri, D.J., Deisseroth, K., Aghajanian, G.K., et al. (2014). Medial prefrontal D1 dopamine neurons control food intake. Nat. Neurosci. *17*, 248–253.

Lattemann, D.F. (2008). Endocrine Links Between Food Reward and Caloric Homeostasis. Appetite *51*, 452–455.

De Lecea, L., Kilduff, T.S., Peyron, C., Gao, X.-B., Foye, P.E., Danielson, P.E., Fukuhara, C., Battenberg, E.L.F., Gautvik, V.T., Bartlett, F.S., et al. (1998). The Hypocretins: Hypothalamus-Specific Peptides with Neuroexcitatory Activity. Proc. Natl. Acad. Sci. *95*, 322–327.

Leinninger, G.M., Jo, Y.-H., Leshan, R.L., Louis, G.W., Yang, H., Barrera, J.G., Wilson, H., Opland, D.M., Faouzi, M.A., Gong, Y., et al. (2009). Leptin acts via leptin receptor-expressing lateral hypothalamic neurons to modulate the mesolimbic dopamine system and suppress feeding. Cell Metab. *10*, 89–98.

Leinninger, G.M., Opland, D.M., Jo, Y.-H., Faouzi, M., Christensen, L., Cappellucci, L.A., Rhodes, C.J., Gnegy, M.E., Becker, J.B., Pothos, E.N., et al. (2011). Leptin action via neurotensin neurons controls orexin, the mesolimbic dopamine system and energy balance. Cell Metab. *14*, 313–323.

Lenoir, M., Serre, F., Cantin, L., and Ahmed, S.H. (2007). Intense Sweetness Surpasses Cocaine Reward. PLoS ONE *2*, e698.

Levine, A.S., Kneip, J., Grace, M., and Morley, J.E. (1983). Effect of centrally administered neurotensin on multiple feeding paradigms. Pharmacol. Biochem. Behav. *18*, 19–23.

Li, J.X., Yoshida, T., Monk, K.J., and Katz, D.B. (2013). Lateral Hypothalamus Contains Two Types of Palatability-Related Taste Responses with Distinct Dynamics. J. Neurosci. *33*, 9462–9473.

Lorenz, K., and Leyhausen, P. (1973). Motivation of human and animal behavior: An ethological view (New York: Van Nostrand Reinhold Company).

Ludwig, D.S., Tritos, N.A., Mastaitis, J.W., Kulkarni, R., Kokkotou, E., Elmquist, J., Lowell, B., Flier, J.S., and Maratos-Flier, E. (2001). Melanin-concentrating hormone overexpression in transgenic mice leads to obesity and insulin resistance. J. Clin. Invest. *107*, 379–386.

Lüscher, C., and Malenka, R.C. (2011). Drug-Evoked Synaptic Plasticity in Addiction: From Molecular Changes to Circuit Remodeling. Neuron *69*, 650–663.

Luttinger, D., King, R.A., Sheppard, D., Strupp, J., Nemeroff, C.B., and Prange, A.J., Jr (1982). The effect of neurotensin on food consumption in the rat. Eur. J. Pharmacol. *81*, 499–503.

Maffei, M., Halaas, J., Ravussin, E., Pratley, R.E., Lee, G.H., Zhang, Y., Fei, H., Kim, S., Lallone, R., Ranganathan, S., et al. (1995). Leptin levels in human and rodent: Measurement of plasma leptin and ob RNA in obese and weight-reduced subjects. Nat. Med. *1*, 1155–1161.

Mantz, J., Thierry, A.M., and Glowinski, J. (1989). Effect of noxious tail pinch on the discharge rate of mesocortical and mesolimbic dopamine neurons: selective activation of the mesocortical system. Brain Res. *476*, 377–381.

Margetic, S., Gazzola, C., Pegg, G.G., and Hill, R.A. (2002). Leptin: a review of its peripheral actions and interactions. Int. J. Obes. Relat. Metab. Disord. J. Int. Assoc. Study Obes. *26*, 1407–1433.

Margolis, E.B., Lock, H., Hjelmstad, G.O., and Fields, H.L. (2006). The Ventral Tegmental Area Revisited: Is There an Electrophysiological Marker for Dopaminergic Neurons? J. Physiol. *577*, 907–924.

Margules, D.L., and Olds, J. (1962). Identical "Feeding" and "Rewarding" Systems in the Lateral Hypothalamus of Rats. Science *135*, 374–375.

Marsh, D.J., Weingarth, D.T., Novi, D.E., Chen, H.Y., Trumbauer, M.E., Chen, A.S., Guan, X.-M., Jiang, M.M., Feng, Y., Camacho, R.E., et al. (2002). Melanin-concentrating hormone 1 receptor-deficient mice are lean, hyperactive, and hyperphagic and have altered metabolism. Proc. Natl. Acad. Sci. U. S. A. *99*, 3240–3245.

Matsui, A., and Williams, J.T. (2011). Opioid-Sensitive GABA Inputs from Rostromedial Tegmental Nucleus Synapse Onto Midbrain Dopamine Neurons. J. Neurosci. *31*, 17729–17735.

Matsumoto, M., and Hikosaka, O. (2007). Lateral habenula as a source of negative reward signals in dopamine neurons. Nature *447*, 1111–1115.

Matsumoto, M., and Hikosaka, O. (2009). Two types of dopamine neuron distinctly convey positive and negative motivational signals. Nature *459*, 837–841.

Matthews, G.A., Nieh, E.H., Vander Weele, C.M., Halbert, S.A., Pradhan, R.V., Yosafat, A.S., Glober, G.F., Izadmehr, E.M., Thomas, R.E., Lacy, G.D., et al. (2016). Dorsal Raphe Dopamine Neurons Represent the Experience of Social Isolation. Cell *164*, 617–631.

Mayer, D.J., Wolfle, T.L., Akil, H., Carder, B., and Liebeskind, J.C. (1971). Analgesia from Electrical Stimulation in the Brainstem of the Rat. Science *174*, 1351–1354.

McCrory, M.A., Fuss, P.J., Hays, N.P., Vinken, A.G., Greenberg, A.S., and Roberts, S.B. (1999). Overeating in America: Association between Restaurant Food Consumption and Body Fatness in Healthy Adult Men and Women Ages 19 to 80. Obes. Res. *7*, 564–571.

Mietus-Snyder, M.L., and Lustig, R.H. (2008). Childhood Obesity: Adrift in the "Limbic Triangle." Annu. Rev. Med. *59*, 147–162.

Mirenowicz, J., and Schultz, W. (1994). Importance of unpredictability for reward responses in primate dopamine neurons. J. Neurophysiol. *72*, 1024–1027.

Mogenson, G.J., and Stevenson, J.A.F. (1966). Drinking and self-stimulation with electrical stimulation of the lateral hypothalamus. Physiol. Behav. *1*, 251–IN9.

Mogenson, G.J., Swanson, L.W., and Wu, M. (1983). Neural projections from nucleus accumbens to globus pallidus, substantia innominata, and lateral preoptic-lateral hypothalamic area: an anatomical and electrophysiological investigation in the rat. J. Neurosci. Off. J. Soc. Neurosci. *3*, 189–202.

Montague, P.R., Dayan, P., and Sejnowski, T.J. (1996). A framework for mesencephalic dopamine systems based on predictive Hebbian learning. J. Neurosci. *16*, 1936–1947.

Mora, F., Rolls, E.T., and Burton, M.J. (1976). Modulation during learning of the responses of neurons in the lateral hypothalamus to the sight of food. Exp. Neurol. *53*, 508–519.

Murray, B., and Shizgal, P. (1996a). Behavioral measures of conduction velocity and refractory period for reward-relevant axons in the anterior LH and VTA. Physiol. Behav. *59*, 643–652.

Murray, B., and Shizgal, P. (1996b). Physiological measures of conduction velocity and refractory period for putative reward-relevant MFB axons arising in the rostral MFB. Physiol. Behav. *59*, 427–437.

Nair-Roberts, R.G., Chatelain-Badie, S.D., Benson, E., White-Cooper, H., Bolam, J.P., and Ungless, M.A. (2008). Stereological estimates of dopaminergic, GABAergic and glutamatergic neurons in the ventral tegmental area, substantia nigra and retrorubral field in the rat. Neuroscience *152*, 1024–1031.

Nakamura, K., Ono, T., and Tamura, R. (1987). Central sites involved in lateral hypothalamus conditioned neural responses to acoustic cues in the rat. J. Neurophysiol. *58*, 1123–1148.

Nakazato, M., Murakami, N., Date, Y., Kojima, M., Matsuo, H., Kangawa, K., and Matsukura, S. (2001). A role for ghrelin in the central regulation of feeding. Nature *409*, 194–198.

Narita, M., Nagumo, Y., Hashimoto, S., Narita, M., Khotib, J., Miyatake, M., Sakurai, T., Yanagisawa, M., Nakamachi, T., Shioda, S., et al. (2006). Direct involvement of orexinergic systems in the activation of the mesolimbic dopamine pathway and related behaviors induced by morphine. J. Neurosci. Off. J. Soc. Neurosci. *26*, 398–405.

Narita, M., Nagumo, Y., Miyatake, M., Ikegami, D., Kurahashi, K., and Suzuki, T. (2007). Implication of protein kinase C in the orexin-induced elevation of extracellular dopamine levels and its rewarding effect. Eur. J. Neurosci. *25*, 1537–1545.

Navarro, M., Olney, J.J., Burnham, N.W., Mazzone, C.M., Lowery-Gionta, E.G., Pleil, K.E., Kash, T.L., and Thiele, T.E. (2015). Lateral Hypothalamus GABAergic Neurons Modulate Consummatory Behaviors Regardless of the Caloric Content or Biological Relevance of the Consumed Stimuli. Neuropsychopharmacol. Off. Publ. Am. Coll. Neuropsychopharmacol.

Nestler, E.J., and Carlezon Jr, W.A. (2006). The Mesolimbic Dopamine Reward Circuit in Depression. Biol. Psychiatry *59*, 1151–1159.

Nieh, E.H., Kim, S.-Y., Namburi, P., and Tye, K.M. (2013). Optogenetic dissection of neural circuits underlying emotional valence and motivated behaviors. Brain Res. *1511*, 73–92.

Nieh, E.H., Matthews, G.A., Allsop, S.A., Presbrey, K.N., Leppla, C.A., Wichmann, R., Neve, R., Wildes, C.P., and Tye, K.M. (2015). Decoding neural circuits that control compulsive sucrose seeking. Cell *160*, 528–541.

Nielsen, S.J., and Popkin, B.M. (2004). Changes in beverage intake between 1977 and 2001. Am. J. Prev. Med. *27*, 205–210.

Nielsen, S.J., Siega-Riz, A.M., and Popkin, B.M. (2002). Trends in energy intake in U.S. between 1977 and 1996: similar shifts seen across age groups. Obes. Res. *10*, 370–378.

Niv, Y., Daw, N.D., Joel, D., and Dayan, P. (2006). Tonic dopamine: opportunity costs and the control of response vigor. Psychopharmacology (Berl.) *191*, 507–520.

Noel, M.B., and Wise, R.A. (1995). Ventral tegmental injections of a selective μ or δ opioid enhance feeding in food-deprived rats. Brain Res. *673*, 304–312.

Norgren, R. (1970). Gustatory responses in the hypothalamus. Brain Res. *21*, 63–77.

O'Connor, E.C., Kremer, Y., Lefort, S., Harada, M., Pascoli, V., Rohner, C., and Lüscher, C. (2015). Accumbal D1R Neurons Projecting to Lateral Hypothalamus Authorize Feeding. Neuron *88*, 553–564.

Olds, J. (1956). Pleasure Centers in the Brain. Sci. Am. *195*, 105–117.

Olds, J., and Milner, P. (1954). Positive Reinforcement Produced By Electrical Stimulation of Septal Area and Other Regions of Rat Brain. J. Comp. Physiol. Psychol. *47*, 419–427.

Olshansky, S.J., Passaro, D.J., Hershow, R.C., Layden, J., Carnes, B.A., Brody, J., Hayflick, L., Butler, R.N., Allison, D.B., and Ludwig, D.S. (2005). A Potential Decline in Life Expectancy in the United States in the 21st Century. N. Engl. J. Med. *352*, 1138–1145.

Opland, D., Sutton, A., Woodworth, H., Brown, J., Bugescu, R., Garcia, A., Christensen, L., Rhodes, C., Myers, M., and Leinninger, G. (2013). Loss of neurotensin receptor-1 disrupts the control of the mesolimbic dopamine system by leptin and promotes hedonic feeding and obesity. Mol. Metab. *2*, 423–434.

Owesson-White, C.A., Roitman, M.F., Sombers, L.A., Belle, A.M., Keithley, R.B., Peele, J.L., Carelli, R.M., and Wightman, R.M. (2012). Sources contributing to the average extracellular concentration of dopamine in the nucleus accumbens. J. Neurochem. *121*, 252–262.

Palmiter, R.D. (2007). Is dopamine a physiologically relevant mediator of feeding behavior? Trends Neurosci. *30*, 375–381.

Pavlov, I.P. (1927). Conditioned reflexes: an investigation of the physiological activity of the cerebral cortex (Oxford, England: Oxford Univ. Press).

Pavlov, I.P., and Anrep, G.V. (2003). Conditioned Reflexes (Courier Corporation).

Pelloux, Y., Everitt, B.J., and Dickinson, A. (2007). Compulsive drug seeking by rats under punishment: effects of drug taking history. Psychopharmacology (Berl.) *194*, 127–137.

Perachio, A.A., Marr, L.D., and Alexander, M. (1979). Sexual behavior in male rhesus monkeys elicited by electrical stimulation of preoptic and hypothalamic areas. Brain Res. *177*, 127–144.

Pereira, M.A., Kartashov, A.I., Ebbeling, C.B., Van Horn, L., Slattery, M.L., Jacobs Jr, D.R., and Ludwig, D.S. (2005). Fast-food habits, weight gain, and insulin resistance (the CARDIA study): 15-year prospective analysis. The Lancet *365*, 36–42.

Perrotti, L.I., Bolaños, C.A., Choi, K.-H., Russo, S.J., Edwards, S., Ulery, P.G., Wallace, D.L., Self, D.W., Nestler, E.J., and Barrot, M. (2005). ΔFosB accumulates in a GABAergic cell population in the posterior tail of the ventral tegmental area after psychostimulant treatment. Eur. J. Neurosci. *21*, 2817–2824.

Petreanu, L., Huber, D., Sobczyk, A., and Svoboda, K. (2007). Channelrhodopsin-2-assisted circuit mapping of long-range callosal projections. Nat Neurosci *10*, 663–668.

Peyron, C., Tighe, D.K., van den Pol, A.N., de Lecea, L., Heller, H.C., Sutcliffe, J.G., and Kilduff, T.S. (1998). Neurons containing hypocretin (orexin) project to multiple neuronal systems. J. Neurosci. Off. J. Soc. Neurosci. *18*, 9996–10015.

Phillips, A.G., Atkinson, L.J., Blackburn, J.R., and Blaha, C.D. (1993). Increased extracellular dopamine in the nucleus accumbens of the rat elicited by a conditional stimulus for food: an electrochemical study. Can. J. Physiol. Pharmacol. *71*, 387–393.

Phillips, P.E.M., Stuber, G.D., Heien, M.L.A.V., Wightman, R.M., and Carelli, R.M. (2003). Subsecond dopamine release promotes cocaine seeking. Nature *422*, 614–618.

Phillipson, O.T. (1979). Afferent projections to the ventral tegmental area of Tsai and interfascicular nucleus: a horseradish peroxidase study in the rat. J. Comp. Neurol. *187*, 117–143.

Pissios, P., Frank, L., Kennedy, A.R., Porter, D.R., Marino, F.E., Liu, F.-F., Pothos, E.N., and Maratos-Flier, E. (2008). Dysregulation of the Mesolimbic Dopamine System and Reward in MCH−/− Mice. Biol. Psychiatry *64*, 184–191.

Popkin, B.M., and Nielsen, S.J. (2003). The Sweetening of the World's Diet. Obes. Res. *11*, 1325–1332.

Powell, L.M., Szczypka, G., Chaloupka, F.J., and Braunschweig, C.L. (2007). Nutritional content of television food advertisements seen by children and adolescents in the United States. Pediatrics *120*, 576–583.

Qu, D., Ludwig, D.S., Gammeltoft, S., Piper, M., Pelleymounter, M.A., Cullen, M.J., Mathes, W.F., Przypek, R., Kanarek, R., and Maratos-Flier, E. (1996). A role for melanin-concentrating hormone in the central regulation of feeding behaviour. Nature *380*, 243–247.

Rescorla, R., and Wagner, A. (1972). A theory of Pavlovian conditioning: Variations in the effectiveness of reinforcement and nonreinforcement. In Classical Conditioning II: Current Research and Theory, (Appleton-Century-Crofts), pp. 64–99.

Rick, C.E., and Lacey, M.G. (1994). Rat substantia nigra pars reticulata neurones are tonically inhibited via GABAA, but not GABAB, receptors in vitro. Brain Res. *659*, 133–137.

Roberts, D.C.S., and Koob, G.F. (1982). Disruption of cocaine self-administration following 6-hydroxydopamine lesions of the ventral tegmental area in rats. Pharmacol. Biochem. Behav. *17*, 901–904.

Robinson, T.E., and Berridge, K.C. (1993). The neural basis of drug craving: An incentive-sensitization theory of addiction. Brain Res. Rev. *18*, 247–291.

Romo, R., and Schultz, W. (1990). Dopamine neurons of the monkey midbrain: contingencies of responses to active touch during self-initiated arm movements. J. Neurophysiol. *63*, 592–606.

Rompré, P.-P. (1995). Psychostimulant-like effect of central microinjection of neurotensin on brain stimulation reward. Peptides *16*, 1417–1420.

Rompré, P.-P., Bauco, P., and Gratton, A. (1992). Facilitation of brain stimulation reward by mesencephalic injections of neurotensin-(1–13). Eur. J. Pharmacol. *211*, 295–303.

Rosenkranz, J.A., and Grace, A.A. (2002). Dopamine-mediated modulation of odour-evoked amygdala potentials during pavlovian conditioning. Nature *417*, 282–287.

Rossi, M., Choi, S.J., O'Shea, D., Miyoshi, T., Ghatei, M.A., and Bloom, S.R. (1997). Melanin-concentrating hormone acutely stimulates feeding, but chronic administration has no effect on body weight. Endocrinology *138*, 351–355.

Rossi, M., Beak, S.A., Choi, S.-J., Small, C.J., Morgan, D.G.., Ghatei, M.A., Smith, D.M., and Bloom, S.R. (1999). Investigation of the feeding effects of melanin concentrating hormone on food intake — action independent of galanin and the melanocortin receptors. Brain Res. *846*, 164–170.

Saddoris, M.P., Cacciapaglia, F., Wightman, R.M., and Carelli, R.M. (2015). Differential Dopamine Release Dynamics in the Nucleus Accumbens Core and Shell Reveal Complementary Signals for Error Prediction and Incentive Motivation. J. Neurosci. Off. J. Soc. Neurosci. *35*, 11572–11582.

Sahu, A. (1998). Evidence Suggesting That Galanin (GAL), Melanin-Concentrating Hormone (MCH), Neurotensin (NT), Proopiomelanocortin (POMC) and Neuropeptide Y (NPY) Are Targets of Leptin Signaling in the Hypothalamus. Endocrinology *139*, 795–798.

Saito, Y., Cheng, M., Leslie, F.M., and Civelli, O. (2001). Expression of the melanin-concentrating hormone (MCH) receptor mRNA in the rat brain. J. Comp. Neurol. *435*, 26–40.

Sakurai, T. (2007). The neural circuit of orexin (hypocretin): maintaining sleep and wakefulness. Nat. Rev. Neurosci. *8*, 171–181.

Sakurai, T., Amemiya, A., Ishii, M., Matsuzaki, I., Chemelli, R.M., Tanaka, H., Williams, S.C., Richardson, J.A., Kozlowski, G.P., Wilson, S., et al. (1998). Orexins and orexin receptors: a family of hypothalamic neuropeptides and G protein-coupled receptors that regulate feeding behavior. Cell *92*, 573–585.

Salamone, J.D., and Correa, M. (2012). The mysterious motivational functions of mesolimbic dopamine. Neuron *76*, 470–485.

Salamone, J., Correa, M., Mingote, S., and Weber, S. (2005). Beyond the reward hypothesis: alternative functions of nucleus accumbens dopamine. Curr. Opin. Pharmacol. *5*, 34–41.

Salamone, J.D., Cousins, M.S., McCullough, L.D., Carriero, D.L., and Berkowitz, R.J. (1994). Nucleus accumbens dopamine release increases during instrumental lever pressing for food but not free food consumption. Pharmacol. Biochem. Behav. *49*, 25–31.

Saper, C.B., Swanson, L.W., and Cowan, W.M. (1979). An autoradiographic study of the efferent connections of the lateral hypothalamic area in the rat. J. Comp. Neurol. *183*, 689–706.

Saunders, B.T., and Robinson, T.E. (2012). The role of dopamine in the accumbens core in the expression of Pavlovian conditioned responses. Eur. J. Neurosci. *36*, 2521–2532.

Schultz, W. (2007). Behavioral dopamine signals. Trends Neurosci. *30*, 203–210.

Schultz, W., and Romo, R. (1987). Responses of Nigrostriatal Dopamine Neurons to High-Intensity Somatosensory Stimulation in the Anesthetized Monkey. J. Neurophysiol. *57*, 201–217.

Schultz, W., Dayan, P., and Montague, P.R. (1997). A Neural Substrate of Prediction and Reward. Science *275*, 1593–1599.

Schwartzbaum, J.S. (1988). Electrophysiology of taste, feeding and reward in lateral hypothalamus of rabbit. Physiol. Behav. *44*, 507–526.

Senn, V., Wolff, S.B.E., Herry, C., Grenier, F., Ehrlich, I., Gründemann, J., Fadok, J.P., Müller, C., Letzkus, J.J., and Lüthi, A. (2014). Long-range connectivity defines behavioral specificity of amygdala neurons. Neuron *81*, 428–437.

Shearman, L.P., Camacho, R.E., Sloan Stribling, D., Zhou, D., Bednarek, M.A., Hreniuk, D.L., Feighner, S.D., Tan, C.P., Howard, A.D., Van der Ploeg, L.H.T., et al. (2003). Chronic MCH-1 receptor modulation alters appetite, body weight and adiposity in rats. Eur. J. Pharmacol. *475*, 37–47.

Shimada, M., Tritos, N.A., Lowell, B.B., Flier, J.S., and Maratos-Flier, E. (1998). Mice lacking melanin-concentrating hormone are hypophagic and lean. Nature *396*, 670–674.

Simansky, K.J., Bourbonais, K.A., and Smith, G.P. (1985). Food-related stimuli increase the ratio of 3,4-dihydroxyphenylacetic acid to dopamine in the hypothalamus. Pharmacol. Biochem. Behav. *23*, 253–258.

Simon, H., Le Moal, M., and Calas, A. (1979). Efferents and afferents of the ventral tegmental-A10 region studied after local injection of [3H]leucine and horseradish peroxidase. Brain Res. *178*, 17–40.

Singh, J., Desiraju, T., and Raju, T.R. (1996). Comparison of Intracranial Self-Stimulation Evoked From Lateral Hypothalamus and Ventral Tegmentum: Analysis Based on Stimulation Parameters and Behavioural Response Characteristics. Brain Res. Bull. *41*, 399–408.

Skofitsch, G., Jacobowitz, D.M., and Zamir, N. (1985). Immunohistochemical localization of a melanin concentrating hormone-like peptide in the rat brain. Brain Res. Bull. *15*, 635–649.

Small, D.M., Jones-Gotman, M., and Dagher, A. (2003). Feeding-induced dopamine release in dorsal striatum correlates with meal pleasantness ratings in healthy human volunteers. NeuroImage *19*, 1709–1715.

Snyder, S.L. (1992). Movies and Product Placement: Is Hollywood Turning Films into Commercial Speech. Univ. Ill. Law Rev. *1992*, 301.

Solinas, M., and Goldberg, S.R. (2005). Motivational effects of cannabinoids and opioids on food reinforcement depend on simultaneous activation of cannabinoid and opioid systems. Neuropsychopharmacol. Off. Publ. Am. Coll. Neuropsychopharmacol. *30*, 2035–2045.

Spyraki, C., Fibiger, H.C., and Phillips, A.G. (1982). Dopaminergic substrates of amphetamine-induced place preference conditioning. Brain Res. *253*, 185–193.

Stamatakis, A.M., and Stuber, G.D. (2012). Activation of lateral habenula inputs to the ventral midbrain promotes behavioral avoidance. Nat. Neurosci. *15*, 1105–1107.

Sternson, S.M. (2013). Hypothalamic Survival Circuits: Blueprints for Purposive Behaviors. Neuron *77*, 810–824.

Stricker, E.M., Swerdloff, A.F., and Zigmond, M.J. (1978). Intrahypothalamic injections of kainic acid produce feeding and drinking deficits in rats. Brain Res. *158*, 470–473.

Stuber, G.D., and Wise, R.A. (2016). Lateral hypothalamic circuits for feeding and reward. Nat. Neurosci. *19*, 198–205.

Stuber, G.D., Klanker, M., de Ridder, B., Bowers, M.S., Joosten, R.N., Feenstra, M.G., and Bonci, A. (2008). Reward-Predictive Cues Enhance Excitatory Synaptic Strength onto Midbrain Dopamine Neurons. Science *321*, 1690–1692.

Sugita, S., Johnson, S.W., and North, R.A. (1992). Synaptic inputs to GABAA and GABAB receptors originate from discrete afferent neurons. Neurosci. Lett. *134*, 207–211.

Sugrue, L.P., Corrado, G.S., and Newsome, W.T. (2005). Choosing the greater of two goods: neural currencies for valuation and decision making. Nat. Rev. Neurosci. *6*, 363–375.

Swanson, L.W. (1982). The projections of the ventral tegmental area and adjacent regions: A combined fluorescent retrograde tracer and immunofluorescence study in the rat. Brain Res. Bull. *9*, 321–353.

Swanson, L.W., and Cowan, W.M. (1979). The connections of the septal region in the rat. J. Comp. Neurol. *186*, 621–655.

Swanson, L.W., Sanchez-Watts, G., and Watts, A.G. (2005). Comparison of melanin-concentrating hormone and hypocretin/orexin mRNA expression patterns in a new parceling scheme of the lateral hypothalamic zone. Neurosci. Lett. *387*, 80–84.

Szczypka, M.S., Rainey, M.A., Kim, D.S., Alaynick, W.A., Marck, B.T., Matsumoto, A.M., and Palmiter, R.D. (1999a). Feeding behavior in dopamine-deficient mice. Proc. Natl. Acad. Sci. U. S. A. *96*, 12138–12143.

Szczypka, M.S., Mandel, R.J., Donahue, B.A., Snyder, R.O., Leff, S.E., and Palmiter, R.D. (1999b). Viral Gene Delivery Selectively Restores Feeding and Prevents Lethality of Dopamine-Deficient Mice. Neuron *22*, 167–178.

Szczypka, M.S., Kwok, K., Brot, M.D., Marck, B.T., Matsumoto, A.M., Donahue, B.A., and Palmiter, R.D. (2001). Dopamine Production in the Caudate Putamen Restores Feeding in Dopamine-Deficient Mice. Neuron *30*, 819–828.

Tabuchi, E., Yokawa, T., Mallick, H., Inubushi, T., Kondoh, T., Ono, T., and Torii, K. (2002). Spatio-temporal dynamics of brain activated regions during drinking behavior in rats. Brain Res. *951*, 270–279.

Tan, K.R., Yvon, C., Turiault, M., Mirzabekov, J.J., Doehner, J., Labouèbe, G., Deisseroth, K., Tye, K.M., and Lüscher, C. (2012). GABA Neurons of the VTA Drive Conditioned Place Aversion. Neuron *73*, 1173–1183.

Tanda, G., Pontieri, F.E., and Chiara, G.D. (1997). Cannabinoid and Heroin Activation of Mesolimbic Dopamine Transmission by a Common μ1 Opioid Receptor Mechanism. Science *276*, 2048–2050.

Tasker, R.A.R., Choinière, M., Libman, S.M., and Melzack, R. (1987). Analgesia produced by injection of lidocaine into the lateral hypothalamus. Pain *31*, 237–248.

Thompson, R.H., and Swanson, L.W. (2010). Hypothesis-driven structural connectivity analysis supports network over hierarchical model of brain architecture. Proc. Natl. Acad. Sci. U. S. A. *107*, 15235–15239.

Tinbergen, N., and Van Iersel, J.J.A. (1947). "Displacement reactions" in the three-spined stickleback. Behaviour *1*, 56–63.

Tsai, H.-C., Zhang, F., Adamantidis, A., Stuber, G.D., Bonci, A., De Lecea, L., and Deisseroth, K. (2009). Phasic Firing in Dopaminergic Neurons Is Sufficient for Behavioral Conditioning. Science *324*, 1080–1084.

Tschöp, M., Smiley, D.L., and Heiman, M.L. (2000). Ghrelin induces adiposity in rodents. Nature *407*, 908–913.

Tschöp, M., Weyer, C., Tataranni, P.A., Devanarayan, V., Ravussin, E., and Heiman, M.L. (2001). Circulating Ghrelin Levels Are Decreased in Human Obesity. Diabetes *50*, 707–709.

Turner, L.H., Solomon, R.L., Stellar, E., and Wampler, S.N. (1975). Humoral factors controlling food intake in dogs. Acta Neurobiol. Exp. (Warsz.) *35*, 491–498.

Tye, K.M., and Deisseroth, K. (2012). Optogenetic investigation of neural circuits underlying brain disease in animal models. Nat. Rev. Neurosci. *13*, 251–266.

Tye, K.M., Stuber, G.D., De Ridder, B., Bonci, A., and Janak, P.H. (2008). Rapid strengthening of thalamo-amygdala synapses mediates cue–reward learning. Nature *453*, 1253–1257.

Tye, K.M., Prakash, R., Kim, S.-Y., Fenno, L.E., Grosenick, L., Zarabi, H., Thompson, K.R., Gradinaru, V., Ramakrishnan, C., and Deisseroth, K. (2011). Amygdala circuitry mediating reversible and bidirectional control of anxiety. Nature *471*, 358–362.

Uhl, G.R., Kuhar, M.J., and Snyder, S.H. (1977). Neurotensin: immunohistochemical localization in rat central nervous system. Proc. Natl. Acad. Sci. *74*, 4059–4063.

Ungless, M.A., and Grace, A.A. (2012). Are you or aren't you? Challenges associated with physiologically identifying dopamine neurons. Trends Neurosci.

Valenstein, E.S., Cox, V.C., and Kakolewski, J.W. (1968). Modification of Motivated Behavior Elicited by Electrical Stimulation of the Hypothalamus. Science *159*, 1119–1121.

Vanderschuren, L.J.M.J., and Everitt, B.J. (2004). Drug Seeking Becomes Compulsive After Prolonged Cocaine Self-Administration. Science *305*, 1017–1019.

Vanderschuren, L.J.M.J., Ciano, P.D., and Everitt, B.J. (2005). Involvement of the Dorsal Striatum in Cue-Controlled Cocaine Seeking. J. Neurosci. *25*, 8665–8670.

Volkow, N.D., Wang, G.-J., Fowler, J.S., Logan, J., Jayne, M., Franceschi, D., Wong, C., Gatley, S.J., Gifford, A.N., Ding, Y.-S., et al. (2002). "Nonhedonic" food motivation in humans involves dopamine in the dorsal striatum and methylphenidate amplifies this effect. Synap. N. Y. N *44*, 175–180.

Volkow, N.D., Wang, G.-J., and Baler, R.D. (2011). Reward, dopamine and the control of food intake: implications for obesity. Trends Cogn. Sci. *15*, 37–46.

Wang, B., You, Z.-B., and Wise, R.A. (2009). Reinstatement of cocaine-seeking by hypocretin (orexin) in the ventral tegmental area: Independence from the local CRF network. Biol. Psychiatry *65*, 857–862.

Watabe-Uchida, M., Zhu, L., Ogawa, S.K., Vamanrao, A., and Uchida, N. (2012). Whole-Brain Mapping of Direct Inputs to Midbrain Dopamine Neurons. Neuron *74*, 858–873.

Vander Weele, C.M., Porter-Stransky, K.A., Mabrouk, O.S., Lovic, V., Singer, B.F., Kennedy, R.T., and Aragona, B.J. (2014). Rapid dopamine transmission within the nucleus accumbens: Dramatic difference between morphine and oxycodone delivery. Eur. J. Neurosci. *40*, 3041–3054.

White, N.M., Packard, M.G., and Hiroi, N. (1991). Place conditioning with dopamine D1 and D2 agonists injected peripherally or into nucleus accumbens. Psychopharmacology (Berl.) *103*, 271–276.

Willuhn, I., Burgeno, L.M., Everitt, B.J., and Phillips, P.E.M. (2012). Hierarchical recruitment of phasic dopamine signaling in the striatum during the progression of cocaine use. Proc. Natl. Acad. Sci. *109*, 20703–20708.

Wise, R.A. (2002). Brain Reward Circuitry. Neuron *36*, 229–240.

Wise, R.A. (2004). Dopamine, learning and motivation. Nat. Rev. Neurosci. *5*, 483–494.

Wise, R.A. (2005). Forebrain substrates of reward and motivation. J. Comp. Neurol. *493*, 115–121.

Wise, R.A. (2006). Role of brain dopamine in food reward and reinforcement. Philos. Trans. R. Soc. Lond. B Biol. Sci. *361*, 1149–1158.

Wise, R.A., Spindler, J., deWit, H., and Gerberg, G.J. (1978). Neuroleptic-Induced "anhedonia" in Rats: Pimozide Blocks Reward Quality of Food. Science *201*, 262–264.

Woodworth, C.H. (1971). Attack elicited in rats by electrical stimulation of the lateral hypothalamus. Physiol. Behav. *6*, 345–353.

Wren, A.M., Seal, L.J., Cohen, M.A., Brynes, A.E., Frost, G.S., Murphy, K.G., Dhillo, W.S., Ghatei, M.A., and Bloom, S.R. (2001). Ghrelin enhances appetite and increases food intake in humans. J. Clin. Endocrinol. Metab. *86*, 5992.

Wyvell, C.L., and Berridge, K.C. (2000). Intra-Accumbens Amphetamine Increases the Conditioned Incentive Salience of Sucrose Reward: Enhancement of Reward "Wanting" without Enhanced "Liking" or Response Reinforcement. J. Neurosci. *20*, 8122–8130.

Yamaguchi, T., Sheen, W., and Morales, M. (2007). Glutamatergic neurons are present in the rat ventral tegmental area. Eur. J. Neurosci. *25*, 106–118.

Yamamoto, T., Matsuo, R., Kiyomitsu, Y., and Kitamura, R. (1989). Response properties of lateral hypothalamic neurons during ingestive behavior with special reference to licking of various taste solutions. Brain Res. *481*, 286–297.

You, Z.-B., Chen, Y.-Q., and Wise, R.A. (2001). Dopamine and glutamate release in the nucleus accumbens and ventral tegmental area of rat following lateral hypothalamic self-stimulation. Neuroscience *107*, 629–639.

Young, L.R., and Nestle, M. (2002). The Contribution of Expanding Portion Sizes to the US Obesity Epidemic. Am. J. Public Health *92*, 246–249.

Zellner, D.A., Lankford, M., Ambrose, L., and Locher, P. (2010). Art on the plate: Effect of balance and color on attractiveness of, willingness to try and liking for food. Food Qual. Prefer. *21*, 575–578.

Zellner, D.A., Siemers, E., Teran, V., Conroy, R., Lankford, M., Agrafiotis, A., Ambrose, L., and Locher, P. (2011). Neatness counts. How plating affects liking for the taste of food. Appetite *57*, 642–648.

van Zessen, R., Phillips, J.L., Budygin, E.A., and Stuber, G.D. (2012). Activation of VTA GABA Neurons Disrupts Reward Consumption. Neuron *73*, 1184–1194.

Zhang, S.-J., Ye, J., Miao, C., Tsao, A., Cerniauskas, I., Ledergerber, D., Moser, M.-B., and Moser, E.I. (2013). Optogenetic Dissection of Entorhinal-Hippocampal Functional Connectivity. Science *340*, 1232627.

Zheng, H., Lenard, N.R., Shin, A.C., and Berthoud, H.-R. (2009). Appetite control and energy balance regulation in the modern world: reward-driven brain overrides repletion signals. Int. J. Obes. 2005 *33 Suppl 2*, S8–S13.

Zimmerman, F.J. (2011). Using Marketing Muscle to Sell Fat: The Rise of Obesity in the Modern Economy. Annu. Rev. Public Health *32*, 285–306.